DIPLOMARBEIT

Simulation of VLBI Intensive Sessions for the Estimation of UT1

zur Erlangung des akademischen Grades

Diplom-Ingenieur/in

ausgeführt am Department für

Geodäsie und Geoinformation

Forschungsbereich Höhere Geodäsie

der Technischen Universität Wien

unter Anleitung von

Univ.Prof. Dipl.-Ing. Dr.techn. Johannes Böhm

und

Dipl.-Ing. Dr.techn. Matthias Schartner

durch

Lisa Kern BSc

Matrikelnummer: 01604671

Wien, im Juli 2021

Unterschrift (Verfasser/in)

Unterschrift (Betreuer/in)

Eidesstattliche Erklärung

Ich erkläre an Eides statt, dass die vorliegende Arbeit nach den anerkannten Grundsätzen für wissenschaftliche Abhandlungen von mir selbstständig erstellt wurde. Alle verwendeten Hilfsmittel, insbesondere die zugrunde gelegte Literatur, sind in dieser Arbeit genannt und aufgelistet. Die aus den Quellen wörtlich entnommenen Stellen, sind als solche kenntlich gemacht.

Das Thema dieser Arbeit wurde von mir bisher weder im In- noch Ausland einer Beurteilerin/einem Beurteiler zur Begutachtung in irgendeiner Form als Prüfungsarbeit vorgelegt. Diese Arbeit stimmt mit der von den Begutachterinnen/Begutachtern beurteilten Arbeit überein.

Wien, im Juli 2021 _____

Acknowledgements

Throughout the study of this master thesis I received a great deal of support and valuable guidance.
First, I would like to pay my special regards to Prof. Johannes Böhm for his assistance and support from the beginning. Since I joined his research group, he always had a sympathetic ear and wise counsel, which helped me to achieve a great deal.
I would also like to show my deepest gratitude to Matthias Schartner, whose expertise and insight into the subject guided me through this research. I want to thank you for your patient support and for all of the opportunities I was given to further my research.
In addition, I would like to thank all my colleagues at the higher geodesy research group at TU Wien for their helpful and friendly attitude, motivation and support. It is a great pleasure for me to have a chance to work with all of you.
Another thank goes out to my friends for being there for me and always encouraging me to do my best.
Finally, I want to express my very profound gratitude to my family for providing me with continuous encouragement and support. Without their assistance, I would not have been able to accomplish everything I have set for myself in life so far.

Kurzfassung

Very Long Baseline Interferometry (VLBI) ist das einzige moderne geodätische Weltraumverfahren mit dem alle fünf Erdorientierungparameter (EOP) und der Internationalen Celestial Referenzrahmen (ICRF) bestimmt werden können. Das Messprinzip umfasst weltweit verteilte Radioteleskope, die Messungen zu Quasaren durchführen und daraus die Differenz der Ankunfszeiten als primäre Beobachtungsgröße ableiten. Neben den 24 Stunden Sessions, an denen oft mehrere VLBI Stationen beteiligt sind, finden sogenannte Intensive Sessions statt. Diese einstündigen Sessions mit nur zwei oder drei Stationen dienen ausschließlich der Bestimmung der Weltzeit UT1 in Bezug auf UTC (*dUT1*) mit einer kurzen Latenz, was für Positions- und Navigationszwecke erforderlich ist. In dieser Studie werden mithilfe der Scheduling-Software VieSched++ bestimmte Basislinien und Netzwerke für die Bestimmung von *dUT1* getestet. Dazu werden Monte Carlo Simulationen durchgeführt.

Der erste Teil der Studie befasst sich mit möglichen Basislinien zwischen bestehenden Stationen des VLBI Global Observing System (VGOS) und des Very Long Baseline Array (VLBA). Ziel ist es, die optimalen Basislinien zwischen zwei und drei Stationen zu finden und unterschiedliche Beobachtungsdauern im Bereich von einer bis vier Stunden zu untersuchen. In Bezug auf das VGOS Netzwerk würde die Basislinie ISHIOKA nach WESTFORD oder GGAO12M die besten Schätzwerte für *dUT1* liefern, etwa 15 % besser als die tatsächlich beobachtete Intensive Session zwischen WETTZ13S und KOKEE12M. Betrachtet man die VLBA Stationen, würde die Basislinie MAUNA KEA nach HANCOCK zu signifikant besseren Werten im Vergleich zur derzeitig beobachteten Basislinie MAUNA KEA nach PIETOWN führen.

Im zweiten Teil werden Basislinien in einem künstlichen globalen Netzwerk von VLBI Antennen ausgewertet, was zu fast 3000 untersuchten Basislinien führt. Im Allgemeinen zeigen die optimalen Basislinien einen kleinen Winkel zur Äquatorebene, z. B. zwischen Teleskopen hoher bis mittlerer Breite und Teleskopen niedriger bis mittlerer Breite, während sie eine Basislinienlänge von etwa 8000 bis 11 000 km haben. Baseline mit einem Mittelpunkt nahe der äquatorialen Ebene führen zu schlechteren *dUT1*-Schätzungen und werden daher für VLBI Intensive Sessions nicht empfohlen.

Abstract

Very Long Baseline Interferometry (VLBI) is the only space geodetic technique capable of estimating all five Earth orientation parameters (EOP) and the International Celestial Reference Frame (ICRF). The measurement principle includes globally distributed radio telescopes observing quasars, thereby deriving the difference in arrival time as the primary observable. In addition to 24 hour sessions, which often involve several VLBI stations, so-called Intensive sessions are observed. These one hour long sessions include only two or three stations and the sole purpose is the determination of Universal Time UT1 with respect to UTC (*dUT1*) with a short latency, which is required for positioning and navigation purposes. In this study, the scheduling software VieSched++ is used to test the suitability of certain Intensive baselines and networks for the determination of *dUT1* in Monte Carlo simulations.

The first part of this study deals with possible baselines between existing stations of the VLBI Global Observing System (VGOS) and the Very Long Baseline Array (VLBA). The target is to find the optimal baselines between two and three stations and to assess different session durations in the range from one to four hours. For VGOS, the baseline ISHIOKA to WESTFORD or GGAO12M would deliver the best estimates of *dUT1*, about 15 % better than the actually observed Intensive session between WETTZ13S and KOKEE12M. For VLBA, the baseline MAUNA KEA to HANCOCK would lead to significantly improved values compared to the baseline MAUNA KEA to PIETOWN, which is currently observed.

Furthermore, this work assesses baselines in a global artificial network of VLBI antennas, leading to almost 3000 investigated baselines. In general, the optimal baselines show a small angle with the equatorial plane, e.g., between high-to-mid-latitude and low-to-mid-latitude telescopes, while having a baseline length of about 8000 to 11 000 km. Baselines with a midpoint close to the equatorial plane result in worse *dUT1* estimates and are therefore not recommended for VLBI Intensive sessions.

Contents

List of Figures

List of Tables

List of Abbreviations

CRS Celestial Reference System

DORIS Doppler Orbitography and Radiopositioning Integrated by Satellite

dUT1 Difference between UT1 and UTC

EOP Earth Orientation Parameter

GAST Greenwich Apparent Sidereal Time

Gbps Gigabits per second

GGOS Global Geodetic Observing System

GNSS Global Navigation Satellite Systems

GSFC Goddard Space Flight Center

ICRF International Celestial Reference Frame

IERS International Earth Rotation and Reference Systems Service

ITRF International Terrestrial Reference Frame

IVS International VLBI Service for Geodesy and Astrometry

LOD Length of Day

LSM Least Squares Method

NRAO National Radio Astronomy Observatory

SEFD System Equivalent Flux Density

SLR Satellite Laser Ranging

SNR Signal to Noise Ratio

TRS Terrestrial Reference System

UT1 Universal Time

UTC Coordinated Universal Time

VGOS VLBI Global Observing System

VieVS Vienna VLBI and Satellite Software

VLBA Very Long Baseline Array

VLBI Very Long Baseline Interferometry

ZWD Zenith Wet Delay

1. Introduction

Very Long Baseline Interferometry (VLBI) is one of the four space-geodetic techniques including the Global Navigation Satellite System (GNSS), Satellite Laser Ranging (SLR), and Doppler Orbitography and Radiopositioning Integrated by Satellite (DORIS).

The geodetic VLBI measurement principle includes a minimum of two VLBI antennas measuring the difference in arrival times of the signals emitted by extragalactic radio sources at radio frequencies. VLBI is not only critical for the realization of the International Celestial Reference Frame (ICRF) but also the realization and, more importantly, for the determination of the scale of the International Terrestrial Reference Frame (ITRF). Furthermore, VLBI is the only technique capable of providing the complete set Earth Orientation Parameters (EOP), representing the transformation parameters between those two reference systems, ensuring the unique position of this space-geodetic technique. The orientation of the Earth in space is essential for positioning and navigation purposes.

So-called Intensive sessions or short "Intensives" are one hour long VLBI sessions with only a few participating stations, and the primary goal to estimate the highly variable Earth's phase of rotation, which is parametrized as the difference *dUT1* between the Universal Time (UT1) and the Coordinated Universal Time (UTC). This explains the importance of Intensive sessions and why various researches in the last decade aimed to improve these short VLBI sessions.

1.1. Objectives of the thesis

In general, this study aims to analyze the impact of specific parameters on the performance of simulated Intensive sessions, as for example the session duration, the number of participating stations as well as the baseline length and geometry. Therefore, Intensive baselines between actual telescopes of the VLBI Global Observing System (VGOS) and Very Long Baseline Array (VLBA) network are simulated and investigated. On this occasion, the impact of different session durations from one to four hours and station networks with two to three telescopes are analyzed. However, the central part of this study is the generation of a global artificial station network and the analysis of the geometry of these simulated Intensive sessions. The goal is to closely examine all possible baselines concerning their performance in the estimation of *dUT1*. Furthermore, it is possible, to analyse what is common knowledge in the VLBI community since decades: that the highest sensitivity and therefore the highest precision concerning the Earth's rotation phase can be achieved by observing long baselines with an east-west extension.

1.2. Thesis structure

This thesis is structured as follows: firstly, an introduction to the principle of geodetic VLBI and in more detail to Intensive sessions can be found in section 2. The following section 3 covers the used methodology, including a detailed insight on the scheduling and simulation process. Since two primary investigations were carried out in the course of this study, the following two sections 4 and 5 are dedicated to the individual large-scale simulation studies, dealing with the experiment setup, the scheduling and simulation approaches, as well as with the results and discussion. Section 4 deals with an investigation based on existing VLBI networks (VGOS and VLBA) and is further divided into two subsections concerning the corresponding network, whereas section 5 covers the information of an investigation based on an artificial station network. Regarding the presented and discussed experiments, section 6 provides a summary and a final conclusion.

2. Theoretical Background

This section provides an overview of the space-geodetic technique VLBI as well as Intensive sessions in more detail. The VLBI measurement principle is geometrical and, therefore, simple and straightforward. Before the actual observation can be made, the whole so-called session needs to be scheduled. The processing of the observed VLBI data includes the correlation and analysis. This section also gives a brief overview of the products of VLBI observations. Additionally, the relevant VLBI station networks, VGOS and VLBA, are introduced and the most important information is summarized.
The second part of this section is dedicated to Intensive sessions, which are of significant importance for this study. At first, the different existing types of Intensives are presented, followed by a short insight view on the principle of these one hour long sessions in more detail. A few studies dedicated to improve the performance of Intensive sessions are mentioned to show the general and widespread interest in this area.

2.1. Very Long Baseline Interferometry

The idea of VLBI was invented in the 1960s by astronomers to synthesize a telescope aperture of many thousand kilometers to improve the imaging of extragalactic objects (Nothnagel, 2019b). Since the 1970s, VLBI is used as a geodetic space technique to determine the orientation and rotation of the Earth in space. This is primarily made possible by the fact that VLBI directly measures quasars in the ICRF at radio frequencies with VLBI telescopes located on the Earth's surface in the ITRF (Haas et al., 2021). The unique position of VLBI is shown in figure 2.1 which lists the contribution of the individual techniques. Whereas from VLBI observations, no direct access to gravity field information or geocenter motion is provided, it is crucial for the determination of the highly variable daily rotation, the long term nutation, and for the realization of the ICRF by a catalog of well-defined quasars (Schuh and Behrend, 2012) (Klopotek et al., 2020).

Parameter	VLBI	GNSS	DORIS	SLR	LLR	Altimetry
ICRF (quasars)	X					
Nutation	X	(X)		(X)	X	
Polar motion	X	X	X	X	X	
UT1	X					
Length of day	(X)	X	X	X	X	
ITRF (stations)	X	X	X	X	X	(X)
Geocenter		X	X	X		X
Gravity field		X	X	X	(X)	X
Orbits		X	X	X	X	X
LEO orbits		X	X	X		X
Ionosphere	X	X	X			X
Troposphere	X	X	X			X
Time/frequency	(X)	X		(X)		

Figure 2.1: An overview of the space-geodetic techniques and their capability to estimate different parameters, figure from Schuh and Behrend (2012).

2.1.1. Measurement principle

In geodetic VLBI, a minimum of two radio telescopes simultaneously observe a radio source emitting an electromagnetic signal. These compact sources are up to billions of light-years away and are called quasars (Campbell, 2000).

In figure 2.2 the basis concept of VLBI is shown. The quasar's signal arrives on Earth as a planar wavefront due to the long distance between the Earth and the sources. Therefore, the direction to the source, which is represented as $\vec{s}_0$ is parallel for all ground-based stations. These incoming signals are now digitized, time-stamped and recorded at the VLBI stations at locations 1 and 2, forming a so-called baseline $\vec{b}$. In the case of the legacy S/X system, the signal is recorded in two bands in the radio frequency domain. The primary frequency is the X-band (8.4 GHz) and S-Band (2.3 GHz) to eliminate the ionosphere's dispersive effects. Hence, the actual observable is not the time delay τ but the group delay τ_{gr} as it is determined from a spectrum of frequencies rather than just monochromatic radiation. For the sake of simplicity, the group delay is just written τ throughout this document.

Due to the separation of the two (or more) stations, a difference in arrival time τ occurs, which can be determined by the cross-correlation of the recorded signals at the correlator. Consequently, the geometric principle of VLBI can be reduced to a rectangular triangle, which provides a direct and straightforward relation between the direction of the observed source $\vec{s}_0$ and the baseline vector $\vec{b}$ scaled by the speed of light c and the time delay τ, see equation 2.1 (Schuh and Behrend, 2012).

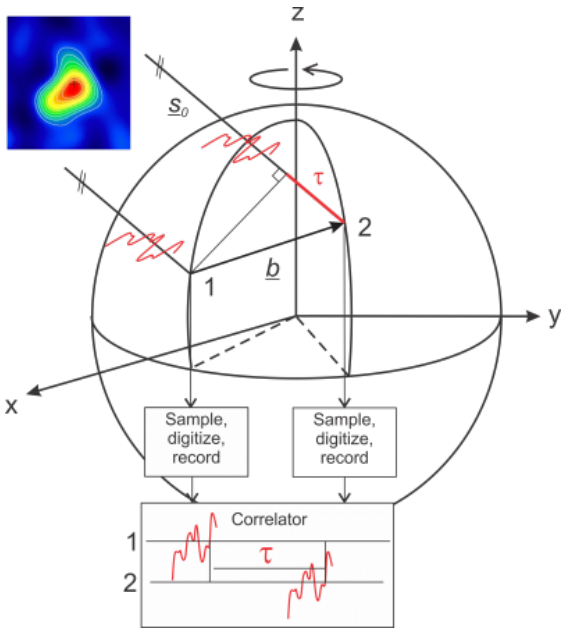

Figure 2.2: The VLBI measuring principle containing a minimum of two telescopes placed at the locations 1 and 2, which are forming a baseline $\vec{b}$ and are observing a quasar in the direction $\vec{s}_0$. τ represents the observed time delay between the stations, figure from Schuh and Behrend (2012).

$$\tau = -\frac{\vec{b} \cdot \vec{s}_0}{c} = t_2 - t_1 \tag{2.1}$$

However, since $\vec{b}$ is provided in an Earth fixed system (Terrestrial Reference System, TRS) and $\vec{s}_0$ in a celestial reference system (Celestial Reference System, CRS), the baseline vector needs to be transformed using the five Earth Orientation Parameters (EOPs), which describe the orientation and rotation of the Earth in space. Therefore, EOPs are essential for positioning and navigation on the Earth's surface and in space, leading to the following fundamental equation of VLBI

$$\tau = -\frac{\mathbf{Q}(t) \cdot \mathbf{R}(t) \cdot \mathbf{W}(t) \cdot \vec{b} \cdot \vec{s}_0}{c}, \tag{2.2}$$

where $\mathbf{W}(t)$, $\mathbf{R}(t)$ and $\mathbf{Q}(t)$ represent transformation matrices with a set of rotations about the axes of the coordinate frame. $\mathbf{W}(t)$ arises from the so-called **polar motion**, which describes the terrestrial motion of the Earth's rotation axis using two angles x_p and y_p. The motion of the Earth's rotation axis with respect to the celestial reference frame is called **precession** and **nutation**, also described by two angles (dX, dY) which can be found in the calculation of $\mathbf{Q}(t)$ (Petit and Luzum, 2010).

The last and the most important one concerning this study is the quantity that describes the **Earth's rotation** around its axis, parametrized as *dUT1* and represented in equation 2.2 by $\mathbf{R}(t)$ (Schuh and Behrend, 2012).

As can be seen from equation 2.3, *dUT1* is the difference between the two time scales UT1 and UTC.

$$UT1 - UTC = dUT1 \tag{2.3}$$

The Universal Time (UT1) is the Greenwich hour angle of the mean sun corrected for polar motion. Hence, it defines the actual nonuniform rotation of the Earth, including all variations. The time scale, referred to as the Coordinated Universal Time (UTC), is highly uniform and adapts well to UT1. However, due to the steady decrease in the Earth rotation phase and consequently the increase in the Length of Day (LOD), *dUT1* would progressively increase. This phenomenon is restricted by the adaption of the epoch of UTC to UT1 by inserting a leap second when *dUT1* is about to exceed 0.9 s (see equation 2.3) (Seeber, 2003).

Strong variations in UT1 arise due to mainly solid Earth tides, atmospheric movements, ocean tides and currents as well as effects of the liquid outer core. Therefore, *dUT1* is subject to strong fluctuations making it hard to predict (Landskron and Böhm, 2019).

The observed time delay τ is mainly influenced by the geometric delay τ_{geom} but also contains contributions from error sources that need to be accounted for (see equation 2.4) (Schuh and Behrend, 2012):

$$\tau = \tau_{\text{geom}} + \tau_{\text{ab}} + \tau_{\text{clk}} + \tau_{\text{inst}} + \tau_{\text{trop}} + \tau_{\text{iono}} + \tau_{\text{rel}} \tag{2.4}$$

with

- τ_{geom} is the geometric delay,
- τ_{ab} is the contribution caused by the dirunal abberation,
- τ_{clk} is induced by the delay from incorrect synchronized reference station clocks,
- τ_{inst} is caused by possible propagation delays through the instrument,
- τ_{tropo} is the tropospheric non-dispersive delay,
- τ_{iono} represents the ionospheric dispersive delay,
- τ_{rel} is the relativistic contribution to the geometric delay.

In order to estimate the true time delay τ_{geom}, it is essential to account for the above listed contributions. There exist several methods to eliminate these error sources: the contributions from the aberration and the relativity are eliminated using known physics, the signal delay caused by the instrument itself by calibration, the delay induced by the clocks and the troposphere are derived in the least squares adjustment by modeling and the ionospheric delay can be removed using dual-frequency observations, due to its dispersive properties (Schuh and Behrend, 2012).

2.1.2. Scheduling

As already mentioned, when using the VLBI technique certain conditions need to be considered in the planning of a VLBI session. For example, it is crucial that at least two telescopes observe one source at the same time. Otherwise, no baseline is formed, no arrival delay τ can be determined and further, no VLBI products can be estimated. Moreover, the VLBI stations are placed all over the Earth and consequently, the mutually visible sky could be somewhat restricted. Due to the ongoing development and improvement of not only the processing and analysis of VLBI data but also the telescopes and antennas, the slewing speed of the stations varies as well as the recording rate and antenna sensitivities (Schartner and Böhm, 2019b).

A so-called schedule is necessary to plan the observation by coordinating the telescopes. This observation plan contains the start and stop times of all participating stations for every individual observation. If a network of n stations observes a source simultaneously, it is called a scan. Whereas when two telescopes forming a baseline point at the same quasar for the same period of time it is called an observation. Consequently, one scan to the same source can consist of $n \cdot (n-1)/2$ individual observations (Nothnagel, 2019b).

Theoretically, there are infinite possible constellations for a scan, making the scheduling of a VLBI session a complex task. As the observation plan defines the geometric configuration of a scan/ the whole session, it is crucial for the quality of the geodetic parameters. Therefore the generation of schedules can be seen as an optimization process (Schartner and Böhm, 2019b). In geodetic VLBI, several optimization criteria are often considered when generating a schedule. For example, the scan duration, the sky coverage or the idle time.

Some of these optimization parameters contradict each other whilst all being important for the accurate determination of geodetic parameters, some of course more than others. One of the challenges is now to find the sweet spot between competing criteria like the sky coverage and the number of observations (Gipson, 2010) (Schartner and Böhm, 2019b). Typically a combination of several criteria is used to generate the optimal schedule (Schartner and Böhm, 2019a).

There are various software packages for analyzing VLBI data, but only a few are dedicated to generate VLBI schedules. sked is a software developed by the Goddard Space Flight Center's (GSFC) International VLBI Service for Geodesy and Astrometry (IVS) Analysis Center, which is currently widely used in the VLBI community (Vandenberg, 1999) (Gipson, 2010). Another package used mainly for astronomic schedules is called Sched by the National Radio Astronomy Observatory (NRAO) (Walker, 2018). Furthermore, the Matlab-based software package VIE_SCHED is part of the Vienna VLBI and Satellite Software (VieVS) and was used to schedule AUSTRAL sessions carried out by the AuScope geodetic VLBI array in Australia (Sun, 2013) (Böhm et al., 2018b) (Plank et al., 2017). Another more recently developed scheduling software is called VieSched++ and is written in C++ (Schartner and Böhm, 2019b).

Typically, a schedule is generated scan after scan (see sked, VI_SCHED and VieSched++) using a brute force approach. As an example, VieSched++ selects a certain scan from a large pool of possible scans based on a total score. The total score is determined by the individual score a scan achieved per optimization criterion multiplied by a corresponding weight factor w (see equation 2.5). These weight factors w define the contribution of the individual criteria for the scan selection (Schartner and Böhm, 2019b). Consequently, the selection of a good set of optimization parameters and corresponding weight factors are the key to generating an optimal schedule. Based on these evaluations, the best scan is selected and this whole process is repeated until the session is fully scheduled (Schartner and Böhm, 2019a).

$$score_{\text{scan}} = \sum_{i=0}^{n} w_{\text{i}} \cdot score_{\text{i}} \tag{2.5}$$

Unfortunately, there is no way finding one "perfect set of parameters" as they strongly depend on the station network and the session task. Consequently, for each session, an individual set of parameters and weight factors should be specified (Schartner et al., 2017). In the end, the scan with the highest total score is selected and the whole process starts again until there is no time within the session left (Schartner and Böhm, 2019a).

2.1.3. Observation

The finished optimized schedules are sent out to all participating stations in the session and following this observation plan, the telescopes rotate and observe autonomously. In geodetic VLBI, the quasars' electromagnetic radiation is observed at the X-band (8.4 GHz) and S-Band (2.3 GHz) concerning the standard S/X system and in the frequency range of 2 to 14 GHz regarding the next generation VLBI Global Observing System (VGOS). In general, small bands with bandwidths up to 16 MHz are extracted due to the limited recording capacity. Furthermore, the signal is digitized and time stamped using the station's atomic clock.

In the following, the recorded bitstreams from every station are transferred to the correlator (Nothnagel, 2019b). Nowadays, parts of the data can be transmitted over the internet, called eVLBI. Only the high connection costs of powerful wires prevent an increased use of eVLBI. In general, the data is shipped via portable disk systems, which has a high impact on the latency of the VLBI products (BKG, 2021).

2.1.4. Correlation

The correlation process includes comparing the recorded bitstreams of stations forming a baseline to derive the fundamental observable of VLBI, the time delay. The mathematical principle behind this process is the cross-correlation theorem (Whitney, 2000). In the correlator, the cross-correlation coefficient is calculated while the two bitstreams are shifted in time relative to each other. At a certain time shift the correlation function is maximized representing the difference in signal arrival times τ (Nothnagel, 2019a).

2.1.5. Simulation

Simulations in VLBI are a valuable tool to assess the accuracy of the parameters of interest while considering possible error sources to ensure that they can provide realistic results. Concerning Monte Carlo simulations, the mathematical model and a set of input parameters with known stochastic behavior are essential for generating a large number of simulations. However, simulated sessions do not reflect the actual performance of the corresponding Intensive session but can be used for testing new scheduling strategies or network constellations. Since real VLBI experiments are expensive but in great demand, simulations are widely used (Schartner and Böhm, 2019a).

The simulated time delay τ can be expressed by the sum of the geometric delay, the three most important stochastic error sources, i.e., troposphere, station clocks and measurement errors of the receiving system as well as the contribution of other systematic errors, for example, the thermal deformation of the telescopes or the structure of the sources (Pany et al., 2010).

The geometric delay is calculated using the so-called Consensus Model (Petit and Luzum, 2010). To predict the performance of a session the three main error sources are alternated in the Monte Carlo simulation process (Klopotek et al., 2020). In general, the troposphere is simulated using the following three parameters: a tropospheric turbulence parameter C_n, the tropospheric height H and the wind speed. The C_n value for different VLBI stations can be found in Petrachenko et al. (2009), which are assumed to be constant up to a height H of 2000 m (Nilsson et al., 2007). The stochastic errors of the station clocks can be modeled using the sum of random walk and integrated random walk stochastic processes (Herring et al., 1990). The receiving system's measurement errors or "white noise" is the standard deviation of Gaussian distributed noise. The sum of these three error sources $\Delta\tau_{\text{tropo}}$, $\Delta\tau_{\text{clk}}$ and $\Delta\tau_{\text{wn}}$ equals the difference between the observed and computed values $(o-c)$ in the least squares adjustment (see equation 2.6).

$$(o-c) = \Delta\tau_{\text{tropo}} + \Delta\tau_{\text{clk}} + \Delta\tau_{\text{wn}} \tag{2.6}$$

2.1.6. Analysis and Products

In the following section, at first the analysis of the VLBI data using the Gauss-Markow Least Squares Method (LSM) is described briefly, focusing on the analysis of Intensive sessions. Secondly, the general products of VLBI, combined and published by the International VLBI Service for Geodesy and Astrometry (IVS) are introduced.

Analysis - Least Squares Adjustment

In the analysis of the VLBI data, the parameters of interest are derived, e.g., EOPs and station coordinates. As already mentioned, the observed delay is influenced by several contributions, which need to be accounted for. Some of these effects can be predicted or modeled, using models according to the International Earth Rotation and Reference Systems Service (IERS) and IVS Conventions. Others can be eliminated to a certain extent, like the ionospheric delay using dual-frequency observations. However, some other parameters, like the clock drifts and the troposphere, especially the wet delay, enormously fluctuate and are hard to predict.

Consequently, it is necessary to estimate these strongly variable quantities along with the parameters of interest using the Gauss-Markow Least Squares Method (LSM). Therefore, a theoretical delay using a priori information, models on the station and source coordinates and furthermore, e.g., the deformation and orientation of the Earth, is calculated. For the computation of this theoretical delay, the IERS Conventions 2010 recommend the application of the Consensus Model. Detailed information can be found in Spicakova (1991) and Petit and Luzum (2010). The LSM uses the difference between the observed delay and the calculated theoretical delay $(o-c)$ or short $\mathbf{l}$ to estimate the unknown parameters $\mathbf{x}$. This method has the task to minimize the weighted sum of the squares of the residuals $\mathbf{v}$ in an overdetermined system, which means that a higher number of observations n compared to unknown parameters u is necessary. Additionally, the mathematical model, which represents the relationship between the unknown parameters and the observations, must be known and the observation equations need to be linearized by a first-order Taylor polynomial (Kahmen, 2006).

$$\mathbf{x} = \mathbf{N}^{-1}\mathbf{A}^T\mathbf{P}\mathbf{l} \quad with \quad \mathbf{N} = \mathbf{A}^T\mathbf{P}\mathbf{A} \tag{2.7}$$

$$\mathbf{v} = \mathbf{A}\mathbf{x} - \mathbf{l} \tag{2.8}$$

Equation 2.7 represents the fundamental relationship between the unknown parameters $\mathbf{x}$ and the Jacobian matrix $\mathbf{A}$, which contains the first derivatives of the function of the observations with respect to the parameters.

Furthermore, it contains the weight matrix **P**, with the weighting of the observations, the normal equation matrix **N** and the vector **l**. Using the derived parameter vector **x**, it is possible to calculate the residuals **v** of the individual observations, as can be seen from equation 2.8. By multiplying the so-called variance factor a posteriori s_0^2 with the inverse of **N**, the covariance matrix **Q** can be determined (see equation 2.9). The diagonal elements of **Q** contain the variances or the square root of the formal errors of each parameter, whereas the off-diagonal elements define the covariances (Kahmen, 2006).

$$\mathbf{Q} = s_0^2 \cdot \mathbf{N}^{-1} \quad with \quad s_0^2 = \frac{\mathbf{v}^T \mathbf{P} \mathbf{v}}{n-u} \tag{2.9}$$

Since this study is mainly based on Intensive sessions, in the following more detailed informations on these short VLBI sessions are provided. As already mentioned, an overdetermined system is necessary to estimate the parameters of interest using the LSM. Concerning Intensive sessions, the highly limited session duration results in a low n and therefore fewer parameters can be estimated, to still receive a redundancy. To be more precise, only the following five quantities are derived (Landskron and Böhm, 2019):

- a linear function describing the clock difference between two stations, which contains one clock offset $CL0$ and clock rate $CL1$,
- a zenith wet delay per station and session $ZWD_{1,2}$ and
- one *dUT1* offset with respect to the a priori value.

This leads to the fact, that other parameters, like the station and source coordinates, the polar motion and the nutation need to be fixed to their a priori value, respectively. Hence, the usage of very accurate a priori values is essential and crucial for the determination of *dUT1* with the highest precision (Raut et al., 2020).

Furthermore, in a least squares adjustment, it is essential that the partial derivatives of the parameters with respect to τ are variable and differ from each other to avoid correlations. The partial derivatives of these five parameters can be found in equation 2.10, where the last two equations concerning the $\frac{\partial \tau}{\partial ZWD_{1,2}}$ and $\frac{\partial \tau}{\partial dUT1}$ are only an approximation or are written in the old nomenclature, which is used for easier interpretation.

$$\begin{aligned} \frac{\partial \tau}{\partial CL0} &= 1 \\ \frac{\partial \tau}{\partial CL1} &= t - t_0 \\ \frac{\partial \tau}{\partial ZWD_{1,2}} &\approx \frac{1}{\sin \varepsilon_{1,2}} \\ \frac{\partial \tau}{\partial dUT1} &\approx -\frac{1}{c} \cdot 1.00273 \cdot cos\delta \cdot ((x_2 - x_1) \cdot \sin h_G + (y_2 - y_1) \cdot \cos h_G) \end{aligned} \tag{2.10}$$

Here, the subscripts 1 and 2 represent the two telescopes, whereas c is the speed of light, δ is the declination of the observed quasar, the coordinates x_1, y_1, x_2 and y_2 describe the location of the telescopes in the equatorial plane and the Greenwich Hour Angle h_G, which can be calculated using the Greenwich Apparent Sidereal Time *GAST* and the right ascension α of the radio source (see equation 2.11).

$$h_G = GAST - \alpha \tag{2.11}$$

Considering these mathematical relations, a dependency between the source position and the partial derivative of *dUT1* exists. As already mentioned, it is crucial to derive variable $\frac{\partial \tau}{\partial dUT1}$ values, mainly a variation of the source position α or h_G and δ (see equation 2.10) is necessary to achieve this. While different δ values from [−90°,90°] result in an $\cos\delta$ value of [0,1], the right ascension α ranges from [0°,360°), leading to a $\sin h_G \mathrel{\widehat{=}} \sin\alpha$ of [−1 ,1], which causes a higher variability of $\frac{\partial \tau}{\partial dUT1}$ than the source declination δ. However, a large extension on the equatorial plane, which can be nearly equated with a large extension of the baseline in east-west direction, can be beneficial (Schartner et al., 2021).

IVS Products

Under the umbrella of the IVS, which is an international collaboration of institutions of geodetic and astrometric VLBI, the results of the Analysis Centers (ACs) are combined and made available to the public. The main IVS products from VLBI observations include the following parameters:

A so-called **reference frame** is a realization of the conceptual reference system, where the coordinate system is defined including the orientation, origin and essential mathematical and physical models (Seeber, 2003). Due to the measurement principle of VLBI, which is the observation of distant radio sources, it is possible to establish a celestial reference frame. While VLBI is the only space-geodetic technique able to realize the ICRF in radio frequencies, the realization of the ITRF includes the products of several techniques, combining the advantages of each one of them. Through observation and a set of points located, for example, on the sky (quasars) or the Earth's surface (stations), catalogs of precise positions and velocities at a certain epoch can be determined. The current versions of the two reference frames are ICRF3 and ITRF2014 (Schuh and Behrend, 2012). The submission for ITRF2020 is currently in progress (Merkowitz and Gipson, 2021).

The **EOPs** are the link between the two reference frames realized through a set of rotations. They describe the orientation and rotation of the Earth in space and are therefore essential for positioning and navigation on the Earth's surface and in space. As already mentioned, VLBI is the only space-geodetic technique that can provide a complete set of EOPs, including *dUT1* and nutation parameters.

Furthermore, VLBI observations can be used to determine geodynamic and astronomical parameters, including the Love and Shida numbers h and l of the solid Earth tides model and the Free Core Nutation (Spicakova et al., 2010), tropospheric parameters and ionospheric models (Hobiger et al., 2006). In addition, the gravitational deflection of the radio signals traveling near the Sun can be observed (Robertson, 1991).

2.1.7. VGOS and VLBA network

Historically, VLBI has only used two frequency bands, the S- and X-band. A map of the current station network can be seen in figure 2.4. To reach the goals of the Global Geodetic Observing System (GGOS) from the early 2000s, which include the determination of station coordinates with an accuracy of 1 mm and velocities of 0.1 mm per year, continuous measurements of station coordinates and EOPs as well as a turnaround time to initial products of less than 24 h, it was necessary to introduce the next generation VLBI system, called **VLBI Global Observing System (VGOS)** (Schuh and Behrend, 2012) (Petrachenko et al., 2012). During the last years more and more stations have been equipped with this next generation system with the following main characteristics in comparison to the commonly used S/X legacy system:

	Legacy system	VLBI2010 system
Antenna size	5–100 m dish	~12 m dish
Slew speed	~0.4–3°/s	~6–12°/s
Sensitivity	200–15,000 SEFD	≤2500 SEFD
Freq. range	2.2–2.4 GHz, 8.2–8.95 GHz	Tunable over ~2–14 GHz
Freq. bands	2 bands (S and X)	4 bands
Recording rate	128–512 Mbps	8–32 Gbps
Delay precision	10–30 ps	~4 ps
Data transfer	Usually ship disks, Some e-transfer	e-Transfer, e-VLBI, Ship disks as needed

Figure 2.3: A comparison of the standard S/X legacy system and the next generation VGOS system, table from Schuh and Behrend (2012).

With VGOS, small and therefore faster slewing antennas with high data rate acquisition, a broadband receiving system with four bands spreading over 2 —14 GHz and further dual polarization observations are used. Not only an increase in the number of observations is achieved using VGOS telescopes (Haas et al., 2021), also the sampling of the sky is improved, which is essential for the decreasing the influence of the troposphere, the restricting factor for geodetic VLBI (Sekido et al., 2021) (Pany et al., 2010).

The so-called **Very Long Baseline Array (VLBA)** network consists of ten identical stations, which are all located in the USA (Napier et al., 1994). Since 2011, observations have been scheduled to estimate the parameter *dUT1* on a daily basis. The 25 m telescopes observe at nine frequency bands between 327 MHzand 96 GHz and are operated by the US Naval Observatory (USNO) (Napier et al., 1994). The array size measures approximately 8611 km, which is the longest possible baseline between the stations MAUNA KEA and SAINT CROIX.

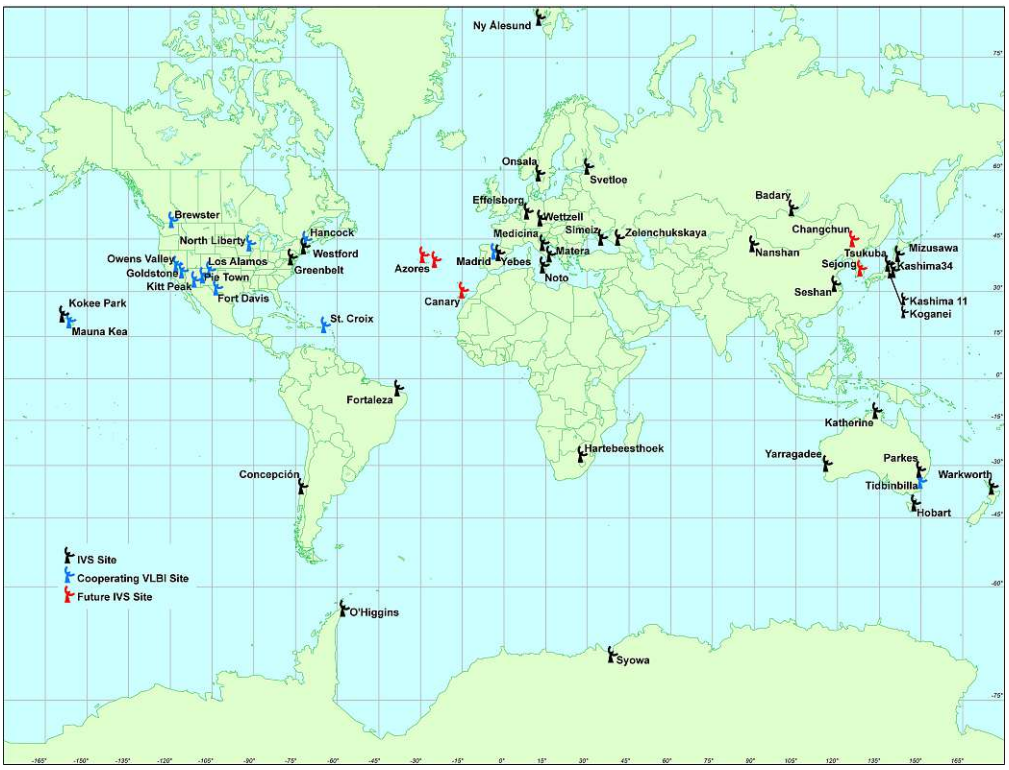

Figure 2.4: A map of the current VLBI station network. Black telescopes mark the IVS antennas, whereas blue telescopes represent mostly VLBA antennas. Red telescopes are planned IVS sites, figure from IVS (2021b).

2.2. Intensive sessions

As already mentioned at the beginning of this chapter, Intensive sessions are one hour single baseline sessions to provide the parameter *dUT1* with a short latency (Böhm et al., 2010). In practice, sometimes more than two stations are participating in one Intensive session to increase the number of observations. There are typically 20-40 observations per one hour S/X legacy session and 50-60 observations in on hour VGOS sessions (Haas et al., 2021). Hence, the precision is reduced compared to 24 h sessions, making the scheduling process itself and the network geometry crucial for the quality of an Intensive session. So far, it is common knowledge in the VLBI community that long east-west baselines are the key to a good performance. In the following section, commonly observed Intensive Sessions are introduced.

2.2.1. Types of Intensive sessions

At the moment, several types of Intensive sessions are observed regularly. They differ in the number and selection of participating stations, in the date and time they take place and in the observing mode (Böhm et al., 2021). The most common ones are the three one hour long Intensive observing programs known as IVS Intensives making use of the S/X legacy-band VLBI system, which have been observed for decades (Haas et al., 2021).

They include the INT1 (or XU) observing program, which is observed regularly on weekdays at 18:30 UTC on the baseline WETTZELL (Germany) - KOKEE (Hawaii, USA). Whereas INT2 (or XK) is usually scheduled for the weekends at 07:30 UTC, including again WETTZELL and ISHIOKA (Japan) or currently MK-VLBA (Hawaii, USA). Lastly, INT3 (also XK) is usually performed on Monday mornings using three to five stations, including ISHIOKA, NYALES20 (Norway), SESHAN25 (China), WETTZELL and WETTZ13N (Germany) (Landskron and Böhm, 2019) (Böhm et al., 2021). Stations participating in IVS Intensives are currently all located in the northern hemisphere. Due to this fact, so-called Southern Intensives were introduced.

The Southern Hemisphere Intensive observing program (SI) was introduced by a collaboration between TU Wien, the HartRAO Observatory and the University of Tasmania to retrieve *dUT1* using VLBI stations located in the Southern Hemisphere. HART15M (South Africa), HOBART12 (Tasmania) and YARRA12M (Western Australia) are the three participating stations in this type of Intensive session starting at 15:30 or 18:30 UTC on Monday or Tuesday (Böhm et al., 2021).

Additionally, during the last years, Intensive sessions between VGOS stations have been investigated. So-called VGOS-B sessions were performed from December 2019 until February 2020 between ISHIOKA and the twin telescopes ONSA13NE and ONSA12SW (Sweden). These VGOS-B sessions were scheduled to be observed simultaneously with the standard INT1 sessions. The comparison of these individual sessions showed that the formal uncertainties of the derived *dUT1* parameter of VGOS-B sessions are three to four times lower than the corresponding uncertainty achieved with the standard S/X legacy Intensive session INT1. This improvement is justified in the improved estimation of the atmospheric delays, which are, as already mentioned, the restricting factor for geodetic VLBI (Haas et al., 2021).

Furthermore, so-called VGOS-2 sessions are scheduled between KOKEE12M (Hawaii, USA) and WETTZ13S (Germany) simultaneously to the VB and INT1 sessions. According to the Intensive Master Schedule published by the IVS, additionally, VGOS-C sessions with the same network as VGOS-B sessions are rarely observed on weekdays in the morning whereas INT1 and VB sessions are scheduled in the evening (IVS, 2021a).

As already mentioned at the beginning of this chapter, all Intensive session types introduced above are one hour long VLBI observations. In the middle of 2018, test sessions between AGGO (Argentina), WETTZELL and WETTZ13N were investigated under the name of INT9 (or X9) with a session duration of two hours. These sessions were scheduled between 16:00 and 18:00 UTC before the regular INT1 session (Plötz et al., 2019).

Beside these global Intensive sessions, more national observations for the determination of *dUT1* exist. For example, since 2011, so-called VLBA Intensives are investigated and observed. They include the following VLBA stations within the USA: MAUNA KEA, PIETOWN and SAINT CROIX (Geiger et al., 2018). Besides the USA, also Russia has its own Intensive sessions, including the following stations: BADARY, ZELENCHK and SVETLOE (Shuygina et al., 2019). These national VLBI Intensive sessions provide the corresponding GNSS (GPS and GLONASS) with *dUT1* values making them not fully dependent on the *dUT1* solution from IVS Intensives. However, in Europe, there is no such Intensive session so far. Böhm et al. (2018b) investigated a European baseline between Santa Maria (Azores, Portugal) and Wettzell for the determination of *dUT1* (see figure 2.5). However, simulations lead to an accuracy of *dUT1* worse than from IVS Intensives. Furthermore, the estimation of *dUT1* from real observations, which were carried out in March 2018, was not possible also due to the low SNR (Signal to Noise Ratio) at the X-band. Unfortunately, investigations in this area are stagnating, although European Intensive sessions would be a precious backup solution.

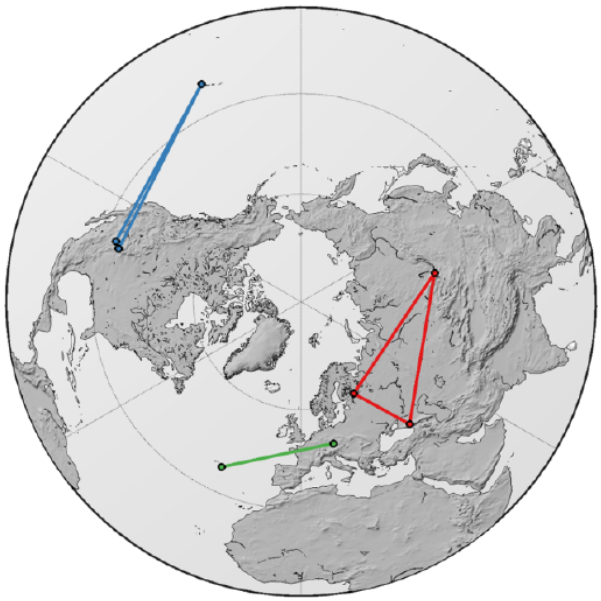

Figure 2.5: A map of national Intensive baselines: VLBA Intensive baseline observed within the USA (blue), Russian baseline (red) and a possible European baseline (green), figure from Böhm et al. (2018b).

2.2.2. Principle of Intensive Sessions

Several general conditions limit the design of schedules for Intensive sessions:

- the small number of participating stations,
- the small number of sources which are commonly visible at all stations due to the highly restricted mutually visible sky arising from the long baselines with large east-west extension,
- the short session duration of one hour and
- the scan duration, which depends on the flux density of the observed source and the antennas' sensitivity to reach a certain minimum *SNR*.

The requirement of a certain minimum *SNR* is necessary, due to the fact that the standard deviation of the observed time delay τ is inversely proportional to the *SNR* and the effective bandwidth of the registration unit B (Schnell, 2006):

$$\sigma_\tau = \frac{1}{2\pi \cdot SNR \cdot B} \tag{2.12}$$

As already mentioned in section 2.1.6, the number of observations for Intensive sessions is rather low, compared to regular 24 h sessions. Only 20-40 (standard S/X legacy system) or 50-60 (VGOS) observations per session can be achieved during this short amount of time. As a result, fewer parameters, namely a clock offset $CL0$ and clock rate $CL1$, a zenith wet delay per station $ZWD_{1,2}$ and one *dUT1* offset can be estimated (Landskron and Böhm, 2019). Besides that, also the accuracy deteriorates, from approximately 5 to 7 μs concerning 24 h sessions up to 15 to 20 μs (Böhm et al., 2010) (Böhm et al., 2018a).

The Earth's rotation among the five EOPs is the most variable and therefore unpredictable quantity. Consequently, it is insufficient to derive *dUT1* solutions only from 24 h sessions where the product delivery time can be up to a week. For this reason and because satellite-based techniques can not distinguish between changes in the Earth's rotation phase and the satellite orbit parameters, Intensive sessions are dedicated VLBI sessions with the sole objective to determine the highly variable parameter on a daily basis with low latency. Therefore, all space-geodetic techniques entirely depend on the determination of UT1 or, more specifically, *dUT1* from geodetic VLBI (Landskron and Böhm, 2019) (Haas et al., 2021).

2.2.3. Improvement of Intensive Sessions

Due to the important role of Intensive sessions for the positioning and navigation on Earth and in space, various researches have been carried out in the last decade to improve the performance of these one hour long VLBI sessions. Since only a few stations are participating in an Intensive session, the network geometry and the scheduling process itself are crucial.

Some of the studies concentrate on improving the scheduling, like in Corbin et al. (2020) by introducing a new mixed-integer linear programming method and using a new sky coverage score, or in Leek et al. (2015), where the impact factors were used in the scheduling to improve the geometry. Additionally, in the study from 2015, the improvement of the performance of Intensive sessions by increasing the number of observations using twin telescopes was investigated. In comparison, Kareinen et al. (2017) suggested adding a tag-along station to get a higher number of observations per session. Whereas Artz et al. (2012) investigated the impact of doubling the session duration from one to two hours.

Other studies also examined the benefits of a proper source selection, like in Uunila et al. (2012), Baver and Gipson (2014) and Baver and Gipson (2020). In the study from 2012, they further found out that observations at the mutually visible sky are the key for high precision concerning Intensive sessions. The following results of this study, as well as similar studies like Baver and Gipson (2015), further confirm this relation.

This particular study aims to optimize Intensive sessions by finding the optimal network constellation regarding the two VLBI station networks, VGOS and VLBA, and analyzing the impact of different conditions, like the session duration or the number of participating stations. However, the main part of this study is based on the study by Schartner et al. (2020), where network geometries are investigated on a global scale. Therefore, a global network with artificial stations has been generated and all possible and unambiguous baselines between two stations are simulated. The target is to examine closer what is common knowledge in the VLBI community for decades, which includes a long east-west baseline extension to achieve the highest precision.

Only recently a similar study concerning the artificial network has been published by (Schartner et al., 2021), which supports the findings of this master thesis.

3. Methodology

3.1. Motivation

In the course of this study, three main experiments, which concern different existing and artificial VLBI station networks, are investigated. All of them focus on improving the performance of Intensive sessions by analyzing mainly the impact of the baseline geometry and baseline length, as well as the session duration and the number of stations participating in a session. As already mentioned, firstly, Intensive sessions between existing VLBI networks (VGOS and VLBA) are analyzed to identify the best single baseline among the available antennas. Secondly, like it has been done in other studies (see section 2.2.3), the impact of a adding a third station to a two station Intensive session and the introduction of different session durations have been examined. Furthermore, different scan duration intervals and the difference between recording with one versus two recorders are investigated concerning one selected VGOS baseline. However, the central part of this study includes a global artificial station network, which is generated to analyze the impact of the geometry of a single baseline Intensive session on a more global scale. This investigation is based on the approach used by Schartner et al. (2020). The motivation is further to analyze common knowledge throughout the VLBI community for decades, stating that long east-west baselines are essential for determining *dUT1* with the highest precision.
Since these experiments are based on Intensive sessions taking place over one whole year with daily or monthly observations and many VLBI antennas or artificial antennas involved, it is not possible to perform these experiments in practice. As already mentioned in the section 2.1.5, using certain software packages, sessions can not only be scheduled but also simulated to assess the accuracy of the parameter of interest, *dUT1*. This certainly does not provide the real performance of the corresponding Intensive session. However, it can be used to compare different baselines regarding their geometry, length and other features. To perform this large-scale simulation study, VieSched++ has been used for the scheduling and simulation of almost 1.3 million Intensive sessions (see table 5.5). The preparation and the analysis has been done using the programming and computing software MATLAB.
In the following, the general concept, including the principles and the scheduling is introduced briefly. Since the experiments differ in their setup as well as in the scheduling process, separate chapters are dedicated to the individual experiments concerning existing networks (see chapter 4) and the global investigation (see chapter 5).

3.2. Software and method

Within this study, the software package VieSched++ is used to execute this large-scale simulations. VieSched++ is the VieVS VLBI scheduling software recently developed at the TU Wien by Matthias Schartner. This scheduling and simulation software written in C++ is already widely used to schedule various observing programs, including AUA, T2, EURR&D, EUR, OHG and INT3.

3.2.1. Scheduling

With VieSched++, the generation of schedules is relatively easy and straightforward. The information, which is essential for the computation of schedules is implemented via so-called sked-catalogs. These catalogs are available on Github (NVI, 2021). Some of the existing catalogs, including information on the following topics, are listed below (Vandenberg, 1997).

- Sources:
  - *source.cat*: source positions
  - *flux.cat*: source fluxes
- Stations:
  - *antenna.cat*: antenna properties
  - *equip.cat*: station equipment
  - *position.cat*: station locations
  - *mask.cat*: local horizon and coordinate masks
- Observing modes:
  - *modes.cat*: observing modes
  - *freq.cat*: frequency setups
  - *rx.cat*: receiver setups

The source catalogs provide information on the source positions (right ascension α, declination δ) at a particular epoch and the source fluxes, including the strength and structure information. The so-called *source.cat.geodetic.good* is a subset of the source catalog and is used for geodetic applications, since only well suited sources are included.

The catalogs regarding the stations are essential for the global investigations carried out in the course of this study, see chapter 5. The antenna file contains information on the antenna properties, such as the mount, axis offsets, limitations and slew rates. The number of recorders at a certain station as well as the System Equivalent Flux Density (SEFD), which defines the sensitivity, are part of the *equip.cat*. The position file again lists the station locations and the *mask.cat* the individual local horizon and coordinate masks.

Precise information on the observing modes, frequency and receiver setup, recording modes and more can be found in the catalogs regarding the observation modes (Vandenberg, 1997).

With this background information, the user can now define the needed parameters concerning the desired schedule, like observing mode, date, duration and participating stations. Furthermore, there are many parameters concerning the stations, like the maximum slew distance, the minimum elevation and concerning the observations to possible sources, for instance the minimum number of stations observing one source simultaneously or the minimum scan duration, that can be specified. Fortunately, there are available templates, which contain the common settings for several types of VLBI sessions, including 24 h sessions and Intensive sessions (Schartner, 2021). Therefore, the user can load a certain template in VieSched++, adjust the settings and run the program to generate the desired schedules. These templates are also used in this particular study. More information on the used scheduling, simulation and analysis parameters for the determination of the individual results in this study can be found in tables in the corresponding chapters 4 and 5.

As already mentioned in section 2.1.2, for the generation of an optimal schedule, optimization criteria are introduced. In the following, some of the most important ones implemented in the scheduling software VieSched++ are listed:

For example, the *duration* of a scan is believed to be one of the essential criteria. The main idea is that shorter scans are better than longer scans, as more observations are possible in the same amount of time. Therefore, fast slewing antennas with higher recording rates and sensitivities are needed. This immediately shows how important it is to consider the different antenna attributes in the process of scheduling which include, for example, slewing speeds, recording rates and antenna sensitivities. The visibility areas per station are accounted for using so-called local horizon masks, which show the limitation of the observable section of the sky. Another important issue are the cable links between the turning parts of a telescope and the fixed ground parts. Therefore, the telescope is limited in the azimuth rotation, making it sometimes necessary to carry out longer movements preventing the elements from over-twisting. In the VLBI community, this problem is referred to as cable wrap (Nothnagel, 2019b).

The *sky coverage* criterion describes how evenly the observed sources are distributed over the sky. Usually, one aims for a high sky coverage as it is beneficial for the estimation of the tropospheric delay, which is considered being the major error source in VLBI observations. Therefore, especially low elevation observations are necessary and telescopes have to slew longer distances between scans to achieve this, leading to fewer time to observe.

Another essential optimization criterion is the *number of observations*. Having a large number of observations increases the redundancy, which usually improves the accuracy of the derived geodetic parameters. In comparison to achieving high sky coverage, it is necessary to keep the slew distances low to get many observations.

Additionally, also the *idle time*, which is the time where a telescope is inactive, can be used as an optimization criterion. Besides that, additional parameters can help optimizing a schedule. For example, introducing a criterion that increases a particular station's weight if it participated in fewer observations than the average. This is also possible for baselines where the number of observations per baseline is analyzed.

In practice, a combination of these criteria is used to generate the optimal schedule. In the case of Intensive sessions, the *number of observations* and *idle time* are usually not used in the process since normally all stations participate in the individual scans. The most critical parameters in the process of finding the optimal schedule are the weight factors of the *duration* and *sky coverage*, which control the impact of an individual parameter (see equation 2.5). Using the multi-scheduling tool implemented in VieSched++, it is possible to automatically vary these weight factors, like it has been done in the course of this study and compare the generated schedules to find the best one (Schartner and Böhm, 2019a).

Since in total, almost 1.3 million schedules are generated in the course of this study, a short MATLAB script is implemented with the scope to adjust the given template semi-automatically and to run VieSched++. The user can specify the type of session by selecting the corresponding template, the date and time of the session, the session duration and the participating stations. More importantly for this study is that it is possible to define a certain period of time and cadence when schedules should be generated, e.g., creating daily schedules over one year. In addition, by defining a list of stations and a number of stations per session, the MATLAB script generates all possible and unambiguous network constellations per session date. For every specified session date and possible station network, an adjusted template is now delivered to VieSched++, where it is processed automatically.

The scheduling output is saved and normally contains the following files, where *x* is a placeholder for the corresponding session name:

- *x.skd*: observation file which is sent to the participating stations
- *x.txt*: operation notes, include interesting statistics and information
- *x.vex*: observation file used by the correlator
- *x_initializer.txt*: information about the session
- *x_iteration_#.txt*: log file of every possible iteration #
- *statistics.csv*: contains a large number of statistics and information, e.g. number of stations, sources and scans to certain sources, observation, slew and idle times of all stations and much more

If the multi-scheduling tool is used and a variety of optimization criteria is selected, an accordingly large number of output file versions is generated. Simulations are now used to find the optimal schedule by making the accuracy (assessed by the mean formal error and the repeatabilities) of the parameters of interest accessible and, therefore, the schedules comparable.

3.2.2. Simulation

With the help of the Monte Carlo simulation tool implemented in VieSched++, the generated schedules can be simulated using a standard least-square adjustment. Therefore, as already mentioned in chapter 2.1.5, it is necessary to specify certain parameters, including the number of simulations (commonly set to 1000) and different quantities per station, which help to simulate possible error sources to ensure realistic results. These include the specification of the

- *white noise* (standard deviation of gaussian distributed noise in $[ps]$),
- *clock ASD* (Allan standard deviation of clock accuracy in $[ps]$),
- *clock duration* (time of minimum of *clock ASD* in $[min]$),
- *tropo* C_n (tropospheric turbulence parameter in $[10^{-7}m^{-1/3}]$),
- *tropo H* (tropospheric scale height in $[m]$),
- *tropo dh* (tropospheric height increment in $[m]$),
- *tropo dhseg* (tropospheric time increment in $[h]$),
- *tropo wzd0* (additional constant zenith wet delay in $[mm]$),
- *tropo ve* (wind velocity towards eastern direction in $[m/s]$) and
- *tropo vn* (wind velocity towards northern direction in $[m/s]$).

These parameters are also based on the freely available templates, just like the scheduling parameters used in this study. The desired performance information of the parameter of interest is accessible via the mean formal error *mfe* and repeatability *rep*. The *mfe* is defined as the mean value of the square root of the corresponding diagonal elements of the inverse normal equation matrix, multiplied by the a posteriori variance factor (see equation 2.9). To calculate the *rep* value of a parameter v, in general, a large number of simulations is necessary.

More precisely, it is defined as the standard deviation of the estimated values of the individual simulations i, see equation 3.1 (Schartner and Böhm, 2019a), where the parameter N represents the total number of simulations and $\bar{v}$ the mean value of v.

$$rep_v = \sqrt{\frac{1}{N-1}\sum_{i=1}^{N}(v_i - \bar{v})^2} \tag{3.1}$$

In general, the output of the simulation contains the *x_simulator.txt* files with a summary of the selected settings and further information on the *mfe* and *rep* values. Again, if multi-scheduling is used, many of these files are generated and saved with the corresponding version number. Within the *simulation_summary.txt*, all results of the different versions are combined in one lucid file, which contains the version number, the number of observations as well as again the *mfe* and *rep* value of *dUT1*. However, also the *statistics.csv* file is updated and now also contains information of the simulation process. It is therefore possible to get all information on the scheduling and simulation process from one file.

3.2.3. Analysis

Additionally, it is necessary to define the parameters concerning the analysis. In the case of Intensive sessions, a linear clock is estimated and one is usually only interested in one of the EOPs, which is *dUT1*. Furthermore, a piecewise linear zenith wet delay per station is derived. The estimation interval [h], as well as a constraint [mas] for the parameters, can be specified by the user.

In the following chapters, 4 and 5, the experiment setups and the different scheduling approaches of the two investigations, which include different station networks (VGOS, VLBA and an artificial global network), are described in more detail. Since the network-based investigations have the same motivation and the method is comparable, the two experiments are summarized in chapter 4, whereas chapter 5 concerns the global investigations.

4. Network-based investigation

This chapter is completely dedicated to the experiments concerning existing networks since similar investigations are performed. Starting with the individual experiment setup, precise information on the scheduling and simulation process as well as the results and discussion of the findings are topics of this part. The following list again summarizes the targets of these experiments, which included

- the determination of the optimal two and three station network among the individual stations and therefore the analysis of the baseline geometry and length,
- the investigation of the impact of adding another station as well as increasing the session duration up to four hours and
- the analysis of the influence of different scan durations (10s, 20, 30s) and recording concepts (one recorder with 4 Gbps or two recorders with double data rate) concerning only the VGOS network.

4.1. Experiment setup

Regarding this particular study, when talking about the **VGOS network**, the following nine stations are meant (see figure 4.1). The commonly used two letter station name can be found in the brackets and will be used from now on. Since one of the main goals is to find the optimal single baseline Intensive session and the best three station network, in total, 36 unambiguous constellations of two and 84 of three station networks are formed and investigated.

- GGAO12M (Gs, USA)
- ISHIOKA (Is, Japan)
- KOKEE12M (K2, USA)
- MACGO12M (Mg, USA)
- ONSA13NE (Oe, Sweden)
- ONSA13SW (Ow, Sweden)
- RAEGYEB (Yj, Portugal)
- WESTFORD (Wf, USA)
- WETTZ13S (Ws, Germany)

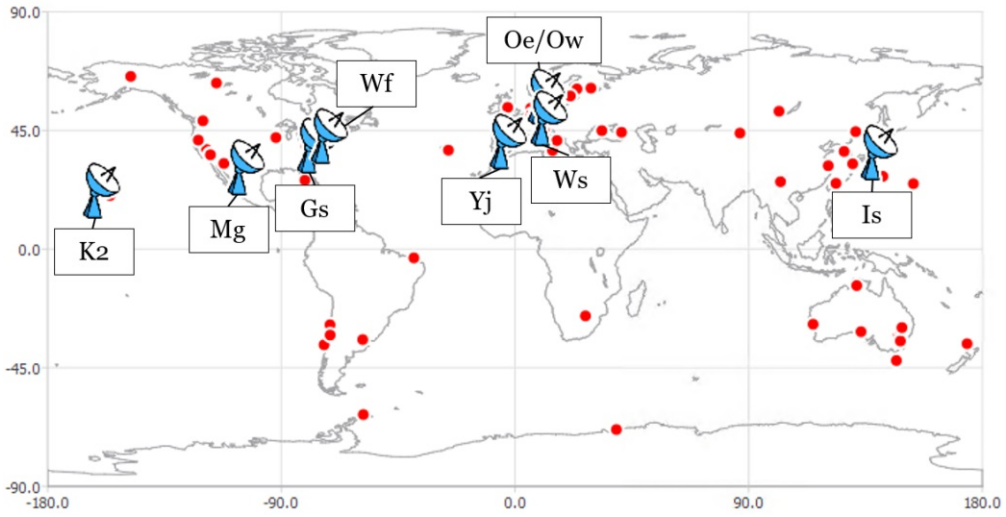

Figure 4.1: A map of the VGOS station network, where *red circles* represent all existing VLBI stations and the *telescope markers* the selected nine VGOS stations, figure from VieSched++.

The longest possible single baseline length measures approximately 10 688 km between K2 and Yj within this network of nine stations. The network with the smallest extension by far includes the twin telescopes Oe and Ow with 75 m followed by the baseline between Gs and Wf with 600 km. More information on the baseline lengths of all possible station networks can be found in table A.1.

The **VLBA network** consists of the following ten antennas, which are all located in the USA. Concerning only VLBA-Stations, there are 45 unambiguous two and 120 three station networks possible.

- Saint Croix (Sc, Virgin Islands)
- Hancock (Hn, New Hampshire)
- North Liberty (Nl, Iowa)
- Fort Davis (Fd, Texas)
- Los Alamos (La, New Mexico)
- Pie Town (Pt, New Mexico)
- Kitt Peak (Kp, Arizona)
- Owens Valley (Ov, California)
- Brewster (Br, Washington)
- Mauna Kea (Mk, Hawaii)

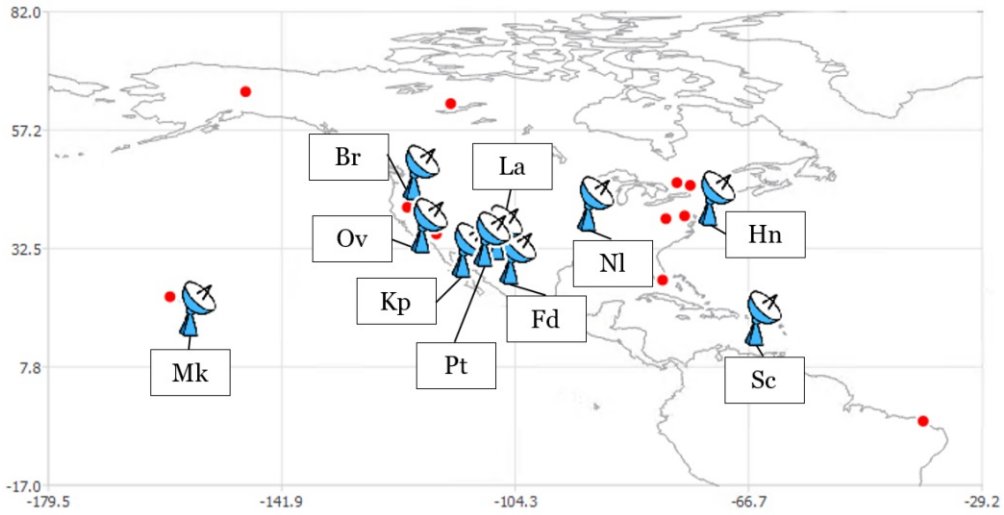

Figure 4.2: A map of the VLBA station network, where *red circles* represent all existing VLBI stations and the *telescope markers* the selected VLBA stations, figure from VieSched++.

The longest VLBA baseline can be formed between Mk and Sc with a total length of approximately 8611 km and the shortest one is between Pt and La with only 236 km. For more information, see table A.3.

4.2. Scheduling and Simulation

As already mentioned in chapter 3, the schedules and simulation results are semi-automatically created based on the user input and the selected template. The most critical parameters concerning both VLBI networks are listed in the following three tables, where the first table 4.1 shows only the parameters included in the scheduling process, the second table 4.2 contains the simulation and the last table 4.3 the analysis quantities and values. Daily schedules are simulated over one year with different session durations (one to four hours) for unambiguous two and three station networks.

Table 4.1: Scheduling parameters for VieSched++.

Scheduling parameters		
parameter	VGOS	VLBA
minimum scan duration [s]	30	20
fixed scan duration [s]	30	-
minimum elevation [deg]	5	
focus corner cadence [s]	600-900	
minimum time between scans to same source [s]	1060-1680	
sky coverage weight factor w_{sky}	- or 0-0.3	
duration weight factor w_{dur}	0-1	

Table 4.2: Simulation parameters for VieSched++.

Simulation parameter		
parameter	VGOS	VLBA
white noise per station [ps]	2.83	17.68
clock ASD [ps]	1	
tropo Cn [$10^{-7}m^{-1/3}$]	1.8	
tropo H [m]	2000	

Table 4.3: Analysis parameters for VieSched++.

Analysis parameter		
parameter	VGOS	VLBA
dUT1 interval [h]	6	
dUT1 constraint [mas]	0.0001	
pwl zenith wet delay interval [h]	1	
pwl zenith wet delay constraint [cm]	1.5	
linear clock	true	
quadratic clock	false	

Scheduling approaches

Since there are many possible ways to generate an optimal schedule using VieSched++ (see section 2.1.2), some of the parameters concerning the scheduling and the simulation, especially the weight factors w, are varied (see table 4.1).

One way to schedule an Intensive session is by using the approach suggested by Uunila et al. (2012) which is implemented in the used software. The idea of the first and second approach is to focus on observations at the corner of the mutually visible sky. Whether a source is located in the corners of the mutually visible sky, can be determined by the elevation angles of the telescopes. When two stations are observing a geodetic source positioned above the midpoint of the baseline, both antennas are oriented nearly straight towards the sky, resulting in a high mean elevation angle. If a source is in the cusps of the visible sky, the antennas need to observe at really low elevations, leading to a low mean elevation angle. Therefore, it is easy to determine if a source is located at the corners. Within VieSched++, this scheduling algorithm works as follows: after a certain time, which is also called the focus corner cadence, see table 4.4), the likelihood of scheduling a scan observing a source at the corners of the mutually visible sky increases by a factor of 1000 Since it is nevertheless always better to observe a brighter source located further away from the corners than a really faint source in the best position, this approach is beneficial as no force is applied in the scheduling processing by using strict rules. In between these corner observations, the scans are scheduled following the standard geodetic scan selection procedure (Schartner and Böhm, 2019b) (Schartner et al., 2021). As can be seen from table 4.4 the focus corner cadence is set to 600 s in the case of the first and 900 s for the second approach.

In addition, the minimum time between two scans to the same source is chosen to be 1680 s. As already mentioned in section 2.1.2, the multi-scheduling tool implemented in VieSched++ can be used to automatically vary the weight factors of, e.g., the sky coverage, duration and number of observations. In this case, eleven sky coverage weight factors between 0 and 0.3 are selected.

The third approach is the standard scheduling procedure, used to schedule Intensive sessions. No explicit corner observations are introduced and the time between two scans to the same source is slightly decreased. However, the multi-scheduling tool is again used to vary not only the sky coverage weight factor w_{sky} between 0 and 1 but also the duration weight factor w_{dur}.

This leads to overall three different scheduling approaches/ versions, which are summarized in the following table 4.4.

Table 4.4: Different scheduling approaches concerning the VGOS and VLBA network.

	Scheduling approaches				
version	focus corner cadence [s]	minimum time between scans [s]	w_{sky}	w_{dur}	number of possible schedules per session
1	900	1680	0-0.3	-	11
2	600	1680	0-0.3	-	11
3	-	1060	0-1	0-1	21

Regarding the first and second approach, eleven different schedules are generated in each case due to the variation of the sky coverage weight factor. Within the classical approach, both the sky coverage and the duration weight factor are altered, leading to twenty-one possible combinations. This leads to the situation, that per session/ day, in total, 43 schedules are generated. This demonstrates, that a lot of work is put into the scheduling process to find the optimal schedule for each simulated Intensive session. Again, a short MATLAB script is generated to identify the best schedule per day out of the 43 available alternatives. This has been executed by determining a total score per scheduled session based on the following quantities:

- the number of observations n_{obs},
- the average sky coverage sky_{cov},
- the simulated mean formal error of dUT1 mfe_{dUT1} [μs] and
- the simulated repeatability of dUT1 rep_{dUT1} [μs].

Before the individual score is calculated, possible outlier-schedules have been detected and eliminated using the 25 % or the 75 % quantile of the corresponding quantity. Concerning the n_{obs} and sky_{cov} the 25 % quantile is determined from all possible schedules and used as a threshold to remove outlier-sessions. For mfe_{dUT1} and rep_{dUT1} the 75 % quantile is derived. Since one aims to get a schedule with a high n_{obs} and sky_{cov} but low mfe_{dUT1} and rep_{dUT1} values, outlier-sessions are defined to have an n_{obs} and sky_{cov} value bigger than the corresponding 25 % quantile and a mfe_{dUT1} and rep_{dUT1} lower than the corresponding 75 % quantile.

If one of these queries is satisfied, the corresponding score for this parameter and the current session is directly set to zero. For the rest of the values of each quantity a score between the corresponding quantile and the minimum - concerning the mfe_{dUT1} and rep_{dUT1} - or maximum value - for n_{obs} and sky_{cov} - is derived using a linear interpolation. Hereby, values of zero to one are assigned, where a score of one is the best.

Hence, in the end the individual scores per parameter are available and one total score per schedule is calculated using the following weighting:

$$score_{total} = 0.7 \cdot n_{obs} + 0.5 \cdot sky_{cov} + 1 \cdot mfe_{dUT1} + 1 \cdot rep_{dUT1} \tag{4.1}$$

The simulated session per day with the highest total score is selected and further investigated. The result of this step is a list of optimal daily schedules per two and three station networks as well as for the different examined session durations over one whole year.

To compare the different network constellations and session durations, first of all, the individual baseline lengths per station network have been derived using the position of the stations. Now, the 3D baseline length bl_{3D} as well as the length of the baseline projected onto the equatorial plane bl_{2D}, which gives an idea of the baseline extension in east-west direction, are calculated for all two station networks, see equations 4.2 and 4.3.

$$bl_{3D} = \sqrt{(x_2 - x_1)^2 + (y_2 - y_1)^2 + (z_2 - z_1)^2} \tag{4.2}$$

$$bl_{2D} = \sqrt{(x_2 - x_1)^2 + (y_2 - y_1)^2} \tag{4.3}$$

Furthermore, the mean values $\overline{mfe}_{dUT1}$ and $\overline{rep}_{dUT1}$ are calculated over the whole investigation period of one year as well as the standard deviations σ_{mfe} and σ_{rep}. These values are used in further investigations concerning the individual network and session duration constellations of the VGOS and VLBA network. Since Baver and Gipson (2018) investigated seasonal variations of the UT1 formal error throughout one year, the computation of the mean value has been essential to neglect this phenomenon to a certain extent.

Table 4.5 summarizes the used approaches and analyzed constellations in the course of this investigation as well as the total number of generated schedules and simulations, where #sched_app represents the number of used scheduling approaches and #stat the number of stations per session.

Table 4.5: Total number of generated schedules using VieSched++ concerning the network-based investigation.

Number of generated schedules						
network	#sched_app	time period	cadence	#stat	durations	total
VGOS	3	1 year	daily	2-3	1-4h	525 600
VLBA	3	1 year	daily	2-3	1-4h	722 700
					In total:	1 248 300

4.3. Results and discussion

In the following section, the results of the two network-based investigations are shown and discussed. To avoid confusion, two separate subsections are introduced, which are identically structured concerning the content. First, the results regarding the two station networks with variable session duration are represented and discussed. In the case of the VGOS network, a short additional experiment concerning the scan duration and recording strategy is attached. This part is then followed by the findings on the three station networks.

4.3.1. VGOS network

Two station network, one to four hours durations

We start with the results from the most common Intensive session setup and one hour session duration including two participating stations, which are displayed using a bar chart in figure 4.3a. All of the following results are shown using the same scale to ensure the comparability of the different experiments. The bars represent the $\overline{mfe}_{dUT1}$ (top) or $\overline{rep}_{dUT1}$ (bottom) value of the individual baselines which can be found on the x-axis. Here, the commonly used two letter codes of the stations are used. The networks are displayed in the order of ascending $\overline{mfe}_{dUT1}$ values in both subplots so that the corresponding mean values of one network can be found easily. Furthermore, the black error bars show the σ_{mfe} and σ_{rep} values. Since one is interested in determining *dUT1* with high precision, the y-axis is limited to 20 or 40 μs. For networks that lead to mean values higher than the selected threshold, the corresponding result is written inside the corresponding blue bar. From now on, for the sake of simplicity the mean values $\overline{mfe}_{dUT1}$ and $\overline{rep_{dUT1}}$ are written as just mfe_{dUT1} and rep_{dUT1}, unless it is stated otherwise.

In the case of the VGOS network, 36 unambiguous two station networks are possible and plotted for every investigated session duration below. Independent of the duration of the simulated Intensive session, among the best baselines are Gs-Is, Is-Wf and Is-Yj concerning the mfe_{dUT1} as well as the rep_{dUT1}. For comparison, the simulation results of the currently and commonly observed VGOS-2 Intensive sessions between K2 and Ws are highlighted in red.

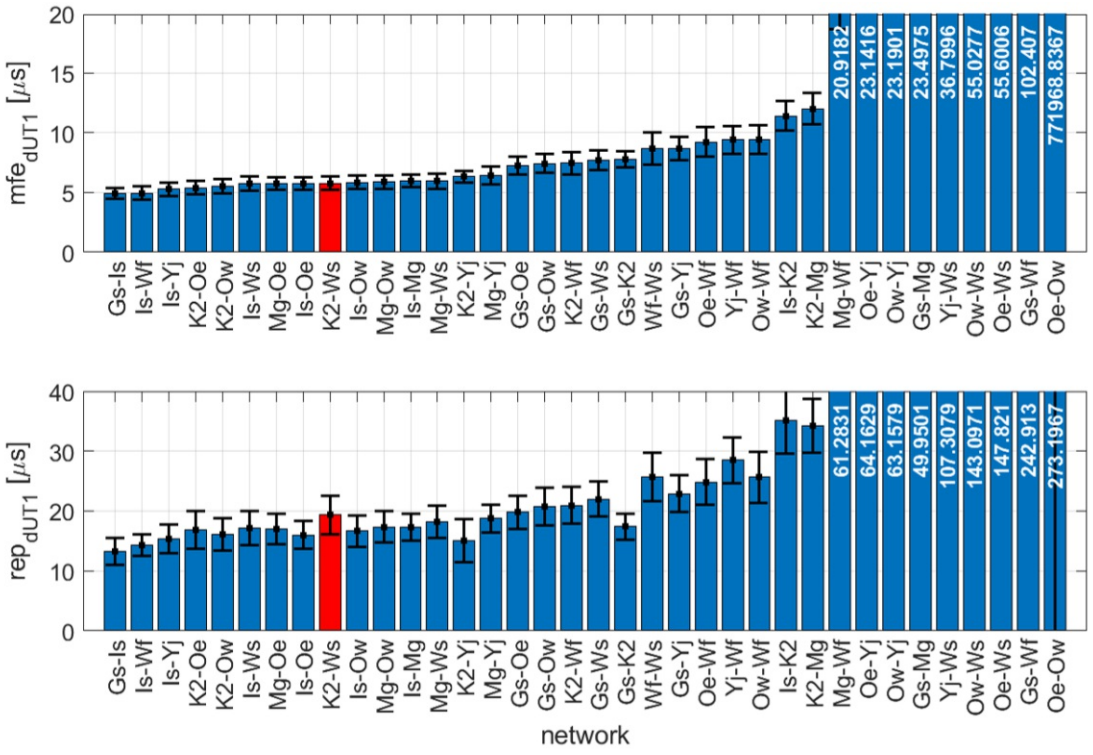

Figure 4.3a: Results of VGOS two station Intensive sessions with one hour duration. The commonly observed Intensive session VGOS-2 (K2-Ws) is highlighted in red.

Comparing the results shown in figure 4.3a with the results concerning two station networks with session durations from two to four hours below (see figures 4.3b, 4.3c and 4.3d), one can see that there are in general only minor differences detectable. However, the three mentioned single baselines are again at the head of the listing. Although, now the optimal baseline is not Gs-Is but Is-Wf. Since the differences between these two single baselines are small, one can conclude that both the Gs-Is and the Is-Wf station network provide the best performance concerning the determination of *dUT1* in this particular case.

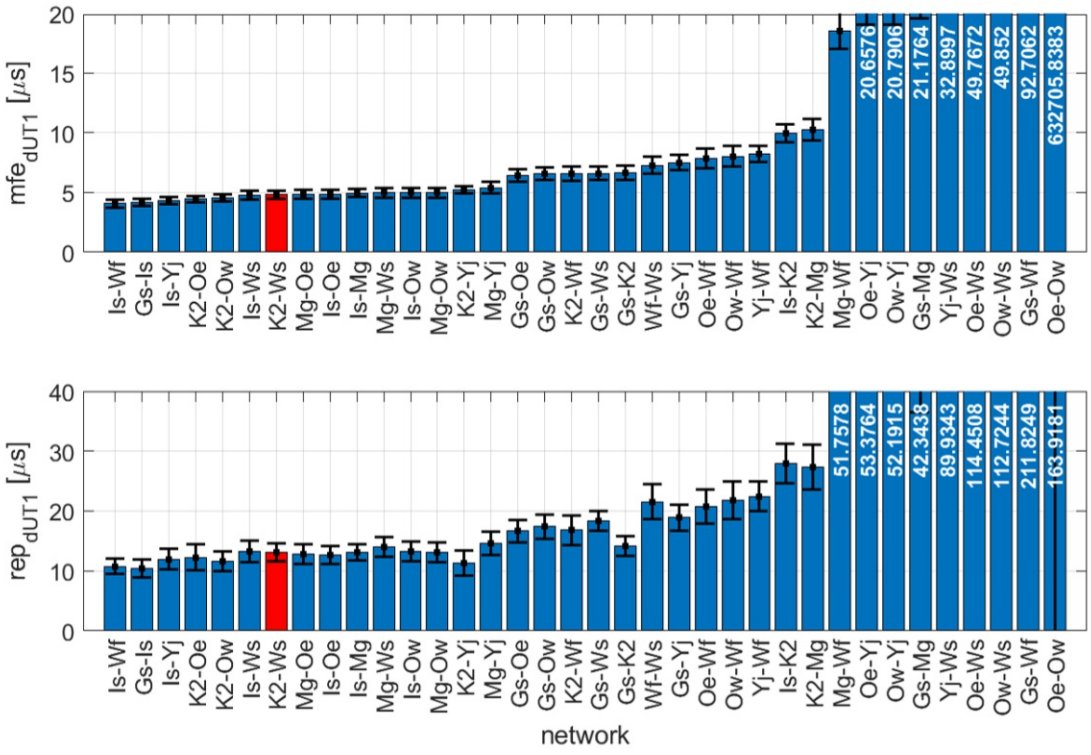

Figure 4.3b: Results of VGOS two station Intensive sessions with two hour duration.

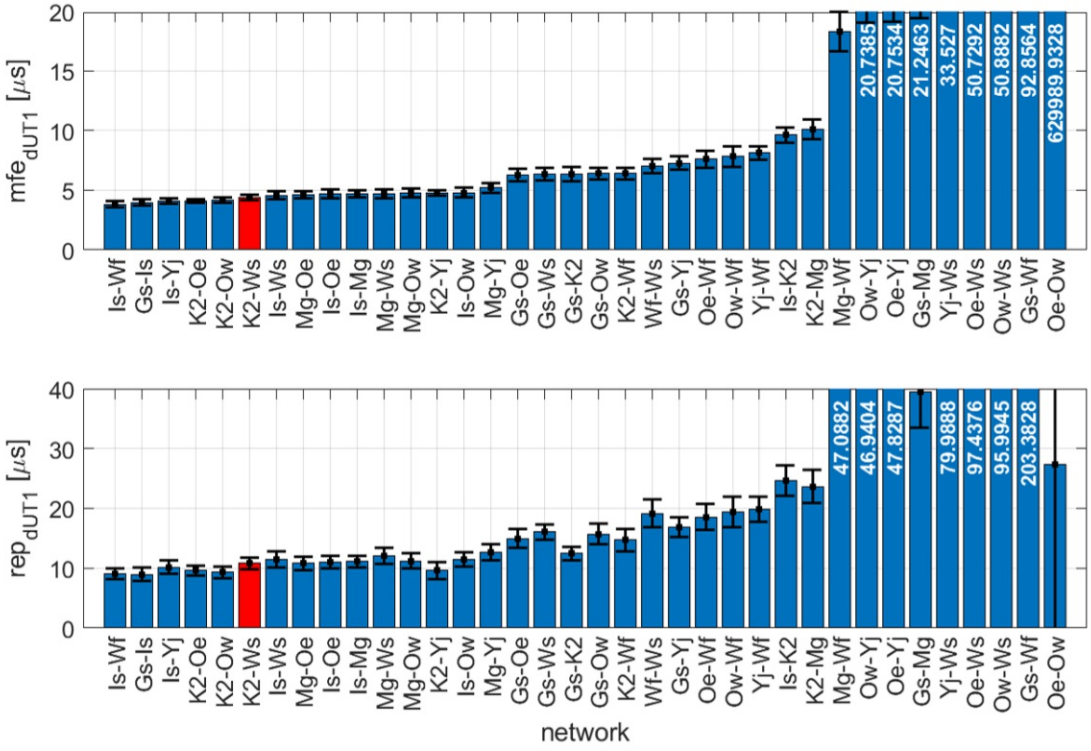

Figure 4.3c: Results of VGOS two station Intensive sessions with three hour duration.

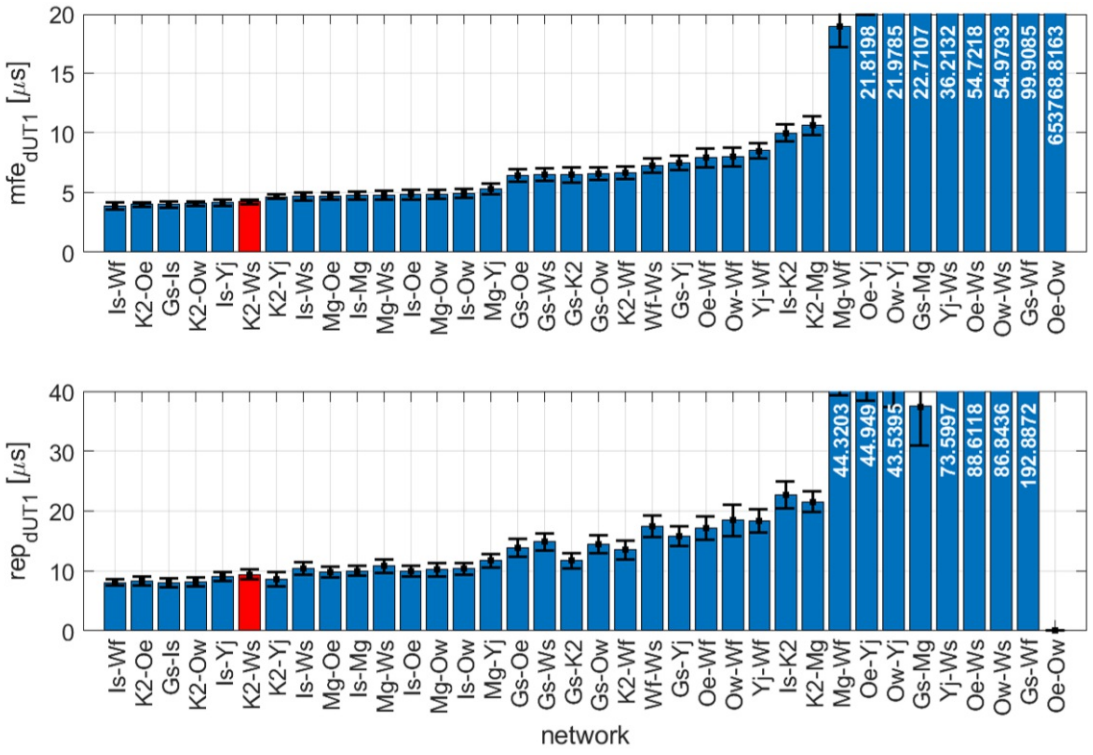

Figure 4.3d: Results of VGOS two station Intensive sessions with four hour duration.

In the following table 4.6 again, the two best single baselines are listed, including more precise information on the simulated accuracy parameters as well as on the baseline length, which include the bl_{3D} and the bl_{2D} in [km]. Additionally, the results concerning the Intensive sessions VGOS-2 (see section 2.2.1) between K2 and Ws are displayed for comparison. A similar but complete list including all examined VGOS single baselines for one hour duration can be found in section A.2.

Table 4.6: This table includes the best single baseline Intensive sessions between VGOS stations for different session durations given in [h], which are Is-Wf and Gs-Is. Furthermore, the results concerning the regularly observed VGOS Intensive session (VGOS-2, see section 2.2.1) between K2-Ws is listed for comparison. bl_{3D} and bl_{2D} are displayed in [km] and the statistical values in [μs].

VGOS two station networks (1-4h)							
network	bl_{3D}	bl_{2D}	dur	mfe_{dUT1}	σ_{mfe}	rep_{dUT1}	σ_{rep}
Is - Wf	9495	9480	1	4.96	0.58	14.28	1.78
			2	4.07	0.36	10.78	1.28
			3	3.83	0.29	9.04	0.91
			4	3.85	0.31	8.09	0.59
Gs - Is	9594	9590	1	4.94	0.45	13.28	2.25
			2	4.18	0.31	10.43	1.46
			3	3.98	0.26	8.97	1.10
			4	4.01	0.27	8.05	0.76
K2 - Ws	10358	10072	1	5.78	0.54	19.33	3.15
			2	4.81	0.31	13.10	1.46
			3	4.39	0.21	10.80	0.96
			4	4.24	0.19	9.42	0.80

Concerning the influence of different session durations, there is a slight improvement regarding the achieved performance with increasing session duration. In the following figure 4.4, again, the mean values and standard deviations of the mfe_{dUT1} and the rep_{dUT1} of the best single baseline Is-Wf is shown. A plot including also the Gs-Is baseline and further also the results from the best three station network can be found in figure 4.9.

In general, the following findings on the impact of the session duration are acquired, analyzing the simulated accuracy values and their standard deviations concerning all 36 possible VGOS two station networks. Increasing the session duration from one to two hours leads to an improvement of the mfe_{dUT1} by 14 %, rep_{dUT1} by 21 % and both σ values by approximately 34 % on average. By extending the session, the performance does not improve further, as can be seen in figure 4.4. The mfe_{dUT1} slightly decreases by 3 %, whereas the rep_{dUT1} by 15 %. Both standard deviations decrease as well (by 12 and 24 %).

Sessions with a duration of four hours did not perform much better in comparison to three hour sessions. To be more precise, even a slight deterioration in the mfe_{dUT1} and the corresponding σ value (by 3 and 2 %) are detectable. However, the rep_{dUT1} is still improving (by 11 and 14 %). A reason for this behaviour could be the modeling of the troposphere, however this investigation is not part of this study.

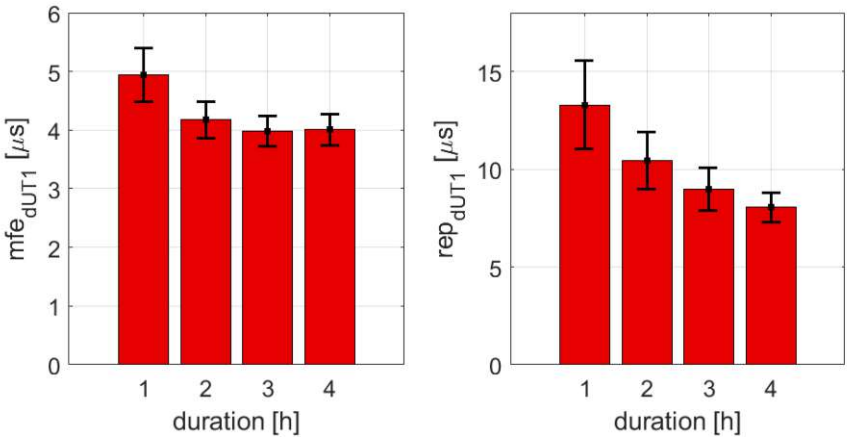

Figure 4.4: A comparison of the best two station network between the VGOS stations Is and Wf concerning different session durations. On the left the mfe_{dUT1} and on the right the rep_{dUT1} is shown.

Comparing the achieved values for one hour with two, three and four hours duration, in sum, the overall biggest improvement can be achieved by increasing the session duration from one to three or four hours. Concerning the mfe_{dUT1} an extension of the session duration to three/four hours leads to an improvement of approximately 17 /14 % and considering the rep_{dUT1} it leads to a better performance by 32 /38 %.

In general, the simulated baselines Is-Wf and Gs-Is provide a good performance concerning the determination of dUT1. Besides the low mfe_{dUT1} and rep_{dUT1} values for both networks, also the standard deviations, displaying the variability of the accuracy values, are small. This shows that the performance of these single baselines can be assumed to be rather stable throughout the year. The baseline between K2 and Ws is among the good networks, but it is not the best one, although it forms the second longest possible baseline with an extension of 10 358 km after the K2-Yj network with 10 688 km. In general, what can be seen from table A.1 is, that against all expectations, the longest baselines do not provide the best simulated performances. This can be explained by the highly restricted commonly visible sky regarding very long baselines and the, therefore, highly restricted source selection/ availability. Figure 4.5 displays the baseline lengths with the corresponding achieved mfe_{dUT1} values. Plotting the baseline lengths against the rep_{dUT1} values shows the same behavior and is therefore not shown here.

Optimal single baseline sessions do not include baselines with an extension of more than 10 000 km, to be more precise, the optimal length would be at around 9500 km concerning the selected VGOS stations. Furthermore, also the σ values decrease with increasing baseline extension. Again, the plot is limited to values <20 μs, which means that formal errors exceeding this threshold are set to 20 μs and no errorbar is shown.

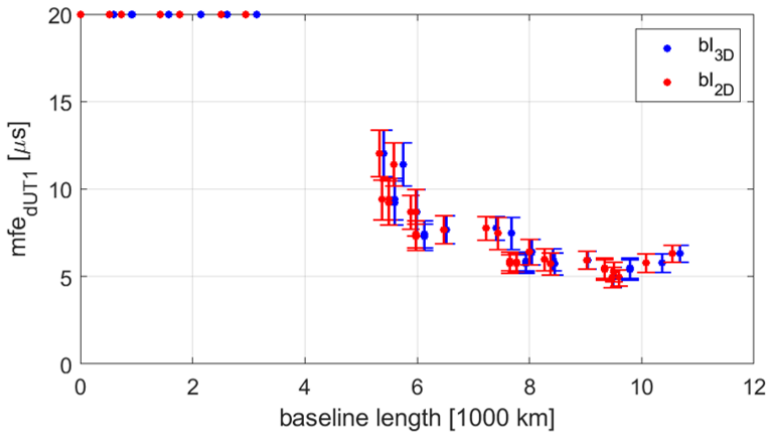

Figure 4.5: The different baseline lengths of all possible two VGOS station networks plotted against the corresponding mfe_{dUT1}. bl_{3D} represents the three-dimensional baseline length, whereas bl_{2D} is the length of the baseline projected onto the equatorial plane.

Furthermore, the network geometries of the two best single baselines Gs-Is (green) and Is-Wf (orange) are plotted in figure 4.6, showing that both of them have a large east-west extension as it is common for Intensive sessions.

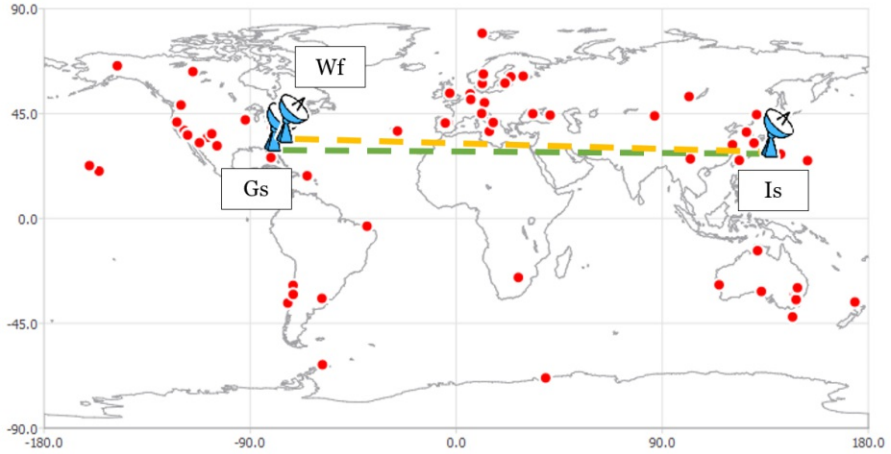

Figure 4.6: A map of the best VGOS station network geometries concerning two stations. The baseline Is-Wf is displayed in orange and the baseline Gs-Is in green.

Different scan durations and recording strategies

Besides the different tested session durations and network constellations for VGOS stations, additional simulations are carried out, including variable scan durations and recording strategies. Concerning VGOS sessions, a fixed scan duration of 30 s is commonly selected, as it has also been done for this particular investigation to ensure a high SNR. In this study, additional schedules with 10 s and 20 s scan and one to four hour session durations are simulated for the two station networks Gs-Is and Is-Wf. Moreover, different recording speeds have been tested. Since for Intensive sessions, normally two recorders with 4 Gbps each are used (resulting in 8 Gbps total), 24 h sessions are performed with only one. This condition is implemented by introducing a minimum slew time (10 , 20 or 30 s) to simulate the different recording rates. The following figure 4.7 shows the results of this experiment for the baseline Gs-Is. The findings concerning the Is-Wf baseline show the same behavior.

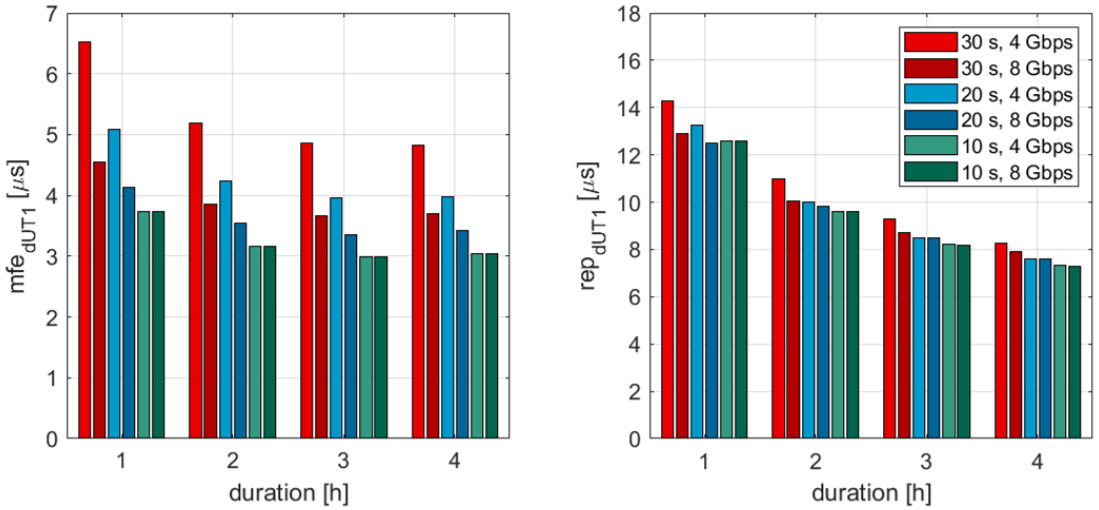

Figure 4.7: The impact of different scan durations 30, 20 and 10s and different recording rates 8 and 4 Gbps on the mfe_{dUT1} (left) and rep_{dUT1} (right) concerning the best single baseline session between the VGOS stations Gs and Is.

Theoretically, the performance can be further improved by decreasing the fixed scan duration. Just by using a scan duration of 20 instead of 30 s, the mfe_{dUT1} can be decreased by approximately 20 % concerning the 4 Gbps recording rate and by 8 % concerning the commonly used 8 Gbps rate. Further reducing the scan duration to 10s results in mfe_{dUT1} values, which are 25 % (4 Gbps) and 10 % (8 Gbps) better than the results from 20 s scan duration schedules. When taking a look at the rep_{dUT1} values, the differences within the same session duration are not as big (around 2 - 5 % improvement between different scan durations with the same recording strategy). In general, when defining a very short scan duration of 10 s, the difference between the 4 and 8 Gbps recording mode is negligibly small.

Overall, again the best results can be achieved by using a session duration of three to four hours, in combination with a fixed scan duration of 10 s using the standard 8 Gbps recording mode. However, as already mentioned in 2.2.2, it needs to be considered, that a certain scan duration is necessary to reach a minimum *SNR*, which depends on the flux density of the observed source and the antennas' sensitivity. Furthermore, the possibility of non-detections arises. Since these effects are not considered in the simulation process, the results of this investigation have to be treated with caution.

Three station network, one to four hours duration

Due to the lack of space and for better clarity, only a few of the 84 three station network constellations are shown in the following figures. A table with the complete data set can be found in section A.2. The stations participating in the best two station networks can be found at the top of this listing. Gs-Is-Wf is without exception the best VGOS three station baseline independent of the session duration. As already mentioned in section 2.2.1, so-called VGOS-B Intensive sessions are observed between Is and the Onsala twin telescopes Oe and Ow. In this simulation study, these particular network does not provide the best performance. To be more precise, independent of the session duration it is always in the last third of this performance listing. However, for comparison reasons, it is included in the following plots displayed in red.

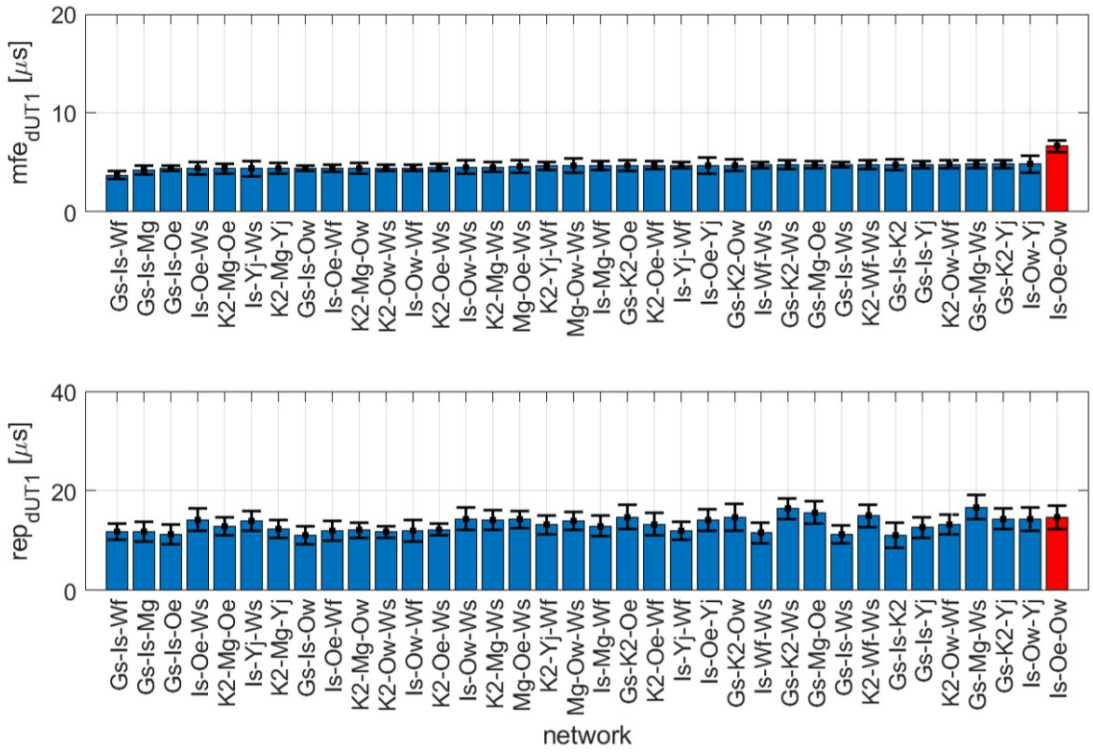

Figure 4.8a: Results of VGOS three station Intensive sessions with one hour duration. The commonly observed Intensive session VGOS-B (Is-Oe-Ow) is highlighted in red. Attention: Since this network is normally in the last third of this performance listing, it has been manually inserted at the end of the visible plot for comparison reasons.

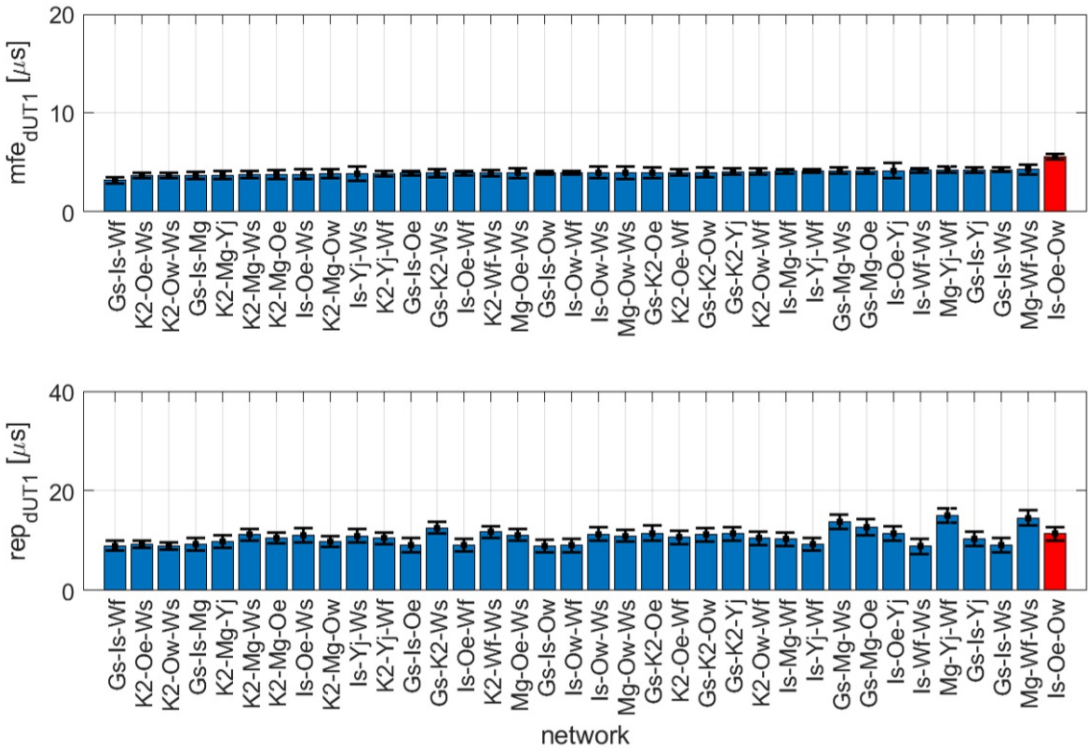

Figure 4.8b: Results of VGOS three station Intensive sessions with two hour duration.

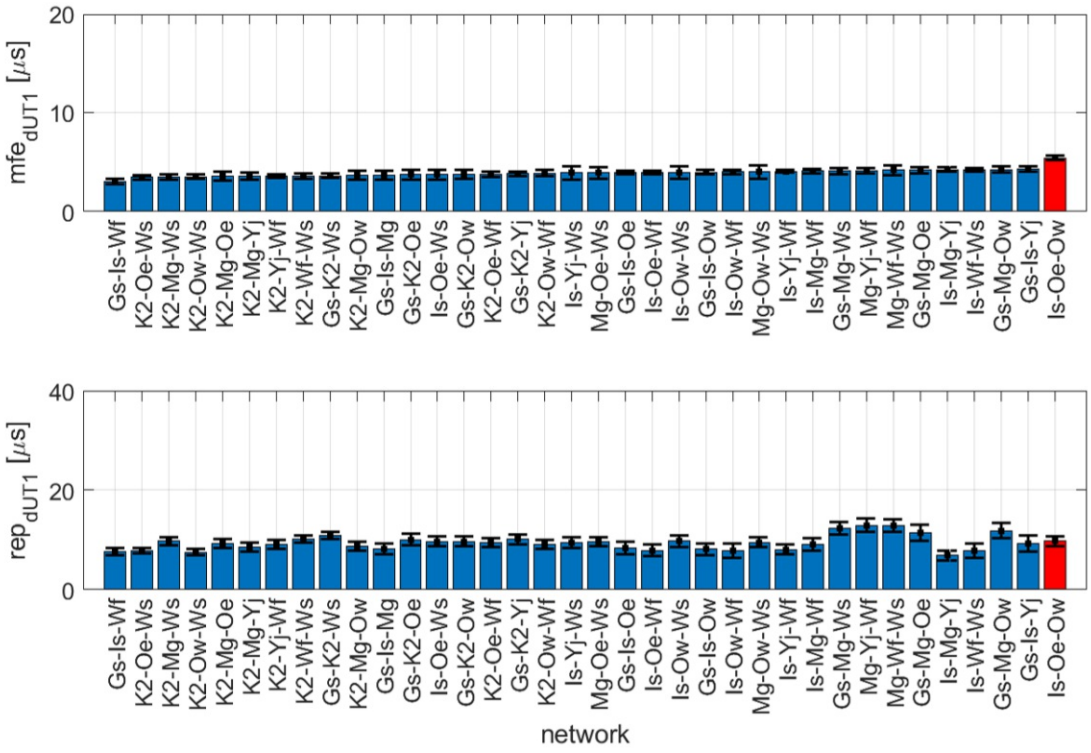

Figure 4.8c: Results of VGOS three station Intensive sessions with three hour duration.

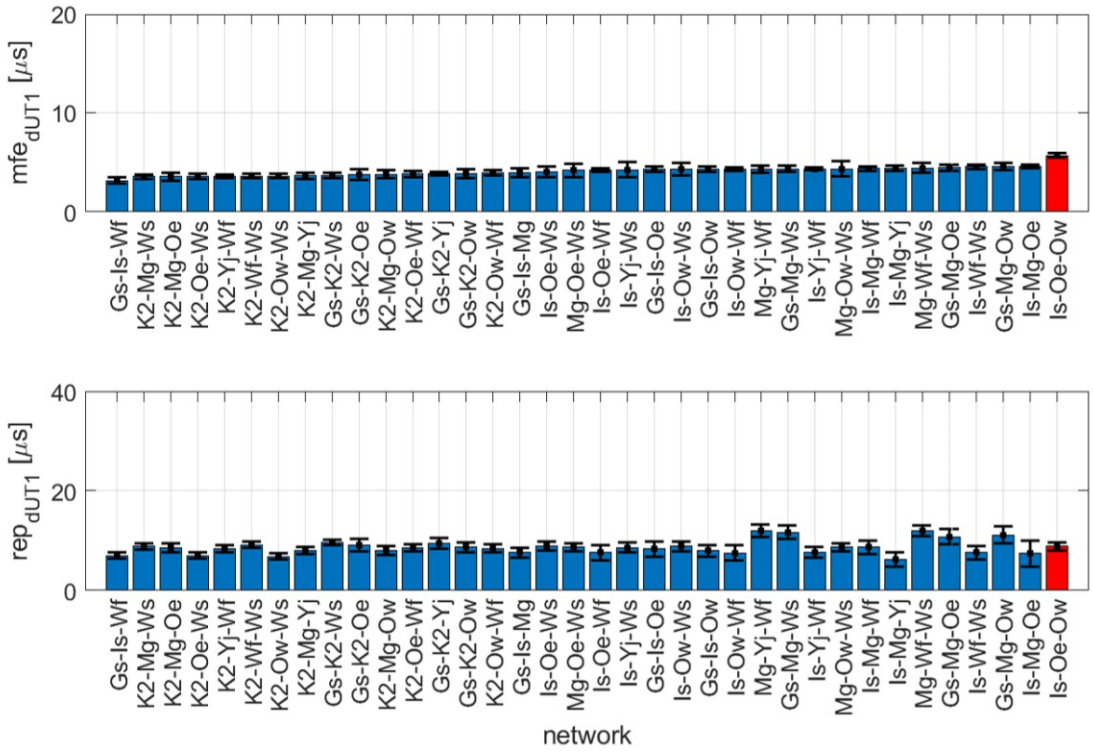

Figure 4.8d: Results of VGOS three station Intensive sessions with four hour duration.

Table 4.7 again lists the accuracy information of the best three station network Gs-Is-Wf per session duration and further contains the same information regarding the VGOS-B session.

Table 4.7: This table includes the best Intensive session between three VGOS stations for different session duration given in [h]. Furthermore, the results concerning the regularly observed VGOS Intensive session (VGOS-B, see section 2.2.1) between Is-Oe-Ow is listed for comparison. The statistical values are given in [μs] and the individual minimums per network are highlighted in green.

VGOS three station networks (1-4h)					
network	dur	mfe_{dUT1}	σ_{mfe}	rep_{dUT1}	σ_{rep}
Gs - Is - Wf	1	3.70	0.40	11.77	1.56
	2	3.20	0.31	8.96	0.98
	3	3.04	0.31	7.71	0.74
	4	3.15	0.34	6.97	0.60
Is - Oe - Ow	1	6.61	0.63	14.60	2.35
	2	5.57	0.30	11.39	1.39
	3	5.41	0.24	9.78	0.99
	4	5.67	0.24	8.83	0.87

Similar to the two station network investigation results, the best performance can be achieved by using three to four hour Intensive sessions. In the following figure 4.9 the results of the best two and three station networks are summarized. In general, it can be seen that by adding a third station to a single baseline Intensive session the performance improves. To quantify this, all two station networks are compared with the corresponding three station networks. Especially for very short baselines, like Oe-Ow, Oe-Ws or Yj-Ws, the improvement ranges from only a few % up to 100 %. However, to show the impact of adding another station to a two station Intensive session, both the 10 % quantile and the 90 % quantile are calculated. Due to the definition of these values, the resulting range includes 80 % of the values, excluding the very low and high values. Therefore, one can state that by introducing a third station to an existing one hour two station network, the mfe_{dUT1} can be improved in the majority of the cases by approximately 7 - 76 % and the rep_{dUT1} by 16 to 75 %. Surprisingly, this analysis also shows that the overall improvement concerning all possible station networks decreases when extending the session duration. This can be seen by the decreasing 10 % quantile values. For example, the same calculations but concerning four hour sessions lead to an improvement of the mfe_{dUT1} in 50 % of the cases only by −9 to 76 %, and the rep_{dUT1} by 2 to 73 %.

Concerning the optimal baselines, which are the Is-Wf and Gs-Is single baselines and the Gs-Is-Wf three station network, the introduction of a third station leads to an improvement of the mean formal error by 25/25 %, the corresponding standard deviation by 31/11 %, the repeatability by 18/11 % and the standard deviation by 12/30 %.

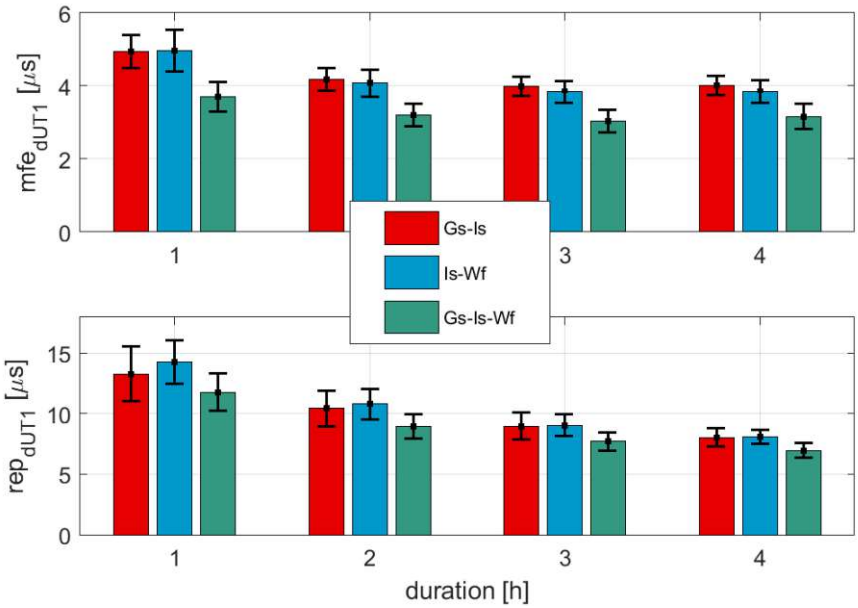

Figure 4.9: A comparison of the best two and three VGOS station networks, concerning the one to four hour investigations.

4.3.2. VLBA network

Two station network, one to four hours duration

Concerning the VLBA network, in total, 45 unambiguous two station networks are possible. As can be seen from the following figures 4.10a, 4.10b, 4.10c and 4.10d, the best single baseline independent of the session duration is Hn-Mk followed by Mk-Sc and Mk-Nl. Again, a commonly observed Intensive session is highlighted in red, which is, in this case, the USA Intensive session between Mk and Pt, see section 2.2.1.

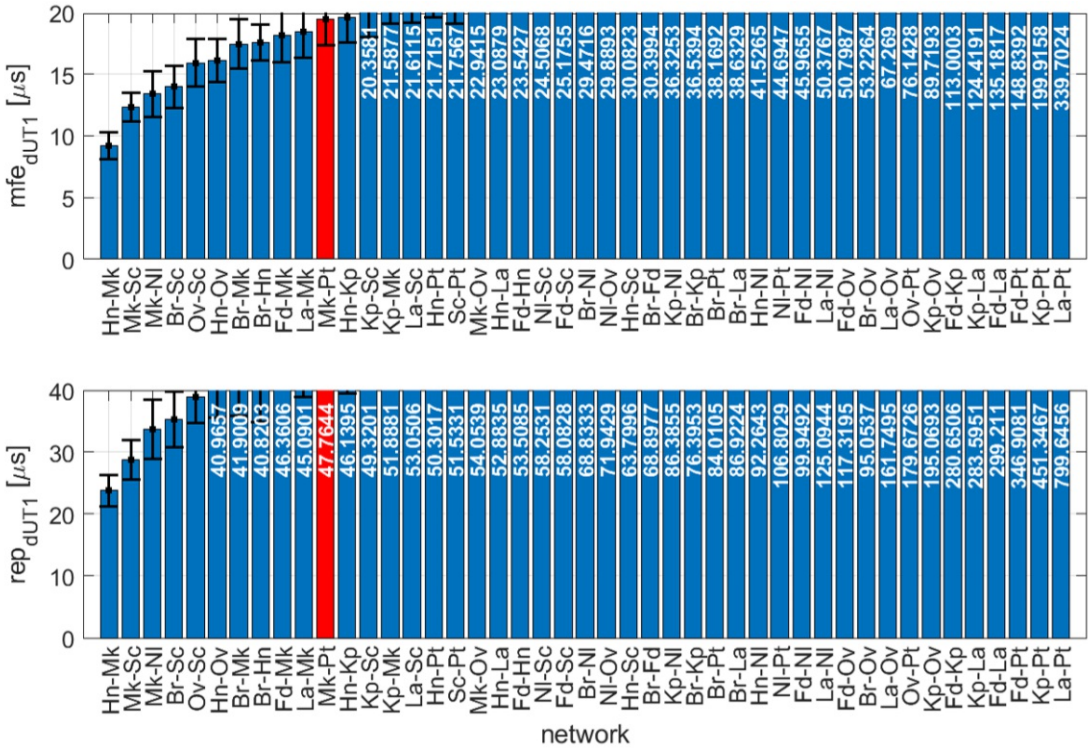

Figure 4.10a: Results of VLBA two station Intensive sessions with one hour duration. The commonly observed VLBA Intensive session (Mk-Pt) is highlighted in red.

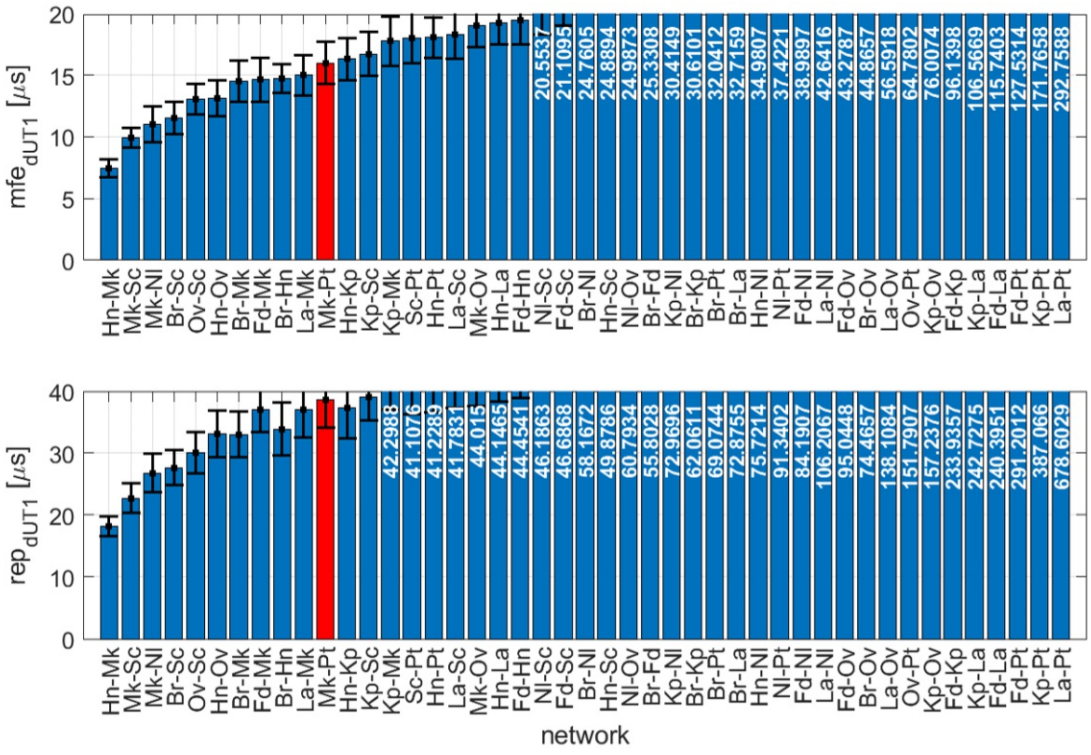

Figure 4.10b: Results of VLBA two station Intensive sessions with two hour duration.

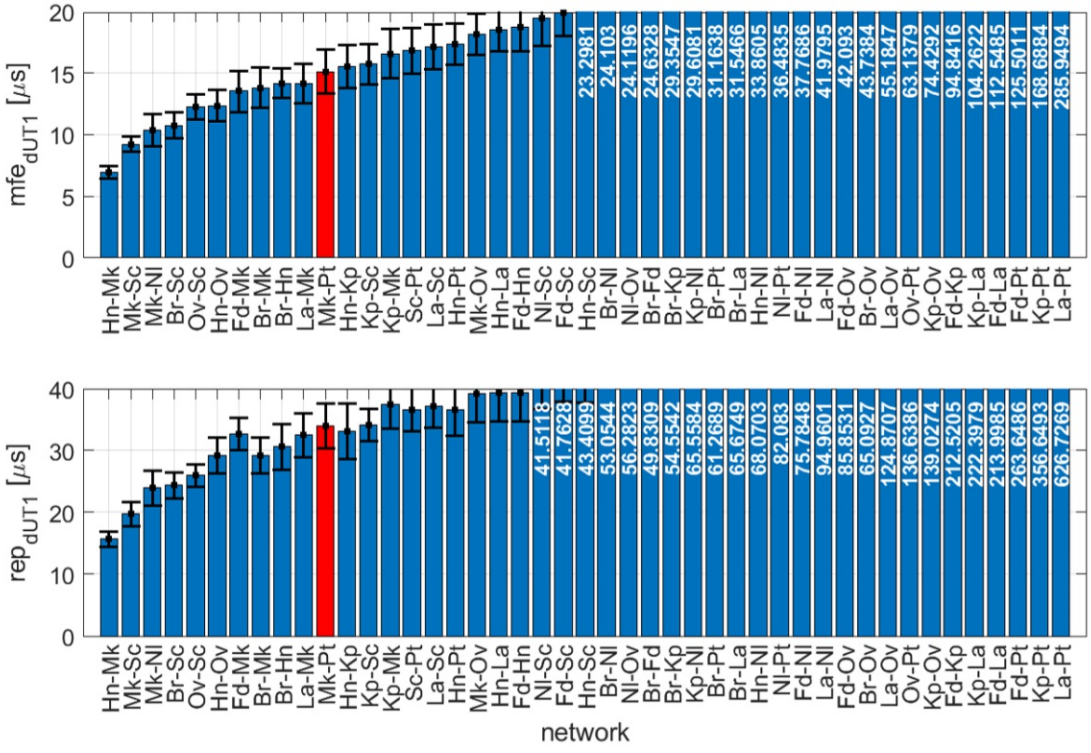

Figure 4.10c: Results of VLBA two station Intensive sessions with three hour duration.

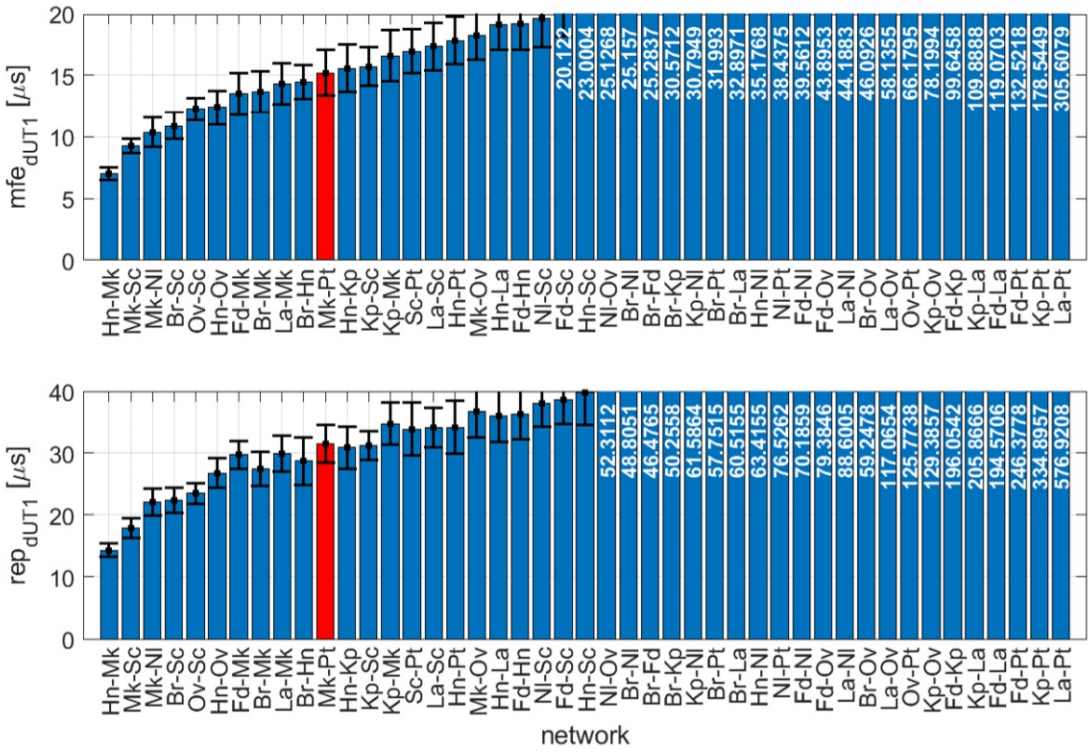

Figure 4.10d: Results of VLBA two station Intensive sessions with four hour duration.

For comparison, the best single baselines are listed in the following table 4.8. Also the simulation results of the actually observed VLBA Intensive session between Mk and Pt for the different session durations are displayed. Again, a complete list concerning all examined VLBA two station networks can be found in section A.2.

Due to the in general shorter baselines between 237 and 8611 km concerning VLBA networks and also the general characteristics of VLBA in comparison to VGOS telescopes (see section 2.1.7), the overall achieved performance is worse than for VGOS networks. Only a few sessions manage to stay below the 20 μs threshold, which has been specified since one is usually interested in high accuracy of *dUT1*. Comparing the best single baseline, Hn-Mk suggested in this study and the regularly observed VLBA Intensive session Mk-Pt, substantial differences can be found in the achieved accuracy values. They differ by a factor of approximately two to three, whereas the corresponding 3D baseline lengths deviate by almost 2700 km.

Table 4.8: This table includes the best single baseline Intensive sessions between VLBA stations for different session durations given in [h], which are Hn-Mk and Mk-Sc. Furthermore, the results concerning the regularly observed VLBA Intensive session (see section 2.2.1) between Mk and Pt is listed for comparison. bl_{3D} and bl_{2D} are displayed in [km] and the statistical values in [μs].

VLBA two station networks (1-4h)							
network	bl_{3D}	bl_{2D}	dur	mfe_{dUT1}	σ_{mfe}	rep_{dUT1}	σ_{rep}
Hn - Mk	7503	7181	1	9.21	1.08	23.77	2.56
			2	7.47	0.70	18.18	1.65
			3	6.95	0.53	15.67	1.25
			4	7.02	0.50	14.34	1.04
Mk - Sc	9594	9590	1	12.33	1.13	28.78	3.17
			2	9.90	0.80	22.75	2.38
			3	9.23	0.64	19.73	1.99
			4	9.24	0.58	17.92	1.63
Mk - Pt	4796	4579	1	19.48	2.16	47.76	6.50
			2	15.99	1.73	38.63	4.50
			3	15.13	1.75	33.94	3.64
			4	15.19	1.85	31.55	3.04

Again, with increasing session duration the performance of the individual session improves, as it can be seen in figure 4.11 illustrative for the best single baseline Hn-Mk.

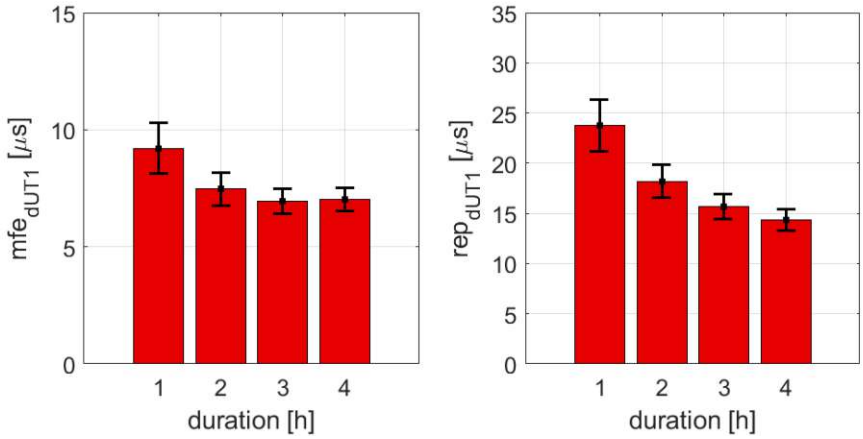

Figure 4.11: A comparison of the best two station network between the VLBA stations Hn and Mk concerning different session durations. On the left the mfe_{dUT1} and on the right the rep_{dUT1} is shown.

A doubling of the session duration from one to two hours leads to an improvement of mfe_{dUT1} by an average of 16 %, σ_{mfe} by 23 %, rep_{dUT1} by 18 %and σ_{rep} by 32 %. Further extending the session from two to three hours influences the values as follows: 4 and 3 % concerning the mfe_{dUT1} (mean value and standard deviation), and 11 and 18 % regarding the rep_{dUT1}. Again, increasing the duration up to four hours, only the rep_{dUT1} values further improve, whereas the mfe_{dUT1} values slightly deteriorate by 3 and 7 % compared to three hour sessions. These findings compared with the results achieved from the same analysis, including the VGOS stations, show a very similar outcome.

Also, for the VLBA network investigation, the overall biggest improvement is achieved by introducing a three or four hour sessions. Compared to the common one hour sessions, the statistical values used in this study can be enhanced by (three/four hours) 20/18 % and 27/33 %.

As already mentioned before, the baseline lengths in the case of VLBA Intensive networks are generally shorter than they are for VGOS stations, which is one reason why less baselines can determine *dUT1* with good accuracy. The following figure 4.12 shows the simulated mfe_{dUT1} plotted against the corresponding 3D and 2D length of the single baseline. Concerning the rep_{dUT1}, a similar relationship can be seen, which is the case why not both plots are displayed here.

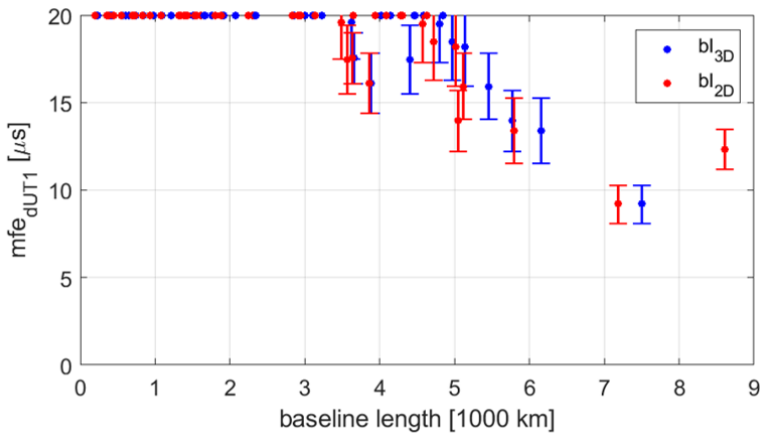

Figure 4.12: The different baseline lengths of all possible two VLBA station networks plotted against the corresponding mfe_{dUT1}. bl_{3D} represents the three-dimensional baseline length, whereas bl_{2D} is the length of the baseline projected onto the equatorial plane.

The network geometries of the two optimal VLBA single baselines, Hn-Mk and Mk-Sc, are displayed in figure 4.13. Against the expectations, which are common knowledge throughout the VLBI community, the shorter single baseline Hn-Mk with no perfect east-west alignment dominates over what is normally suggested to be the perfectly oriented and longer baseline Mk-Sc.

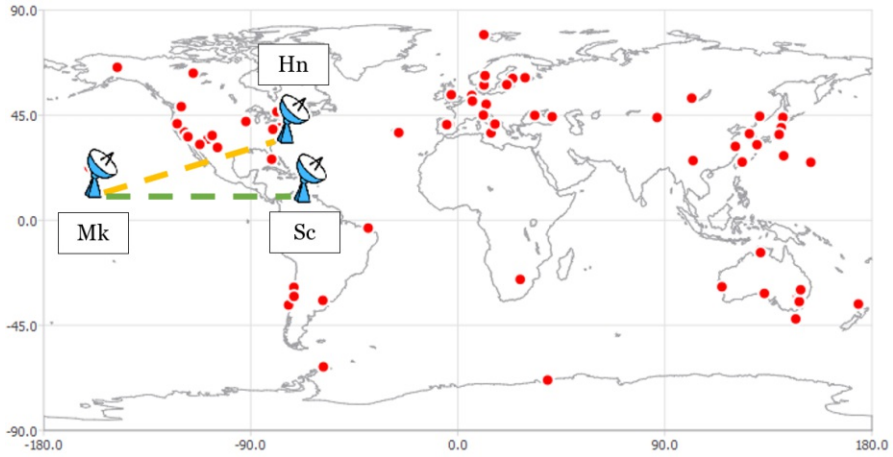

Figure 4.13: A map of the optimal VLBA station network geometries concerning two stations. The baseline Hn-Mk is displayed in orange and the baseline Mk-Sc in green.

Three station network, one to four hours duration

Since there are in total 120 possible three station constellations of VLBA stations, only a small amount can be shown in the following result figures 4.14a, 4.14b, 4.14c and 4.14d. A table with the whole data set can be found in the section A.2. The Fd-Hn-Mk network is the best three station network examined in this investigation concerning Intensive sessions with one hour duration. For longer session durations from two to four hours another three station network dominates, which is the Hn-Mk-Nl network. In Geiger et al. (2018), besides the two station VLBA Intensive session also a three station network Mk-Sc-Pt was mentioned to be observed in the future. In the following result plots this particular network is highlighted for comparison reasons.

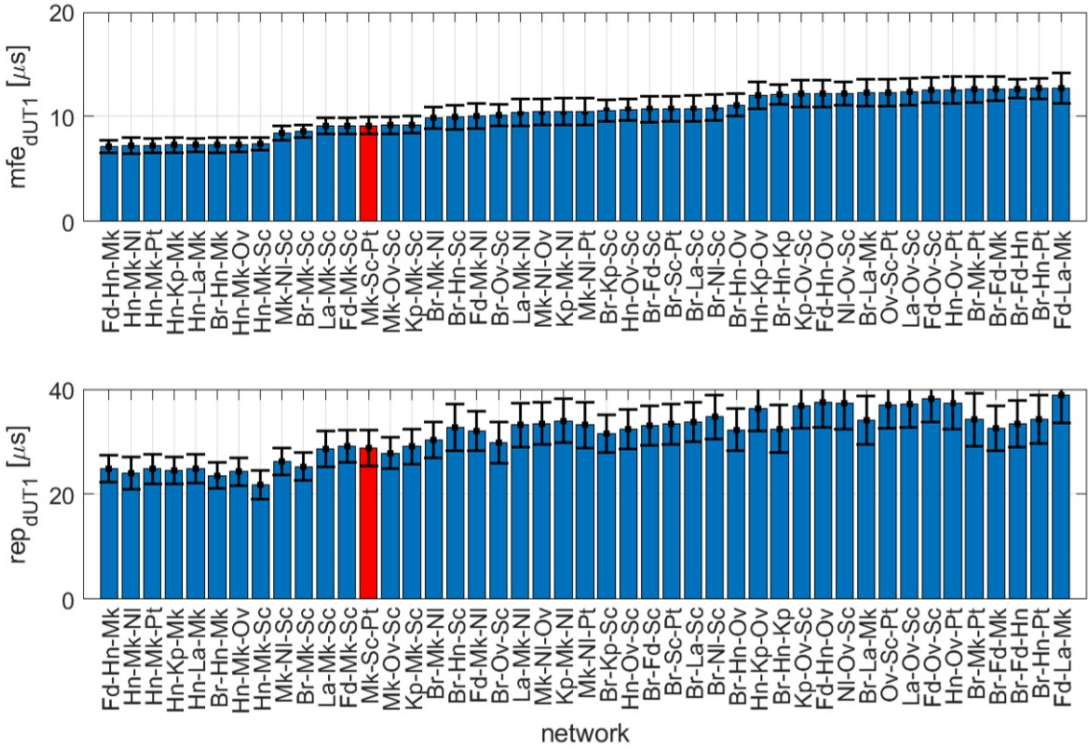

Figure 4.14a: Results of VLBA three station Intensive sessions with one hour duration. The simulation results of the Mk-Sc-Pt network are highlighted in red.

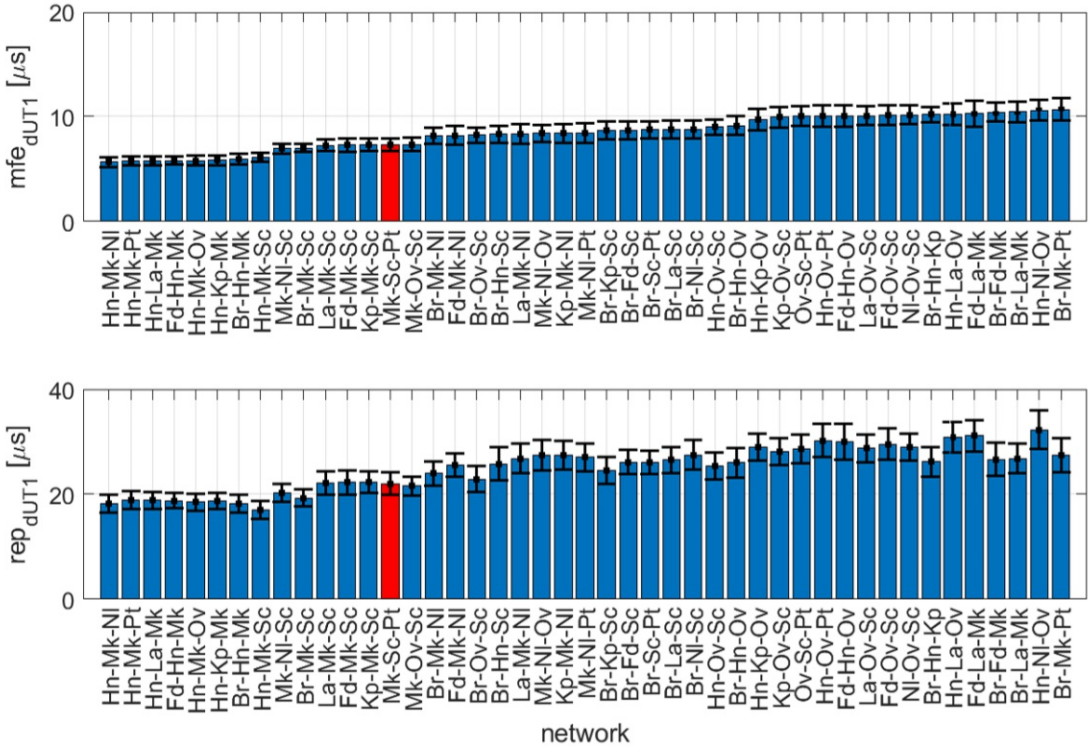

Figure 4.14b: Results of VLBA three station Intensive sessions with two hour duration.

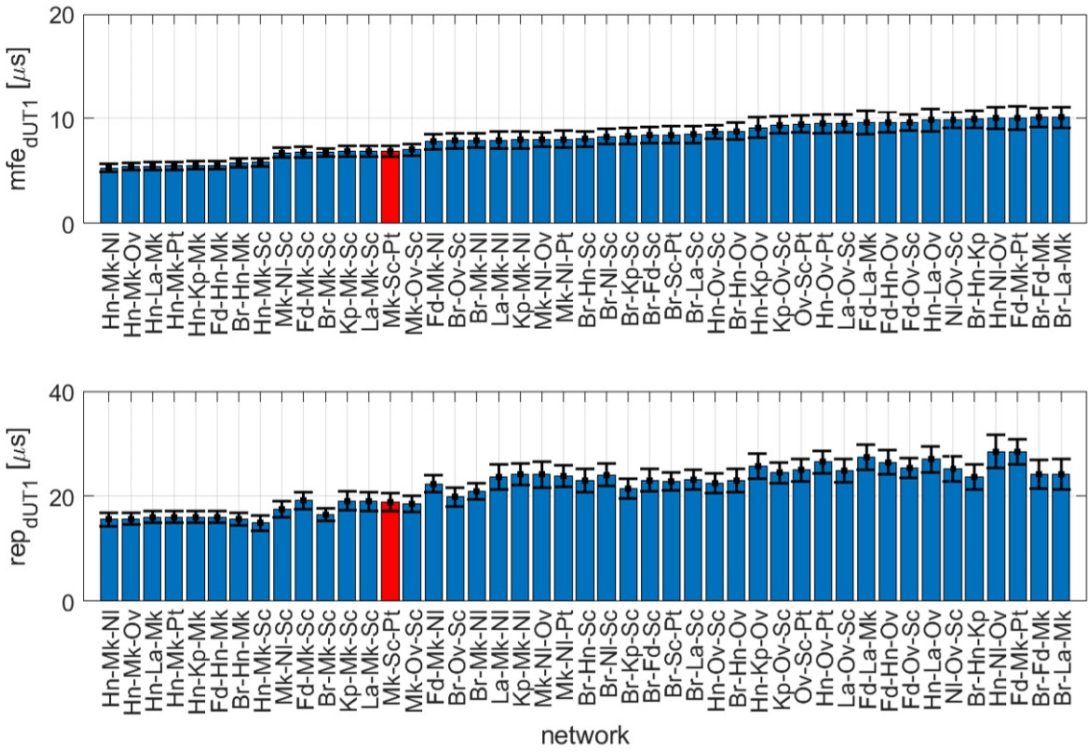

Figure 4.14c: Results of VLBA three station Intensive sessions with three hour duration.

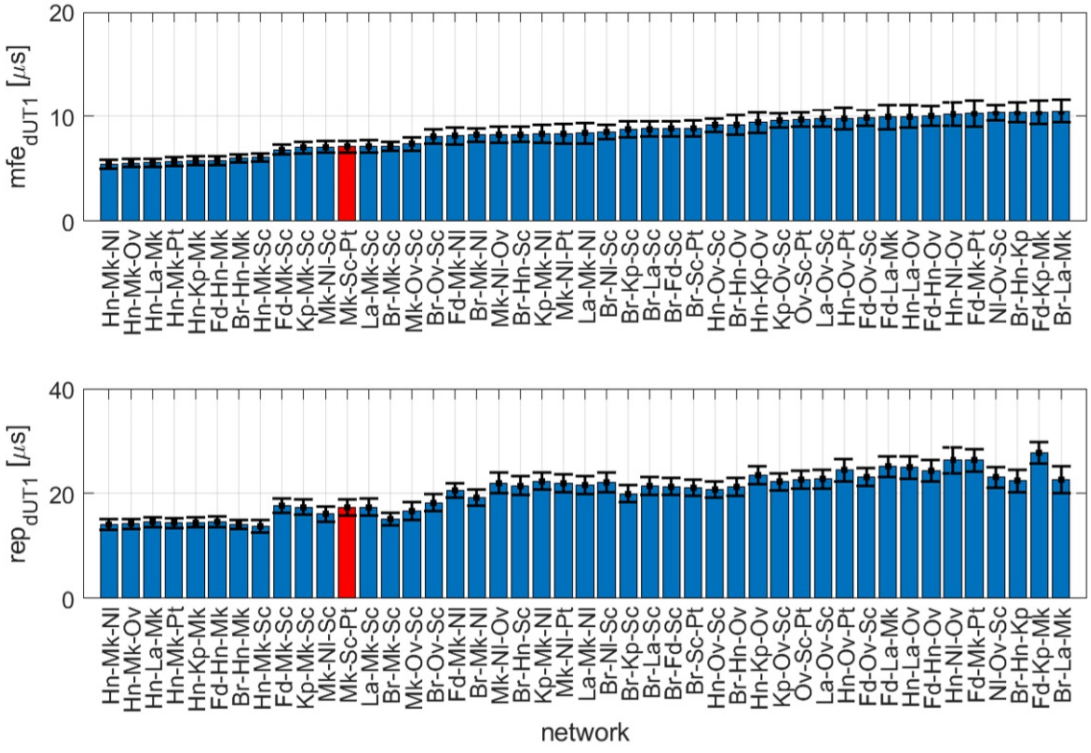

Figure 4.14d: Results of VLBA three station Intensive sessions with four hour duration.

The Mk-Sc-Pt network is among the best networks of 120 possible and unambiguous constellations concerning all examined session durations. However, there are even more perfect ones existing. In the following table, the simulation results of the two best three station sessions are displayed beside the ones from the Mk-Sc-Pt network.

Table 4.9: This table includes the best Intensive sessions between three VLBA stations for different session durations given in [h]. Furthermore, the results concerning the planned three station VLBA session between Mk, Sc and Pt (Geiger et al., 2018) are listed for comparison. The statistical values are given in [μs] and the individual minimums per network are highlighted in green.

VLBA three station networks (1-4h)					
network	dur	mfe_{dUT1}	σ_{mfe}	rep_{dUT1}	σ_{rep}
Fd - Hn - Mk	1	7.14	0.64	24.96	2.56
	2	5.79	0.39	18.79	1.52
	3	5.55	0.37	16.06	1.07
	4	5.77	0.43	14.63	0.97
Hn - Mk - Nl	1	7.24	0.74	23.99	3.02
	2	5.66	0.48	18.19	1.67
	3	5.30	0.35	15.56	1.21
	4	5.44	0.41	14.11	1.09
Mk - Sc - Pt	1	9.14	0.83	28.80	3.42
	2	7.31	0.61	22.02	2.15
	3	6.91	0.52	18.94	1.68
	4	7.10	0.57	17.40	1.52

Just like in all the other investigations in this chapter, the best results regarding the mfe_{dUT1} can be achieved by observing three hour long Intensive sessions, whereas the lowest rep_{dUT1} values can be examined when introducing four hour long sessions. This finding is true for all analyzed constellations.

To examine the effect of adding a third station to the different two station networks again, the improvement is quantified using the 10 % quantile and the 90 % quantile. By introducing a third station to a one hour long two station Intensive session, in the case of the majority of the sessions the mfe_{dUT1} decreases by 28 to 67 % and the rep_{dUT1} by 11 to 64 %. Compared to the same analysis concerning VGOS stations, with increasing session duration, the improvement realized by the additional observing station stagnates. That means that independent of the duration of the session, the improvement is approximately constant.

Concerning the best single baselines according to this study (see figure 4.15), which is Hn-Mk, the introduction of a third station leads to an improvement of the individual accuracy values by an average of 21 and 36 % concerning mfe_{dUT1} and for this particular baseline to no further improvement in the rep_{dUT1} and σ_{rep} values.

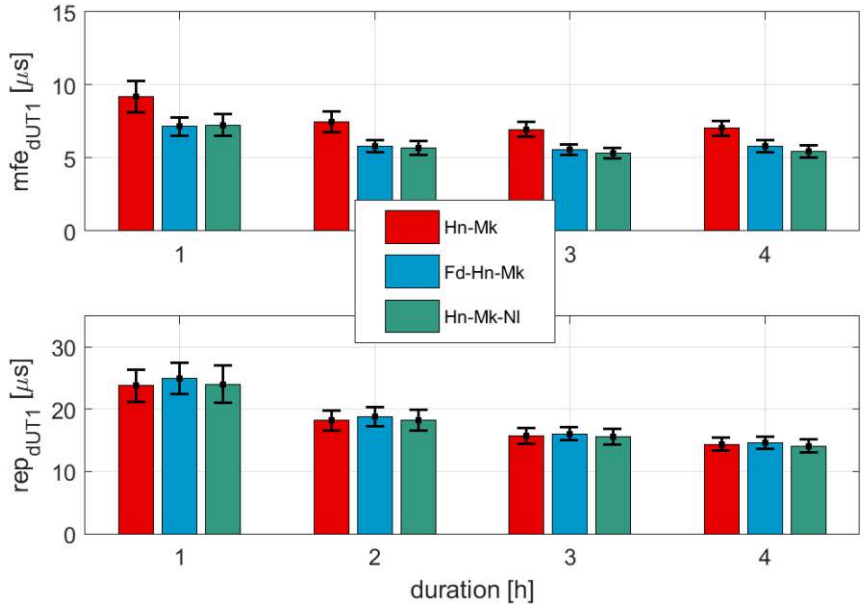

Figure 4.15: A comparison of the best two and three VLBA station networks, concerning the one to four hour investigations.

The network geometry of the optimal three station networks Fd-Hn-Mk and Hn-Mk-Nl can be seen in figure 4.16.

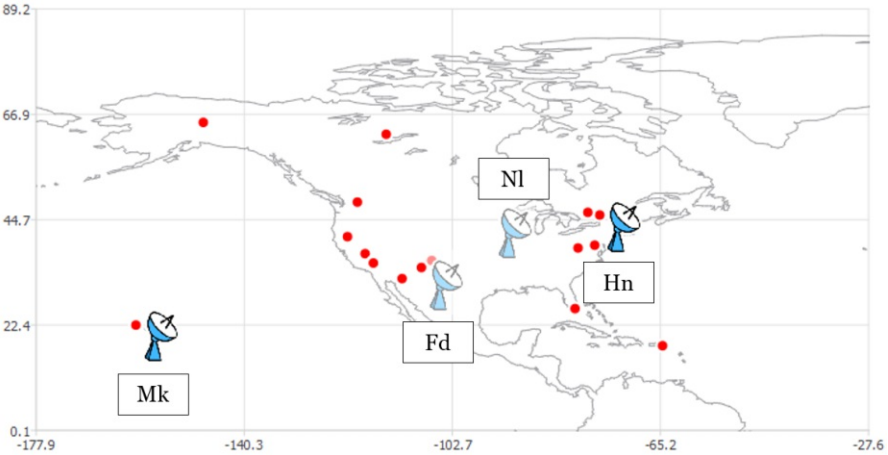

Figure 4.16: A map of the optimal VLBA station network geometries concerning three stations, which are Fd-Hn-Mk and Hn-Mk-Nl. Due to the lack of space the baselines are not marked as dotted line. The two stations (Fd and Nl) that vary between the two optimal three station baselines are displayed more transparently.

In the following final table 4.10 of this chapter, the best baselines regarding both the VGOS and VLBA network are summarized. For comparison, also the commonly observed baselines are displayed.

Table 4.10: Simulated optimal baselines concerning the VGOS and VLBA network compared with the commonly observed baselines.

Optimal baselines - a summary			
network	#stat	simulated	commonly observed
VGOS	2	Is-Wf / Gs-Is	K2-Ws
	3	Gs-Is-Wf	Is-Oe-Ow
VLBA	2	Hn-Mk	Mk-Pt
	3	Fd-Hn-Mk	Mk-Sc-Pt

5. Global investigation

The following chapter discusses the investigation concerning an artificial VLBI station network for the assessment of baselines for *dUT1* determination. The work carried out within this thesis was essential for the work published by Schartner et al. (2021). The study is based on catalogs that are used in VieSched++. Furthermore, again precise information on the scheduling and simulation can be found in the following as well as the results and the further analysis and discussion. The main target of this study is to question what is common knowledge throughout the VLBI community concerning the perfect network geometry for Intensive sessions by examining the impact of the station constellation and baseline length on the determination of *dUT1* on a global scale.

5.1. Experiment setup

To identify the optimal baseline geometry for Intensive sessions on a global-scale, artificial VLBI stations are introduced and placed on a regular 10° x 10° grid. This approach is based on Schartner et al. (2020) and can be realized by adjusting the catalogs with the information on the antennas and their position, which VieSched++ uses in the scheduling and simulation process. Concerning the antennas, they are all assumed to be identical and VGOS-type telescopes, with the same antenna properties as the WETTZ13S telescope in Germany. Before the needed catalogs are generated, the following considerations regarding the global grid are made:

Global Grid

Since baselines between stations located at latitudes higher than 80° would be relatively short and therefore irrelevant especially for Intensive sessions, the latitude (lat) - longitude (lon) grid is limited to a latitude range of −80° to 80°. Furthermore, based on a first approximation of a rotational symmetric Earth, it is sufficient for this study to set longitude limits additionally and decrease the number of investigated schedules.

In general, every baseline can be rotated about the z-axis so that one antenna is located on an arbitrary meridian and the other in the East. In the course of this study, the reference meridian is chosen to be the zero meridian. Hence, it is also considered sufficient to investigate baselines with a difference in longitude from 0° to 180°. This leads to in total 323 artificial stations (see figure 5.1). Short disclaimer: most of these artificial antenna positions would not be realizable in practice since many of them are placed in the middle of oceans. They are only investigated to show how the geometry of an Intensive session affects the performance and the precision of *dUT1* on a global scale.

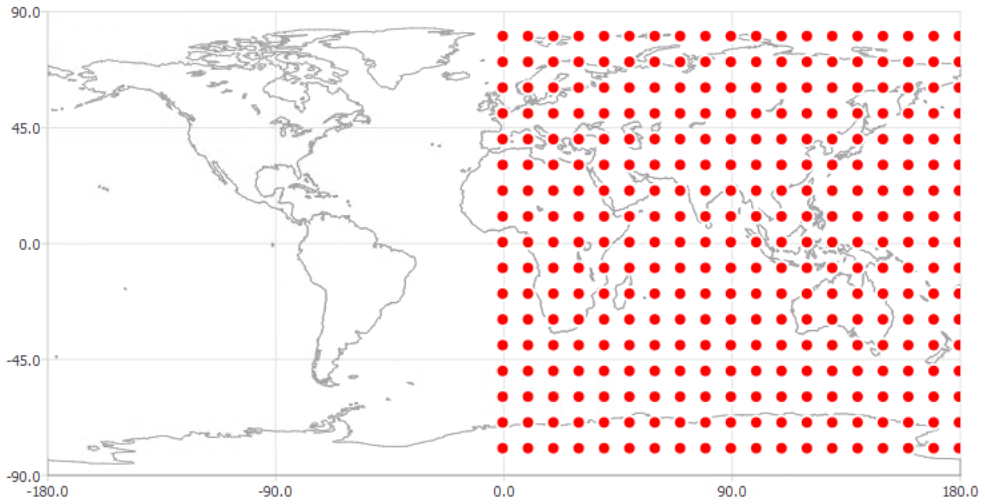

Figure 5.1: A map of the global artificial station network, where *red circles* represent the locations of the artificial VLBI antennas, figure from VieSched++.

The antennas located on the reference meridian are selected as reference stations, meaning that all investigated baselines are formed always between one reference station and one other artificial station. Since baselines including reference stations on the northern hemisphere can be seen as baselines including reference stations on the southern hemisphere mirrored at the equator, their performance is approximately identical. Therefore, only antennas at the reference meridian at $lat \geq 0$ are selected to be reference stations. In practice, this is not entirely true since other sources are available in the northern compared to the southern hemisphere. Furthermore, the sources, which can be observed in the southern hemisphere, are known to be less dense and have higher uncertainties (Charlot et al., 2020) (Plank et al., 2015).

The goal is to form all possible and unambiguous baselines between every reference station to any other artificial station and investigate the simulated performance of these two station networks. Since there are 322 possible baselines per reference station and in total nine of them, this leads to 2898 baselines, which are examined in this study.

Artificial Antenna

As already mentioned in the beginning of this section, to realize this artificial network, it is necessary to provide the needed information to VieSched++ via so-called catalogs. These *.cat* files contain information on the station network including the position and relevant antenna properties for the scheduling process. The currently used sked catalogs for the "real" VLBI station network are available on Github (NVI, 2021). In case of the artificial network, the following four catalogs (see table 5.1) have been generated based on the commonly used information for the VGOS telescope WETTZ13S, and inserted in VieSched++ to simulate the previously described network.

Table 5.1: This table provides an overview of the used scheduling catalogs in VieSched++ for the global investigation.

Scheduling catalogs - an overview	
Antenna information - *antenna.cat*	
station name/ ID	*LAxxxLOyyy*
axis	AZEL
axis offset [m]	0
axis limitations [°]	-90 and 450 / 6 and 90
axis slew rates [°/min]	720 and 360
diameter [m]	13.2
Station equipment - *equip.cat*	
SEFD [Jy]	1400 (X-band) and 1050 (S-band)
equipment/ recorder	MARK6
Station position - *position.cat*	
coordinates	X, Y, Z [m] and *lat*, *lon* [°]
Station horizon masks - *mask.cat*	
step function [°]	0, 5, 360

Horizon masks are defined as series of line segments or step functions to represent the horizon. Concerning the WETTZ13S antenna, the input is given as a step function, with the elevation value (5°) between the 0° and 360° azimuth angles where the elevation applies.

5.2. Scheduling and simulation

In total, 12 monthly schedules have been generated per baseline over one year, resulting in approximately 34800 simulated schedules, which are analyzed in this experiment. In comparison to the investigations carried out in chapter 4, only one scheduling approach is used and only one hour single baselines are analyzed. As already introduced in section 4.2, a scheduling algorithm, which is suggested by Uunila et al. (2012) is used with a focus corner cadence of 900 s. The starting time of each schedule is chosen to be at 07:00 UTC on the first of each month. This has been done to comprise all possible changes in the sidereal time affecting the source selection.

The following tables again summarize the most important parameters involved in the scheduling (see table 5.2), simulation (see table 5.3) and analysis process (see table 5.4).

Table 5.2: Scheduling parameters for VieSched++.

Scheduling parameters	
parameter	value
minimum scan duration [s]	30
fixed scan duration [s]	30
minimum elevation [deg]	5
focus corner cadence [s]	900
minimum time between scans to same source [s]	1500
sky coverage weight factor w_{sky}	0.05
duration weight factor w_{dur}	1

Table 5.3: Simulation parameters for VieSched++.

Simulation parameter	
parameter	value
white noise per station [ps]	2.83
clock ASD after 50 min [ps]	1
tropo Cn [$10^{-7}m^{-1/3}$]	1.8
tropo H [m]	2000

Table 5.4: Analysis parameters for VieSched++.

Analysis parameter	
parameter	value
dUT1 interval [h]	1
dUT1 constraint [mas]	0.0001
pwl zenith wet delay interval [h]	1
pwl zenith wet delay constraint [cm]	1.5
linear clock	true

Based on these 12 schedules per single baseline, again the mean value as well as the standard deviation have been calculated for mfe_{dUT1} and rep_{dUT1} and furthermore also the baseline lengths bl_{3D} and bl_{2D} (see equations 4.2 and 4.3).

In this study, the following numbers of schedules and simulations are generated and analyzed, where #sched_app stands for the number of used scheduling approaches and #stat for the number of stations per session). This shows how much effort has been put into the generation of highly optimized schedules using VieSched++.

Table 5.5: Total number of generated schedules using VieSched++.

Number of generated schedules						
network	#sched_app	time period	cadence	#stat	durations	total
VGOS	3	1 year	daily	2-3	1-4h	525 600
VLBA	3	1 year	daily	2-3	1-4h	722 700
global artificial	1	1 year	monthly	2	1h	34 800
					In total:	1 283 100

5.3. Importance of $\frac{\partial \tau}{\partial dUT1}$ on the performance of Intensive Sessions

Before the results of this investigation are shown and discussed in section 5.4, the findings of a recently published study by Schartner et al. (2021) are briefly described in this section. As already mentioned in section 2.1.6, the variability of the partial derivatives of the estimated parameters is crucial to distinguish the estimated parameters from each other in the least squares adjustment. Hence, the performance of the Intensive sessions in general and the determination of *dUT1* strongly depend on the variability of $\frac{\partial \tau}{\partial dUT1}$.

The following visualizations in figure 5.2 show this variability of $\frac{\partial \tau}{\partial dUT1}$ regarding five equally long baselines. This figure includes a what is believed to be a perfectly oriented baseline *(a)* on the equator, the same baseline *(b)* but located at another latitude level, a north-south oriented baseline *(c)* from one pole to the equator as well as another north-south oriented baseline *(d)* parallel to the Earth's rotation axis and a baseline *(e)* with the mid-point close to the equatorial plane.

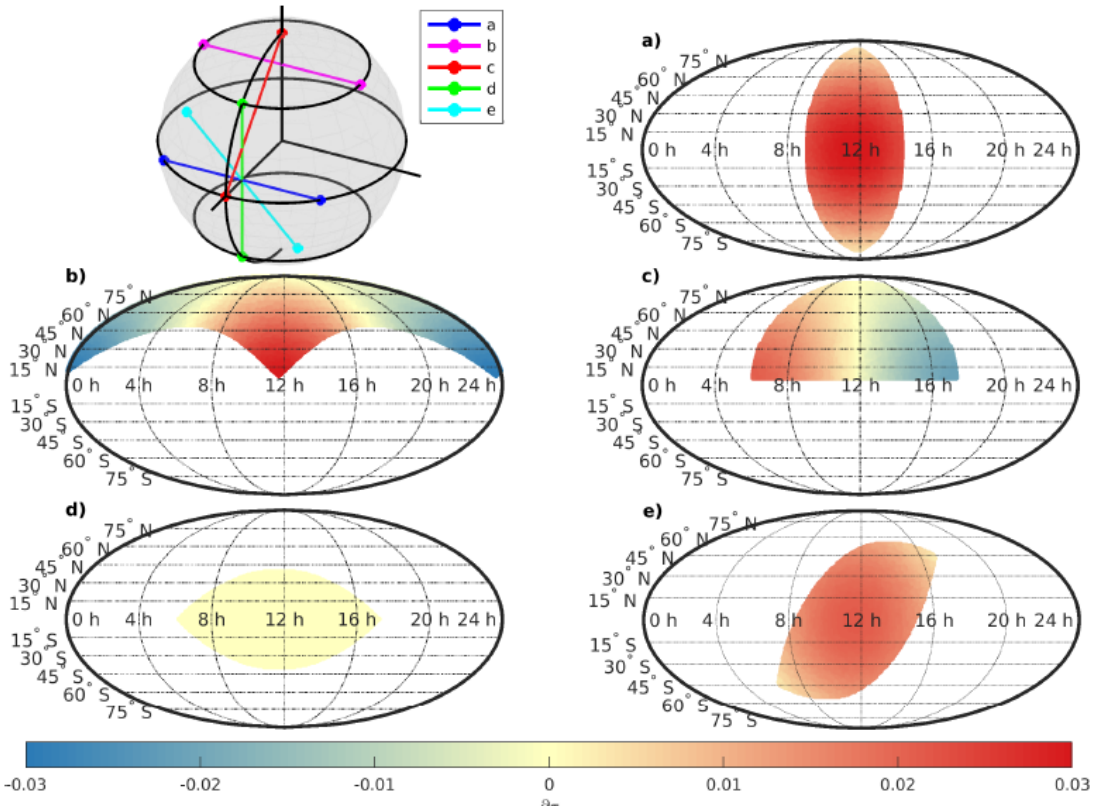

Figure 5.2: The variability of the partial derivative of τ with respect to *dUT1* for five equally long baselines, figure from Schartner et al. (2021).

Due to the highly restricted commonly visible sky, especially concerning the achievable α values, which are crucial for the variability of $\frac{\partial \tau}{\partial dUT1}$, the equatorial baseline *(a)* as well as the north-south oriented baseline parallel to the Earth's rotation axis *(d)* and the baseline with the mid-point close to the equatorial plane *(e)* result in a small variety of the partial derivatives. The two remaining baselines, which include the perfectly oriented baseline in high latitude range *(b)* and further also the north-south oriented baseline between the pole and the equator, cover a much bigger part of the celestial frame (concerning the α) and therefore provide a high variability of $\frac{\partial \tau}{\partial dUT1}$ with positive influence on the performance of these single baseline Intensive sessions. Subsequently, this investigation by Schartner et al. (2021) supports the findings by Uunila et al. (2012) and Baver and Gipson (2015), which state the importance of corner observations, since the minima and maxima of $\frac{\partial \tau}{\partial dUT1}$ are located in the corners of the mutually visible sky.

However, what has to be further considered is, that the polar motion - among other quantities - can not be estimated using Intensive sessions, due to the restricted number of observations. Hence, it is fixed to the a priori information. Therefore, the accuracy of this pair of polar motion values is crucial for the determination of *dUT1*. Since this effect is not accounted for in this master thesis, only a short insight on the impact of erroneous polar motion a priori data from the study by Schartner et al. (2021) is given in section A.1.

5.4. Results and discussion

All results concerning this investigation are plotted using a grid which ranges from −80° to 80° *lat* and 0° to 180° Δ*lon*, where every grid cell represents one artificial VLBI station. The values within the cell show the mfe_{dUT1} or rep_{dUT1} of the corresponding baseline between the station at the location of the cell and the current reference station (marked in black). This means that per figure, the simulation results of one reference station to any other artificial station are displayed, which are in total 322 baselines per reference station. As already mentioned, this large-scale simulation study has been carried out for in total nine reference stations (labeled as *ref*) on the northern hemisphere at the reference meridian at 0° Δ*lon*, which results in nine grid plots for each the mfe_{dUT1} and the rep_{dUT1}. In this chapter, only selected results are displayed and further analyzed. The remaining ones can be found in section A.3. Due to reasons concerning the presentation of the data, baselines with an achieved mfe_{dUT1} of more than 100 μs are marked as *inf*. Additionally, for some constellations, including very long baselines, the estimation is not possible due to the highly restricted commonly visible sky. These cells are also marked with *inf*.

First, the simulation results consisting of the mfe_{dUT1} (top) and rep_{dUT1} (bottom) of the analysis of a reference station at latitudes commonly achieved in Intensive sessions, are displayed. Since the VLBI station Wz (49.15° *lat*, 12.88° *lon*) is usually part of the IVS Intensive sessions, this first result plot shows the reference station's results 50° *lat*. Since INT1 sessions usually observe the baseline between Wz and Kk (22.13° *lat*, −159.66° *lon*), the Δ*lon* equals approximately 172° and is marked in the following figure using a red rectangle. For a long time, INT2 sessions contained the stations Wz and Is (36.21° *lat*, 140.22° *lon*), resulting in a Δ*lon* of 127° (displayed in purple). More recently, Wz and Mk (19.80° *lat*, −155.45° *lon*) participate in INT2 sessions leading to an extension in *lon* direction of approximately 168° (green).

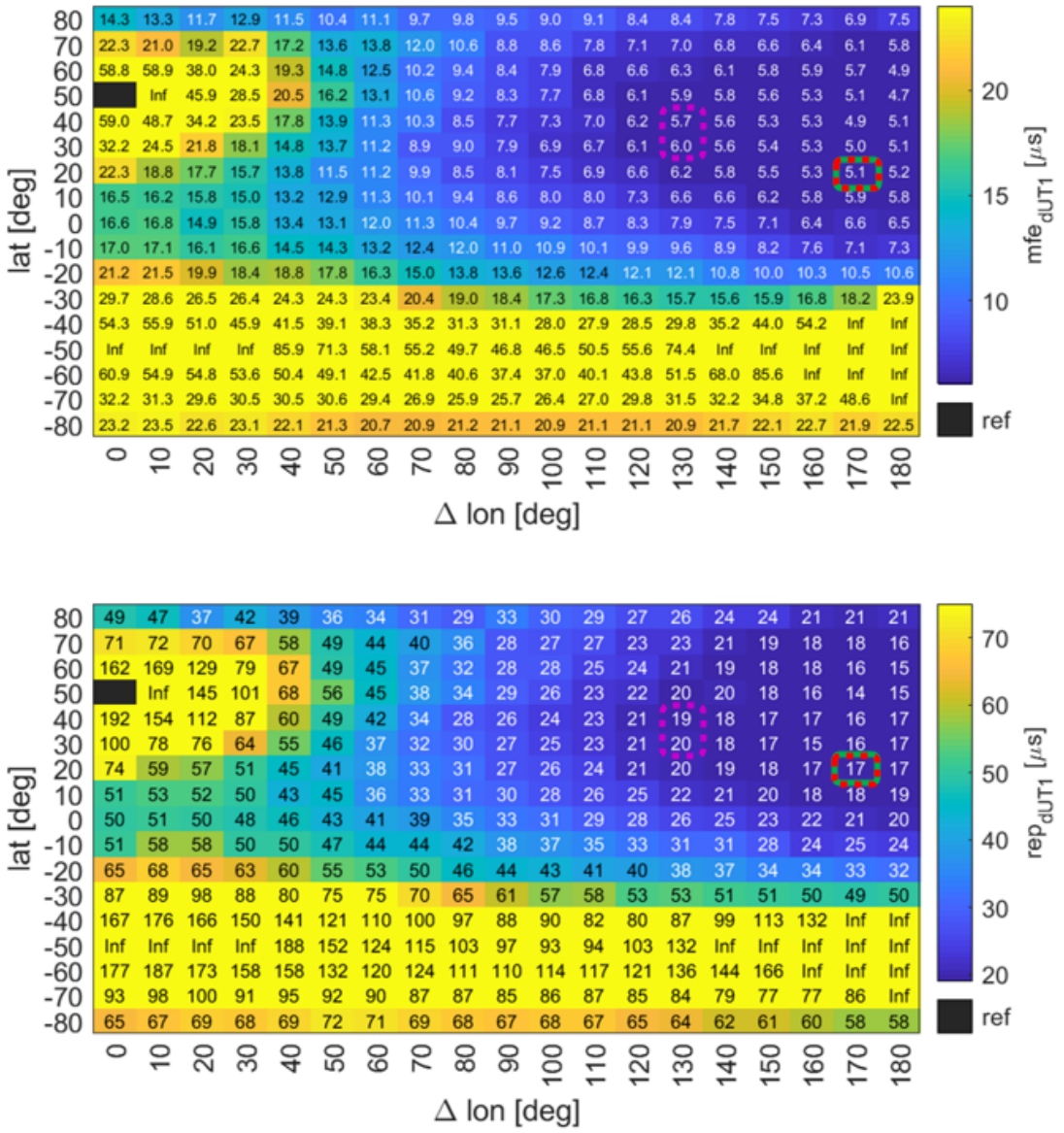

Figure 5.3: Simulation results mfe_{dUT1} (top) and rep_{dUT1} (bottom) concerning a reference station at 50° *lat*, like the real VLBI station Wz at 49.15°, displayed as a black cell. The dotted rectangles mark the locations of the second stations participating in various commonly observed Intensive sessions: INT1 sessions between Wz and Kk (red) and INT2 sessions between either Wz and Is (purple) or Mk (green) (see section 2.2.1).

Due to the resolution of the grid, the baselines Wz-Kk and Wz-Mk result in the same cell grid and therefore lead to the same simulated values of 51 μs in mfe_{dUT1} and 17 μs in rep_{dUT1}. Since the lowest achieved values are 47 and 14 μs, one can say that these baselines have a good performance. In comparison, the baseline between Wz and Is does not perform equally well.

However, with values below 6 and 20 μs, this baseline provides better performance than many other two station networks. As already mentioned, due to the restricted mutually visible sky, very long baselines, which include stations in the southern hemisphere, do not perform well. Furthermore, also very short baselines and baselines with a mid-point close to the equatorial plane result in high mfe_{dUT1} and rep_{dUT1} values. Moreover, perfectly north-south oriented baselines, which are approximately parallel to the Earth's rotation axis perform, as expected, badly. These results support the findings of the study by Schartner et al. (2021) discussed in section 5.3, where these baselines are suggested to lead to high accuracy values due to the low variability of the partial derivative of τ with respect to *dUT1*. This low variability is caused by the restricted mutually visible sky especially in the right ascension range of the observed sources. Furthermore, in figure 5.2, baseline (b) represents a perfect east-west oriented baseline in a mid- to high-latitude range, which resulted in a high variability of $\frac{\partial \tau}{\partial dUT1}$. Concerning the simulation results shown in figure 5.3, the optimal geometry for a single baseline session, starting from a station in the mid- to high-latitude range, includes another station in the mid- to high-latitude range while also having a large Δlon.

Figure 5.4 shows the same plot but regarding a reference station at 0° *lat*. These results can not be compared with a typical Intensive session constellation, since there are no VLBI stations participating in Intensive sessions close to the equator. Actually, FORTLEZA in Brazil with −3.87° *lat* is the only telescope located in this low-latitude level. However, the simulation results still show the theoretical impact of the geometry on Intensive sessions. Again, very long and short baselines result in high mfe_{dUT1} and rep_{dUT1} values. However, against all expectations, equatorial baselines with a perfect east-west extension overall lead to a poor performance in *dUT1*. This finding corresponds with the results from Schartner et al. (2021), where equatorial baselines show a low variability in α and therefore also in $\frac{\partial \tau}{\partial dUT1}$, explaining the bad performance. Optimal baselines in this particular case, are found in the mid- to high-latitude range, showing that not always the perfectly oriented east-west baseline is the best choice. Surprisingly, some north-south oriented baselines lead to results, which are only <20% worse than the optimal baseline. To be more precise, these baselines are far from being parallel to the Earth's rotation axis and hence are located between a telescope at the equator and one close to the pole. Figure 5.2, baselines (c) and (d), display the $\frac{\partial \tau}{\partial dUT1}$ values of both, a north-south aligned baseline parallel to the Earth's rotation vector and one between the pole and the equator. Since the second one allows observations over the whole northern part of the hemisphere and therefore leads to a high variability, the first baseline results in a highly restricted commonly visible sky concerning the α.

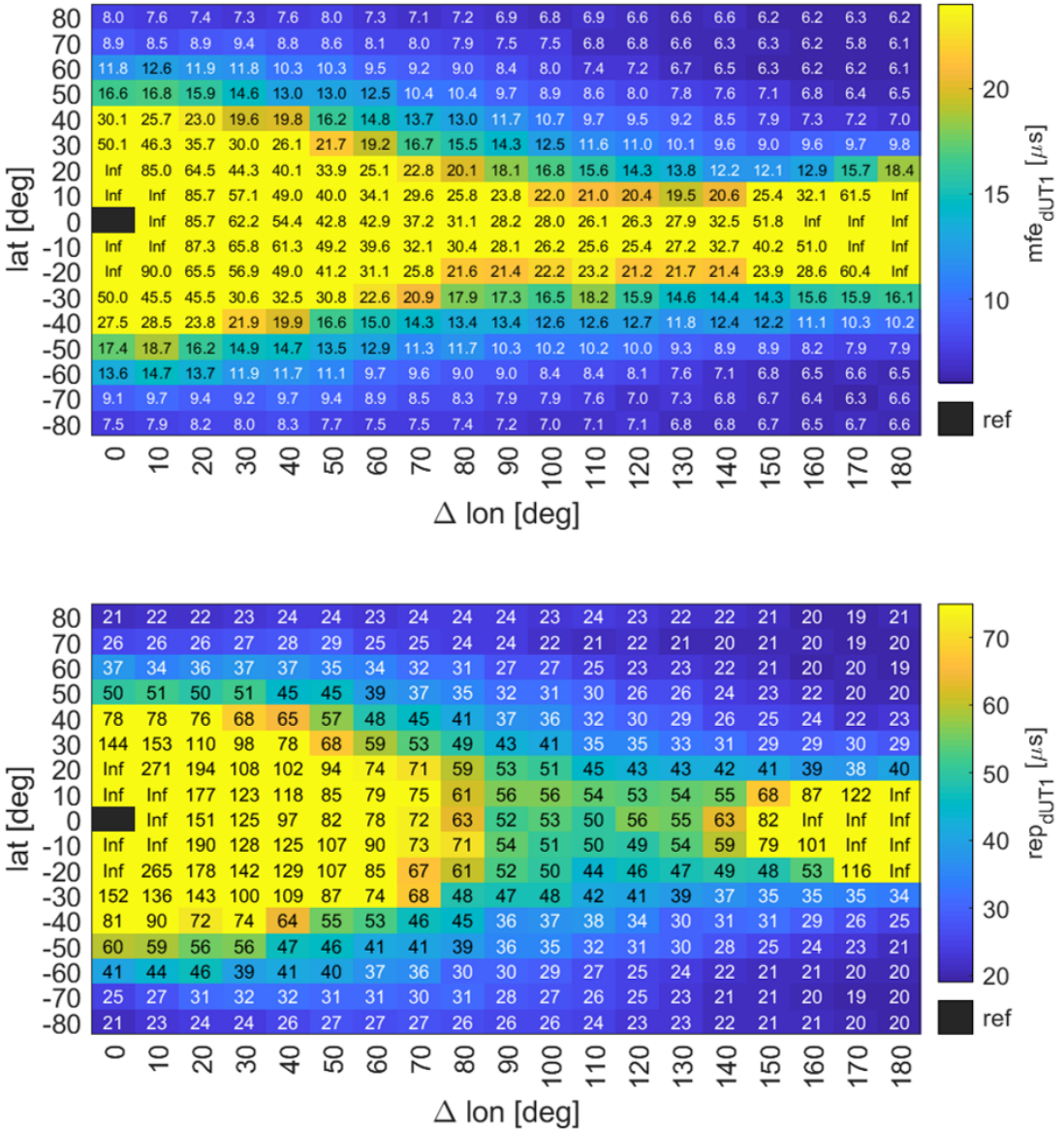

Figure 5.4: Simulation results mfe_{dUT1} (top) and rep_{dUT1} (bottom) concerning a reference station at 0° *lat*.

In the last figure 5.5, again the differences in the simulation results of the north-south oriented baselines can be seen clearly. In this case, the baseline from the pole to the equator at 0° Δlon is again only approximately 25 % worse than the perfect baseline to a telescope at 20° *lat* and 180° Δlon. Once more, baselines with a midpoint close to the equatorial plane lead to a bad performance concerning the estimation of *dUT1*, even though they include the longest possible baseline extension from (80°,0°) to (−80°,180°).

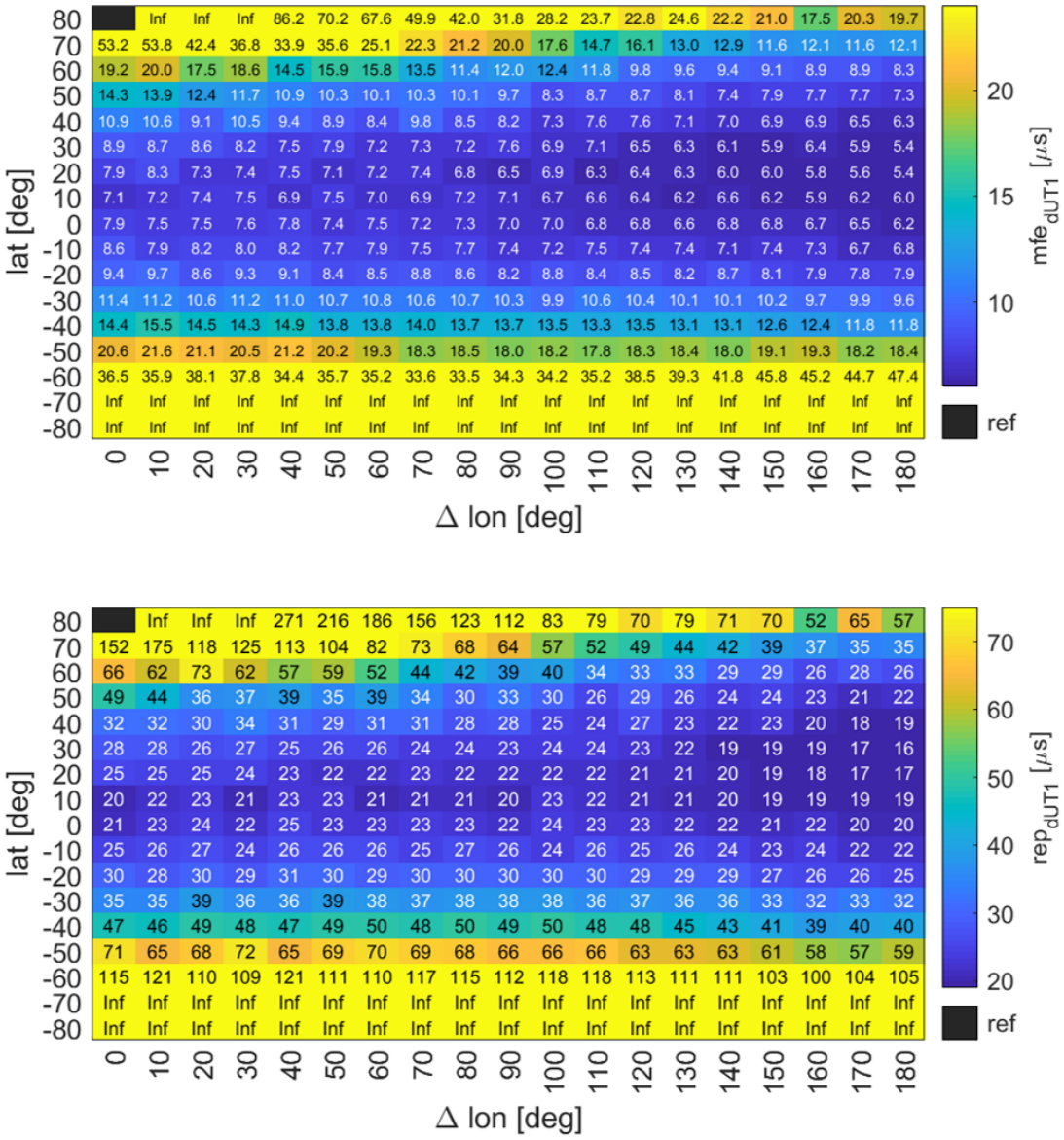

Figure 5.5: Simulation results mfe_{dUT1} (top) and rep_{dUT1} (bottom) concerning a reference station at 80° *lat*.

Just like it has been done for the network-based investigations, the baseline lengths bl_{2D} and bl_{3D} (see equations 4.3 and 4.2) are calculated using the coordinates of the artificial stations and then plotted against the corresponding achieved mfe_{dUT1}, see figure 5.6. Since concerning this global investigation, in total, almost 3000 baselines are analyzed, this plot represents the mathematical relation between these quantities better and a more general statement can be derived regarding the impact of the baseline length on the performance of Intensive sessions.

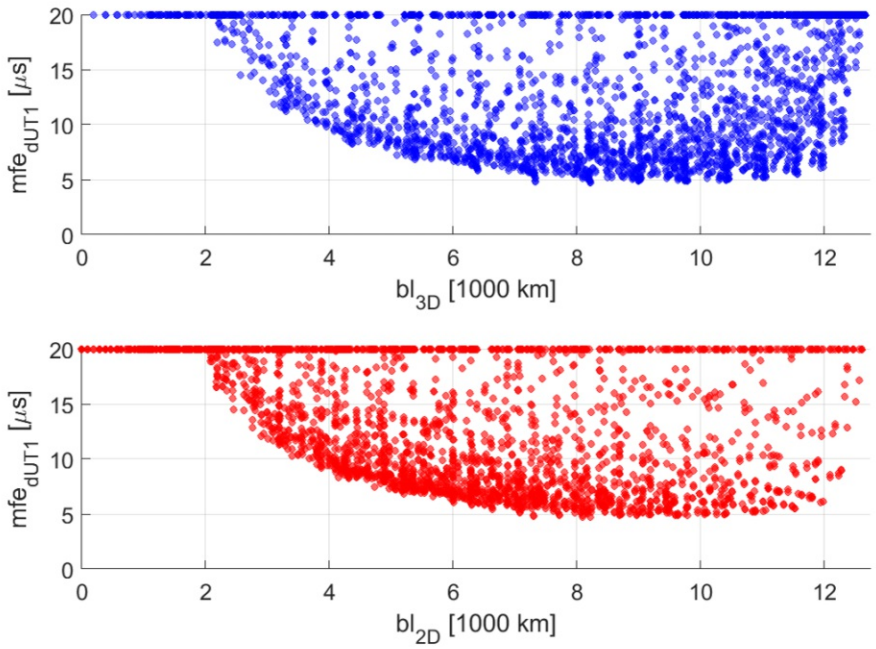

Figure 5.6: The different baseline lengths of all possible artificial networks plotted against the corresponding mfe_{dUT1}. bl_{3D} (top) represents the three-dimensional baseline length, whereas bl_{2D} (bottom) is the length of the baseline projected onto the equatorial plane.

Clearly, the optimal bl_{3D} ranges from approximately 8000 km to 11 000 km, with the minimum of mfe_{dUT1} reached at about 9500 km. For baselines longer than 9500 km the accuracy decreases again. At baseline lengths of over 12 000 km the commonly visible sky is highly restricted and therefore the performance is worse compared to a shorter baseline of about 5000 km. The plot concerning the bl_{2D} shows the same behavior.

In general, when thinking about common knowledge concerning the perfect single baseline geometry, the findings of this study show new insights. Firstly, very long baselines do not always provide the best performance due to the highly restricted commonly visible sky accompanied by restricted source selection. Secondly, it is not crucial to form a perfect east-west extension, since baselines that include a small angle with the equatorial plane provide equally good or even better simulation results. Additionally, network constellations with a midpoint close to the equatorial plane are not recommendable, since they overall result in a poor performance. What is really surprising is that equatorial baselines, which seem to be the optimal one regarding common knowledge, do not lead to good results suggested by this simulation study (see figure 5.4). Furthermore, also certain north-oriented baselines do not perform as poor as expected. These include network geometries that are far away from being parallel to the Earth's rotation axis, like it can be seen in figure 5.5.

6. Summary and Conclusion

In summary, the findings of this master thesis are based on large-scale simulation studies. Therefore, the results do not represent real accuracy information on the individual Intensive session baselines but can be used to compare them. Furthermore, what has to be further considered is, that in this study the influence of erroneous polar motion a priori data is not accounted for and therefore has an direct influence on the determination of *dUT1*. In a similar study by (Schartner et al., 2021) this impact is investigated. A brief overview on the findings of this study can be found in section A.1.

This investigation has been done not only to evaluate an optimal baseline for existing station networks (VGOS and VLBA) and an artificial global network, but also to analyse the effect of different session configurations. This includes the session duration, the number of participating stations and concerning the VGOS station network also the scan duration and recording rate.

In general, a lot of work has been put into the scheduling process, resulting in a total of almost 1.3 million schedules, that have been investigated in the course of this study. In the following the findings of the individual investigations are summarized very briefly.

Starting with the best baselines concerning the existing VLBI station networks VGOS and VLBA, in general, baselines are suggested, which are not commonly observed at the moment. In case of the best two station VGOS network, the baselines Gs-Is and Is-Wf would theoretically perform better than the commonly scheduled baseline between K2 and Ws (VGOS-2). Although the VGOS-2 session forms a longer baseline with an even higher east-west extension than both of the suggested optimal baselines, the mfe_{dUT1} and rep_{dUT1} values are about 15 % and 20 % worse.

The best three station network including VGOS stations is formed between the telescopes Gs, Is and Wf, just like the two optimal two station networks. The VGOS-B Intensive sessions between Is-Oe-Ow did not even perform nearly as good concerning the estimation of *dUT1*. To be more precise, out of the 84 possible and unambiguous baselines this session was always listed in the last third of the performance sorting with mfe_{dUT1} and rep_{dUT1} values approximately 45 % and 22 % worse than the best ones. What has to be considered here is, that in this study, no joint estimation of the troposphere concerning the twin telescopes Oe and Ow has been carried out. Hence, the VGOS-B sessions are very likely to perform better than it is shown in this study.

Regarding the VLBA network, the baselines Hn-Mk and Fd-Hn-Mk provide the highest simulated accuracies. The commonly observed baseline between Mk and Pt showed worse results, by a factor of about two. Furthermore, also the three station network Mk-Sc-Pt did not perform as well.

Coincidentally, only recently, the USNO introduced a new test series of VLBA Intensive session between the stations Hn and Mk with a slightly longer session duration of 1.5 h, starting from the beginning of May 2021 and lasting until the end of August 2021. Considering the results of this master thesis, this particular baseline should provide the best performance concerning the determination of *dUT1*. Furthermore, the increase in the session duration is beneficial.

In general, the session duration has a high impact on the simulated performance of an Intensive session. By doubling the session duration the mfe_{dUT1} and rep_{dUT1} improve by approximately 15 and 20 %. Furthermore, also the σ values of both decrease. Scheduling three or four hour sessions instead of one hour sessions improves the performance further. However, the difference in the decrease of the accuracy values between three and four hours is not that significant. This behaviour can be described most likely by the modeling of the troposphere. Therefore, it is possible, that a decrease of the estimation interval of the ZWD is can lead to a further improvement of the performance of Intensive sessions with increasing session duration.

Moreover, also the extension of a two station Intensive session by a third station leads to an enhancement of the performance. Concerning one hour sessions, the majority of the three station sessions result in accuracy values up to about 75 % better than the two station networks. However, the improvement is not the same for the different session durations. In general, with increasing session duration the enhancement of the performance either stagnates or even decreases slightly. In general, by introducing a third station the possibility arises, that more parameters, like the polar motion, can be estimated. This would solve the issue of the high impact of erroneous polar motion a priori information on the estimate of *dUT1* (see section A.1).

Besides the analysis of the different session durations and number of participating stations, additional schedules have been generated to investigate the effect of different scan durations and recording rates on single baseline VGOS sessions. Usually, VGOS Intensive sessions are observed with a fixed scan duration of 30 s and a recording speed of 8 Gbps. Decreasing the scan duration to 10 s theoretically improves the performance concerning the estimation of *dUT1* as well as the usage of a higher recording speed. However, with a decreasing scan duration the difference between the performance achieved by the 4 and 8 Gbps recording mode is really small. Since two effects, namely reaching a certain minimum *SNR* and non-detections, which arise from a decrease in the scan duration, are not considered in the simulation process these results have to be treated with caution.

In the last section the global investigation concerning the optimal baseline geometry and length for single baseline Intensive sessions is discussed. This global-scaled experiment based on artificial station leads to new insights on what is common knowledge regarding the perfect baseline geometry for these one hour sessions. This simulation study shows, that not always the perfectly east-west aligned baseline provides the highest precision. For example, against all expectations, equatorial baselines lead to low accuracy values. This can be explained by the low variability of the partial derivative $\frac{\partial \tau}{\partial dUT1}$, due to the highly restricted commonly visible sky in α direction (Schartner et al., 2021). In addition, also very long baselines do not perform very well, since again the source selection is highly restricted.

In general, the best baselines can be achieved by forming a baseline including a small angle with the equatorial plane, e.g., between high-to-mid-latitude and low-to-mid-latitude telescopes while also having a baseline length of about 8000 to 11 000 km. As already mentioned, for very long baselines the performance deteriorates progressively.

Another new insight is, that baselines with a midpoint close to the equatorial plane result in high mfe_{dUT1} and rep_{dUT1} and are therefore not recommended as possible Intensive sessions. Moreover and against all expectations, north-south oriented baselines, which are far from being parallel to the Earth's rotation axis, e.g., baselines between the pole and the equator, achieved accuracy values only approximately 25 % worse than the results from the best baseline. Overall, the results of this study support the findings evaluated by Schartner et al. (2021).

A. Appendix

A.1. Impact of erroneous polar motion a priori information on *dUT1*

Beside the variability of the partial derivative $\frac{\partial \tau}{\partial dUT1}$, the influence of erroneous polar motion a priori data has been analysed in the study by Schartner et al. (2021). The impact of uncertainties in the polar motion a priori data dx_p and dy_p can be assessed by analysing the derivatives (see equation A.1).

$$\frac{dUT1}{dx_p} = -\frac{(y_2 - y_1)(z_2 - z_1)}{(y_2 - y_1)^2 + (x_2 - x_1)^2} \quad and \quad \frac{dUT1}{dy_p} = -\frac{(x_2 - x_1)(z_2 - z_1)}{(y_2 - y_1)^2 + (x_2 - x_1)^2} \tag{A.1}$$

In the following figure A.1 the combined effect of both dx_p and dy_p is visualized concerning reference stations at different latitude levels, marked as a red star. Since the impact of errors in the a priori information is very high concerning baselines with a big difference in the z-coordinates, this has to be considered when observing *dUT1* from these baselines. For more details see Schartner et al. (2021).

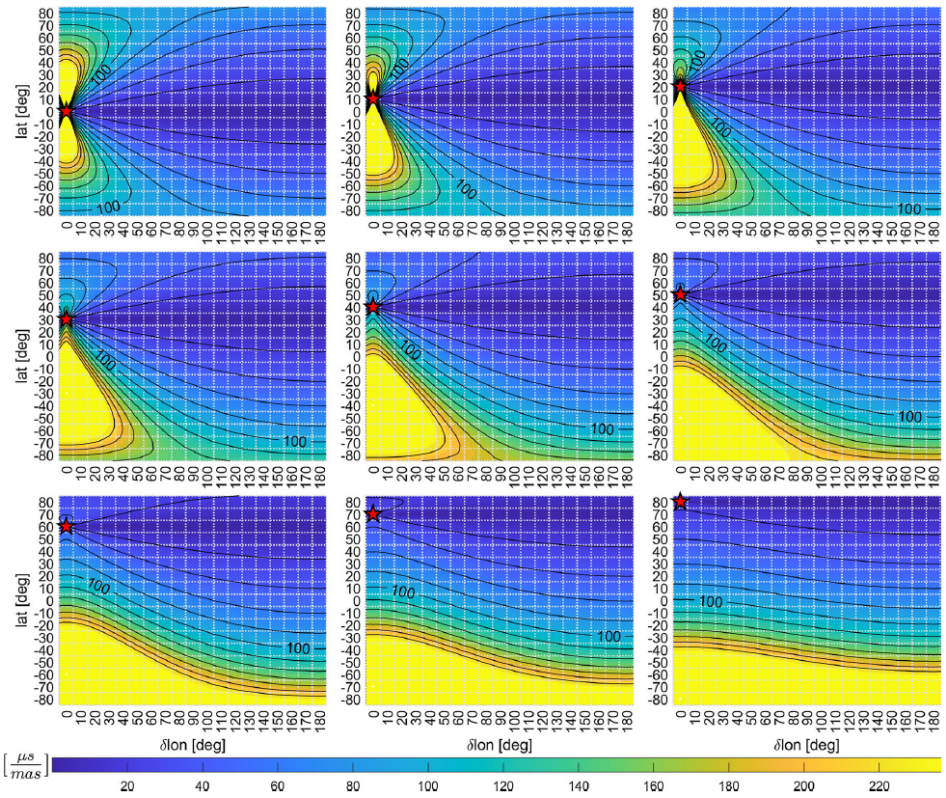

Figure A.1: Combined impact by x- and y-pole of erroneous polar motion a priori information on the determination of *dUT1*, figure from Schartner et al. (2021).

A.2. Network-based investigation

VGOS network results (2 stations, 1h duration)

Table A.1: Results of the VGOS network investigation: bl_{3D} and bl_{2D} represent the 3D and 2D baseline length in [km], mfe_{dUT1} and rep_{dUT1} are the calculated mean values over the whole investigation period in $[\mu s]$ and σ_{mfe} and σ_{rep} are the derived standard deviations of mfe_{dUT1} and rep_{dUT1} in $[\mu s]$.

VGOS network investigation with two stations and one hour duration													
network	bl_{3D}	bl_{2D}	mfe_{dUT1}	σ_{mfe}	rep_{dUT1}	σ_{rep}	network	bl_{3D}	bl_{2D}	mfe_{dUT1}	σ_{mfe}	rep_{dUT1}	σ_{rep}
Oe - Ow	0	0	-	-	-	-	Gs - Ws	6522	6472	7.70	0.81	22.00	2.89
Gs - Wf	601	520	102.41	17.25	242.91	49.23	Gs - K2	7405	7229	7.77	0.67	17.40	2.21
Ow - Ws	920	738	55.03	5.00	143.10	21.18	K2 - Wf	7676	7435	7.46	0.92	20.92	3.05
Oe - Ws	920	738	55.60	5.17	147.82	20.15	Is - Oe	7937	7773	5.75	0.55	16.03	2.36
Yj - Ws	1576	1422	36.80	4.02	107.31	15.02	Is - Ow	7937	7773	5.86	0.57	16.70	2.63
Ow - Yj	2153	1770	23.19	2.54	63.16	10.35	Mg - Ow	7940	7654	5.89	0.55	17.31	2.61
Oe - Yj	2153	1770	23.14	2.53	64.16	10.72	Mg - Oe	7940	7654	5.75	0.53	17.00	2.57
Gs - Mg	2623	2511	23.50	1.82	49.95	8.01	Mg - Yj	8040	7991	6.42	0.74	18.75	2.34
Mg - Wf	3138	2954	20.92	2.20	61.28	8.96	Mg - Ws	8418	8271	5.97	0.63	18.20	2.73
Yj - Wf	5377	5374	9.41	1.15	28.53	3.82	Is - Ws	8442	8376	5.74	0.63	17.16	2.80
K2 - Mg	5402	5335	12.03	1.29	34.19	4.49	Is - Mg	9031	9017	5.95	0.52	17.30	2.27
Ow - Wf	5600	5500	9.44	1.20	25.63	4.26	Is - Wf	9495	9480	4.96	0.58	14.28	1.78
Oe - Wf	5600	5500	9.22	1.24	24.84	3.82	Is - Yj	9508	9500	5.27	0.54	15.35	2.43
Is - K2	5744	5581	11.42	1.23	35.13	5.50	Gs - Is	9594	9590	4.94	0.45	13.28	2.25
Gs - Yj	5893	5891	8.69	0.96	22.92	3.14	K2 - Oe	9793	9334	5.41	0.57	16.87	3.10
Wf - Ws	5998	5977	8.67	1.33	25.67	4.06	K2 - Ow	9793	9334	5.50	0.60	16.04	2.69
Gs - Ow	6130	5978	7.44	0.78	20.78	3.17	K2 - Ws	10358	10072	5.78	0.54	19.33	3.15
Gs - Oe	6130	5978	7.28	0.75	19.78	2.83	K2 - Yj	10688	10546	6.33	0.48	15.06	3.58

VGOS network results (3 stations, 1h duration)

Table A.2: Results of the VGOS network investigation: mfe_{dUT1} and rep_{dUT1} are the calculated mean values over the whole investigation period in [μs] and σ_{mfe} and σ_{rep} are the derived standard deviations of mfe_{dUT1} and rep_{dUT1} in [μs].

VGOS network investigation with three stations and one hour duration									
network	mfe_{dUT1}	σ_{mfe}	rep_{dUT1}	σ_{rep}	network	mfe_{dUT1}	σ_{mfe}	rep_{dUT1}	σ_{rep}
Gs - Is - Wf	3.70	0.40	11.77	1.56	Is - Oe - Yj	4.69	0.81	14.16	2.16
Gs - Is - Mg	4.19	0.48	11.84	2.02	Gs - K2 - Ow	4.70	0.59	14.72	2.66
Gs - Is - Oe	4.35	0.27	11.21	1.98	Is - Wf - Ws	4.71	0.32	11.58	2.08
Is - Oe - Ws	4.35	0.64	14.22	2.30	Gs - K2 - Ws	4.72	0.47	16.41	2.10
K2 - Mg - Oe	4.36	0.51	12.90	1.80	Gs - Mg - Oe	4.74	0.37	15.66	2.23
Is - Yj - Ws	4.36	0.78	14.05	1.98	Gs - Is - Ws	4.74	0.30	11.25	1.76
K2 - Mg - Yj	4.37	0.56	12.41	1.81	K2 - Wf - Ws	4.76	0.47	14.96	2.27
Gs - Is - Ow	4.39	0.28	11.14	1.80	Gs - Is - K2	4.77	0.54	11.02	2.55
Is - Oe - Wf	4.40	0.34	11.95	1.97	Gs - Is - Yj	4.78	0.34	12.63	2.13
K2 - Mg - Ow	4.41	0.56	12.10	1.54	K2 - Ow - Wf	4.79	0.42	13.23	2.05
K2 - Ow - Ws	4.43	0.34	11.72	1.15	Gs - Mg - Ws	4.81	0.43	16.70	2.44
Is - Ow - Wf	4.43	0.33	12.03	2.14	Gs - K2 - Yj	4.81	0.39	14.35	2.07
K2 - Oe - Ws	4.48	0.37	12.24	1.22	Is - Ow - Yj	4.82	0.84	14.26	2.33
Is - Ow - Ws	4.51	0.70	14.40	2.30	Gs - Mg - Ow	4.83	0.42	16.17	2.30
K2 - Mg - Ws	4.52	0.47	14.11	2.01	Mg - Wf - Ws	4.92	0.61	17.94	2.60
Mg - Oe - Ws	4.59	0.64	14.24	1.63	Is - K2 - Wf	4.94	0.40	11.91	1.79
K2 - Yj - Wf	4.64	0.40	13.23	1.88	Is - Mg - Oe	4.99	0.29	10.60	1.97
Mg - Ow - Ws	4.65	0.75	14.01	1.82	Is - Mg - Ow	5.03	0.30	10.72	1.93
Is - Mg - Wf	4.66	0.42	12.93	2.04	Mg - Oe - Wf	5.04	0.49	16.56	2.24
Gs - K2 - Oe	4.67	0.55	14.75	2.44	Mg - Yj - Wf	5.08	0.45	19.29	2.10
K2 - Oe - Wf	4.67	0.41	13.32	2.19	Mg - Ow - Wf	5.16	0.51	16.89	2.47
Is - Yj - Wf	4.68	0.32	12.01	1.78	Gs - Mg - Yj	5.28	0.44	16.82	1.99

Table A.3: Results of the VGOS network investigation: mfe_{dUT1} and rep_{dUT1} are the calculated mean values over the whole investigation period in [μs] and σ_{mfe} and σ_{rep} are the derived standard deviations of mfe_{dUT1} and rep_{dUT1} in [μs].

VGOS network investigation with three stations and one hour duration									
network	mfe_{dUT1}	σ_{mfe}	rep_{dUT1}	σ_{rep}	network	mfe_{dUT1}	σ_{mfe}	rep_{dUT1}	σ_{rep}
Is - Mg - Yj	5.28	0.32	10.82	1.36	Gs - K2 - Mg	6.46	0.47	15.89	1.48
Mg - Yj - Ws	5.29	0.86	14.23	2.12	Mg - Oe - Yj	6.59	0.50	14.26	1.78
K2 - Yj - Ws	5.30	0.80	9.92	1.69	Is - Oe - Ow	6.61	0.63	14.60	2.35
Is - Mg - Ws	5.32	0.28	10.94	1.79	Mg - Ow - Yj	6.65	0.59	15.02	1.81
Is - K2 - Oe	5.41	0.57	11.89	2.40	K2 - Oe - Yj	6.71	1.24	13.58	2.85
Is - K2 - Ow	5.46	0.70	11.98	2.18	Ow - Wf - Ws	6.75	0.75	21.06	3.12
Is - K2 - Mg	5.49	0.75	14.85	2.26	Oe - Wf - Ws	6.79	0.76	21.01	2.86
Gs - Ow - Ws	5.65	0.55	16.83	2.12	K2 - Ow - Yj	6.97	1.67	13.81	3.17
Gs - Oe - Ws	5.76	0.56	16.72	2.15	Mg - Oe - Ow	7.06	0.58	14.87	1.85
Is - K2 - Ws	5.79	0.61	14.10	2.58	Gs - Yj - Wf	7.13	1.02	22.64	2.82
Gs - Yj - Ws	5.79	0.64	17.88	2.17	Oe - Ow - Wf	7.19	0.85	20.87	3.20
Gs - Ow - Yj	5.92	0.75	16.89	2.24	Yj - Wf - Ws	7.35	0.78	21.69	2.85
Gs - Oe - Yj	5.99	0.71	16.82	2.19	Oe - Yj - Wf	7.51	0.67	20.74	3.00
K2 - Mg - Wf	6.04	0.64	19.76	2.35	K2 - Oe - Ow	7.62	1.95	13.16	2.70
Gs - Wf - Ws	6.05	0.85	19.97	3.61	Ow - Yj - Wf	7.63	0.68	20.61	3.13
Gs - Oe - Ow	6.13	0.88	17.34	2.74	Gs - Mg - Wf	17.31	1.95	42.81	6.10
Gs - Oe - Wf	6.17	0.79	18.94	3.77	Oe - Ow - Yj	17.35	1.60	54.11	8.13
Gs - Ow - Wf	6.27	0.75	19.61	4.32	Ow - Yj - Ws	19.40	1.73	62.40	9.28
Gs - K2 - Wf	6.38	0.54	14.47	2.04	Oe - Yj - Ws	19.57	1.75	62.67	8.97
Is - K2 - Yj	6.41	0.50	11.65	2.40	Oe - Ow - Ws	44.85	3.78	117.80	14.60

VLBA network results (2 stations, 1h duration)

Table A.3: Results of the VGOS network investigation: bl_{3D} and bl_{2D} represent the 3D and 2D baseline length in [km], mfe_{dUT1} and rep_{dUT1} are the calculated mean values over the whole investigation period in [μs] and σ_{mfe} and σ_{rep} are the derived standard deviations of mfe_{dUT1} and rep_{dUT1} in [μs].

VLBA network investigation with two stations and one hour duration

network	bl_{3D}	bl_{2D}	mfe_{dUT1}	σ_{mfe}	rep_{dUT1}	σ_{rep}	network	bl_{3D}	bl_{2D}	mfe_{dUT1}	σ_{mfe}	rep_{dUT1}	σ_{rep}
La - Pt	237	195	339.70	40.18	799.65	157.63	Hn - La	3007	2944	23.09	2.15	52.88	8.03
Kp - Pt	417	355	199.92	19.25	451.35	88.06	Fd - Hn	3106	2908	23.54	2.25	53.51	7.81
Fd - Pt	565	449	148.84	15.43	346.91	61.88	Hn - Pt	3227	3139	21.72	2.15	50.30	7.20
Fd - La	609	378	135.18	12.94	299.21	50.16	Hn - Kp	3623	3492	19.58	2.05	46.14	6.71
Kp - La	652	549	124.42	11.77	283.60	54.35	Nl - Sc	3646	2833	24.51	2.94	58.25	10.31
Fd - Kp	744	734	113.00	9.93	280.65	44.75	Br - Hn	3658	3635	17.55	1.46	40.82	5.96
Kp - Ov	845	695	89.72	7.05	195.07	22.44	Hn - Ov	3886	3856	16.12	1.74	40.97	5.34
Ov - Pt	973	937	76.14	5.94	179.67	24.82	Mk - Ov	4015	3642	22.94	2.17	54.05	8.91
La - Ov	1088	1080	67.27	5.70	161.75	22.07	Fd - Sc	4144	3935	25.18	2.92	58.08	7.19
Br - Ov	1215	828	53.23	3.86	95.05	13.07	Br - Mk	4399	3564	17.45	1.98	41.90	5.99
La - Nl	1433	1336	50.38	5.01	125.09	23.92	La - Sc	4459	4090	21.61	2.47	53.05	7.66
Fd - Ov	1508	1381	50.80	4.26	117.32	15.45	Kp - Mk	4467	4300	21.59	2.49	51.89	7.27
Hn - Nl	1611	1608	41.53	3.38	92.26	12.91	Sc - Pt	4580	4275	21.76	2.70	51.53	7.03
Fd - Nl	1655	1322	45.97	4.30	99.95	18.51	Mk - Pt	4796	4579	19.48	2.16	47.76	6.50
Nl - Pt	1664	1531	44.69	4.57	106.80	19.60	Kp - Sc	4840	4626	20.36	2.32	49.32	6.02
Br - La	1757	1432	38.63	3.54	86.92	13.12	La - Mk	4970	4719	18.47	2.18	45.09	6.25
Br - Pt	1806	1392	38.17	3.74	84.01	13.68	Fd - Mk	5134	5019	18.17	2.20	46.36	5.48
Br - Kp	1914	1337	36.54	3.55	76.40	12.65	Ov - Sc	5461	5118	15.93	1.91	38.93	4.26
Kp - Nl	2076	1885	36.33	3.50	86.39	15.08	Br - Sc	5767	5045	13.96	1.73	35.32	4.50
Br - Nl	2300	2246	29.47	2.43	68.83	10.47	Mk - Nl	6157	5795	13.39	1.85	33.74	4.77
Nl - Ov	2328	2296	29.89	2.86	71.94	12.46	Hn - Mk	7503	7181	9.21	1.08	23.77	2.56
Br - Fd	2346	1808	30.40	3.35	68.90	12.10	Mk - Sc	8612	8609	12.33	1.13	28.78	3.17
Hn - Sc	2853	1559	30.08	3.35	63.80	11.05							

VLBA network results (3 stations, 1h duration)

Table A.4: Results of the VLBA network investigation: mfe_{dUT1} and rep_{dUT1} are the calculated mean values over the whole investigation period in $[\mu s]$ and σ_{mfe} and σ_{rep} are the derived standard deviations of mfe_{dUT1} and rep_{dUT1} in $[\mu s]$.

VLBA network investigation with three stations and one hour duration									
network	mfe_{dUT1}	σ_{mfe}	rep_{dUT1}	σ_{rep}	network	mfe_{dUT1}	σ_{mfe}	rep_{dUT1}	σ_{rep}
Fd - Hn - Mk	7.14	0.64	24.96	2.56	Mk - Nl - Ov	10.45	1.26	33.50	4.03
Hn - Mk - Nl	7.24	0.74	23.99	3.02	Kp - Mk - Nl	10.45	1.27	33.95	4.19
Hn - Mk - Pt	7.26	0.68	24.81	2.81	Mk - Nl - Pt	10.47	1.31	33.21	4.35
Hn - Kp - Mk	7.27	0.74	24.55	2.63	Br - Kp - Sc	10.54	1.03	31.51	3.54
Hn - La - Mk	7.27	0.66	24.82	2.76	Hn - Ov - Sc	10.67	1.04	32.42	3.70
Br - Hn - Mk	7.29	0.73	23.59	2.42	Br - Fd - Sc	10.69	1.21	33.11	3.80
Hn - Mk - Ov	7.29	0.70	24.31	2.65	Br - Sc - Pt	10.72	1.17	33.38	3.86
Hn - Mk - Sc	7.41	0.61	21.85	2.75	Br - La - Sc	10.77	1.27	33.83	3.76
Mk - Nl - Sc	8.42	0.69	26.18	2.58	Br - Nl - Sc	10.83	1.25	34.71	4.17
Br - Mk - Sc	8.58	0.58	25.28	2.59	Br - Hn - Ov	11.08	1.07	32.27	4.05
La - Mk - Sc	9.11	0.78	28.68	3.41	Hn - Kp - Ov	11.99	1.26	36.37	4.27
Fd - Mk - Sc	9.11	0.75	29.21	3.06	Br - Hn - Kp	12.08	0.93	32.43	4.56
Mk - Sc - Pt	9.14	0.83	28.80	3.42	Kp - Ov - Sc	12.18	1.26	36.84	4.20
Mk - Ov - Sc	9.16	0.80	27.81	3.01	Fd - Hn - Ov	12.19	1.26	37.49	4.82
Kp - Mk - Sc	9.20	0.81	29.10	3.38	Nl - Ov - Sc	12.20	1.13	37.31	4.92
Br - Mk - Nl	9.88	1.02	30.34	3.37	Br - La - Mk	12.25	1.28	34.10	4.58
Br - Hn - Sc	9.92	1.11	32.73	4.38	Ov - Sc - Pt	12.30	1.28	36.96	4.32
Fd - Mk - Nl	10.03	1.20	32.04	3.78	La - Ov - Sc	12.32	1.29	37.12	4.33
Br - Ov - Sc	10.13	1.01	29.86	3.92	Fd - Ov - Sc	12.51	1.21	38.26	4.47
La - Mk - Nl	10.40	1.26	33.20	4.23	Hn - Ov - Pt	12.52	1.28	37.28	4.86

Table A.5: Results of the VLBA network investigation: mfe_{dUT1} and rep_{dUT1} are the calculated mean values over the whole investigation period in [μs] and σ_{mfe} and σ_{rep} are the derived standard deviations of mfe_{dUT1} and rep_{dUT1} in [μs].

VLBA network investigation with three stations and one hour duration									
network	mfe_{dUT1}	σ_{mfe}	rep_{dUT1}	σ_{rep}	network	mfe_{dUT1}	σ_{mfe}	rep_{dUT1}	σ_{rep}
Br - Mk - Pt	12.59	1.25	34.21	4.99	Kp - Nl - Sc	14.39	1.41	40.82	5.59
Br - Fd - Mk	12.64	1.18	32.52	4.31	Hn - La - Sc	14.55	1.09	37.64	5.09
Br - Fd - Hn	12.65	0.87	33.43	4.51	Hn - Kp - Pt	14.72	1.40	40.84	5.75
Br - Hn - Pt	12.67	1.00	34.22	4.63	Kp - La - Sc	14.84	1.60	42.61	5.41
Fd - La - Mk	12.68	1.46	38.83	5.31	Kp - Mk - Pt	14.85	1.57	42.65	6.49
Hn - La - Ov	12.71	1.21	38.47	5.09	Hn - Kp - La	14.85	1.39	41.75	6.13
Br - Hn - La	12.85	1.03	35.23	5.19	Kp - Sc - Pt	14.99	1.62	42.41	5.44
Hn - Nl - Ov	13.03	1.25	40.27	5.37	Fd - Hn - Kp	15.01	1.43	41.60	5.41
Br - Kp - Mk	13.03	1.28	34.82	5.01	Kp - Mk - Ov	15.12	1.58	44.98	6.20
Br - Mk - Ov	13.16	1.35	37.06	4.75	Nl - Sc - Pt	15.25	1.40	42.10	5.56
Fd - Mk - Pt	13.18	1.54	40.25	5.05	Hn - Kp - Nl	15.48	1.31	44.29	6.32
Fd - Mk - Ov	13.23	1.49	42.19	5.23	La - Nl - Sc	15.59	1.42	43.50	5.95
Hn - Kp - Sc	13.31	1.29	36.24	5.26	Fd - Hn - Sc	15.63	1.22	38.24	5.46
Br - Hn - Nl	13.61	0.97	40.37	6.40	Fd - Kp - Sc	15.68	1.70	45.75	5.87
Fd - Kp - Mk	13.75	1.52	42.49	5.50	La - Sc - Pt	15.81	1.76	43.58	5.58
La - Mk - Pt	13.84	1.48	39.66	5.99	Fd - Hn - Pt	16.25	1.60	43.30	5.65
La - Mk - Ov	13.87	1.47	41.50	5.79	Fd - La - Sc	16.28	1.72	47.22	5.84
Kp - La - Mk	14.15	1.59	41.71	6.03	Hn - La - Pt	16.52	1.54	44.06	6.18
Hn - Sc - Pt	14.23	1.16	37.10	5.01	Fd - Nl - Sc	16.58	1.52	43.37	5.92
Mk - Ov - Pt	14.27	1.43	43.18	5.79	Fd - Sc - Pt	16.59	1.69	46.12	6.17

Table A.5: Results of the VLBA network investigation: mfe_{dUT1} and rep_{dUT1} are the calculated mean values over the whole investigation period in [μs] and σ_{mfe} and σ_{rep} are the derived standard deviations of mfe_{dUT1} and rep_{dUT1} in [μs].

VLBA network investigation with three stations and one hour duration									
network	mfe_{dUT1}	σ_{mfe}	rep_{dUT1}	σ_{rep}	network	mfe_{dUT1}	σ_{mfe}	rep_{dUT1}	σ_{rep}
Fd - Hn - La	16.62	1.54	44.35	5.99	Fd - Kp - Nl	27.70	2.41	77.31	14.81
Hn - Nl - Pt	17.34	1.34	48.57	6.85	Br - La - Pt	28.30	2.59	71.42	12.83
Hn - Nl - Sc	17.64	1.41	45.94	7.19	Kp - Nl - Pt	28.37	2.49	80.85	15.21
Fd - Hn - Nl	18.24	1.41	50.32	6.76	Br - La - Ov	28.59	1.65	65.03	7.94
Hn - La - Nl	18.50	1.53	51.45	7.46	Br - Kp - Ov	28.80	1.88	64.42	9.18
Br - Nl - Ov	19.04	1.30	48.23	6.41	Br - Ov - Pt	29.04	1.78	64.83	7.61
Br - Kp - Nl	19.18	1.28	47.79	5.96	Kp - La - Nl	29.08	2.57	83.00	15.41
Br - Fd - Nl	19.20	1.25	47.92	5.62	Fd - Nl - Pt	32.09	2.97	87.75	16.38
Br - Nl - Pt	20.53	1.42	52.52	7.33	Fd - La - Nl	33.80	2.80	92.19	18.48
Br - La - Nl	21.14	1.51	56.30	8.89	La - Nl - Pt	34.82	3.33	99.03	19.34
Kp - Nl - Ov	21.98	1.56	62.83	10.30	Fd - La - Ov	40.03	2.79	106.53	13.48
Fd - Nl - Ov	22.04	1.48	61.17	9.47	Fd - Ov - Pt	42.23	3.15	110.69	12.70
Nl - Ov - Pt	22.96	1.64	68.37	11.00	Fd - Kp - Ov	42.44	2.99	113.57	14.23
Br - Fd - Kp	23.02	2.09	56.44	8.26	Kp - La - Ov	50.97	3.74	139.44	17.90
Br - Fd - Ov	23.39	1.57	54.49	7.57	La - Ov - Pt	53.10	3.96	143.35	19.31
La - Nl - Ov	23.54	1.95	70.04	11.74	Kp - Ov - Pt	58.79	4.42	156.17	19.86
Br - Fd - La	23.95	2.41	63.78	10.74	Fd - Kp - La	73.31	4.61	191.56	25.64
Br - Fd - Pt	24.07	2.43	62.31	11.27	Fd - Kp - Pt	84.74	6.50	232.35	32.79
Br - Kp - La	26.74	1.93	64.25	8.86	Fd - La - Pt	100.16	9.30	263.32	41.07
Br - Kp - Pt	26.92	2.41	65.71	9.94	Kp - La - Pt	106.82	9.42	273.89	52.67

A.3. Global investigation

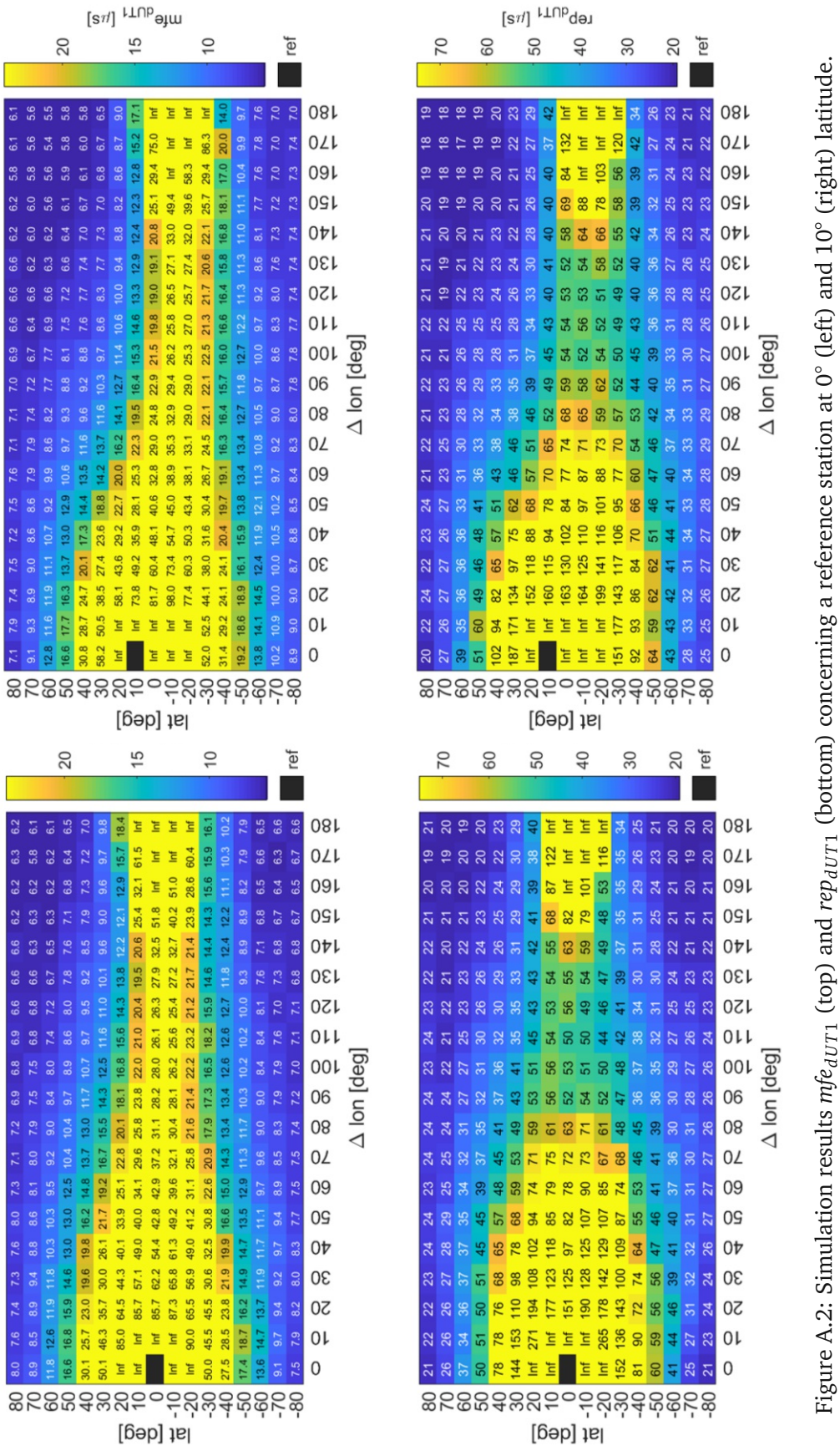

Figure A.2: Simulation results mfe_{dUT1} (top) and rep_{dUT1} (bottom) concerning a reference station at 0° (left) and 10° (right) latitude.

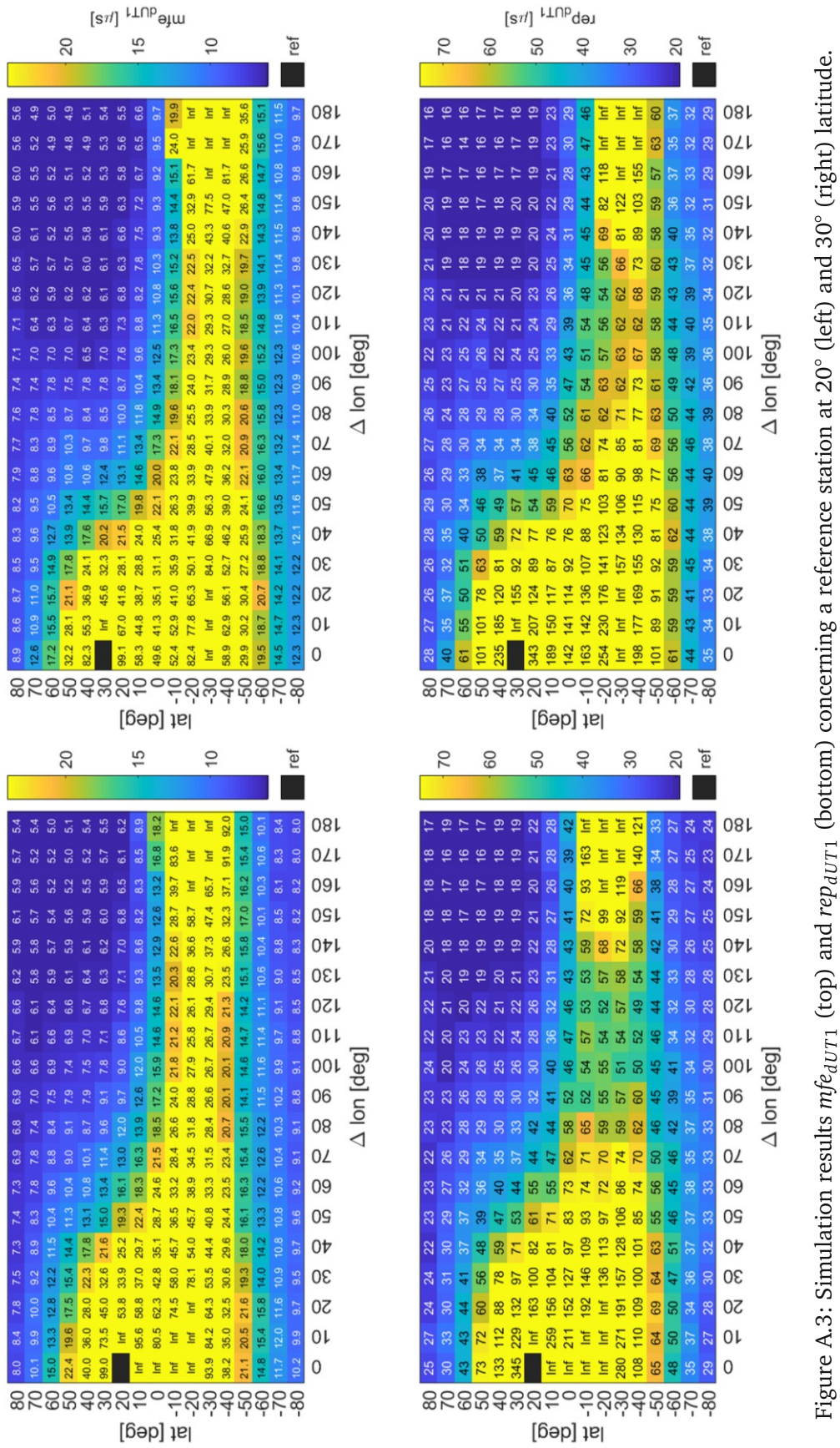

Figure A.3: Simulation results mfe_{DUT1} (top) and rep_{DUT1} (bottom) concerning a reference station at 20° (left) and 30° (right) latitude.

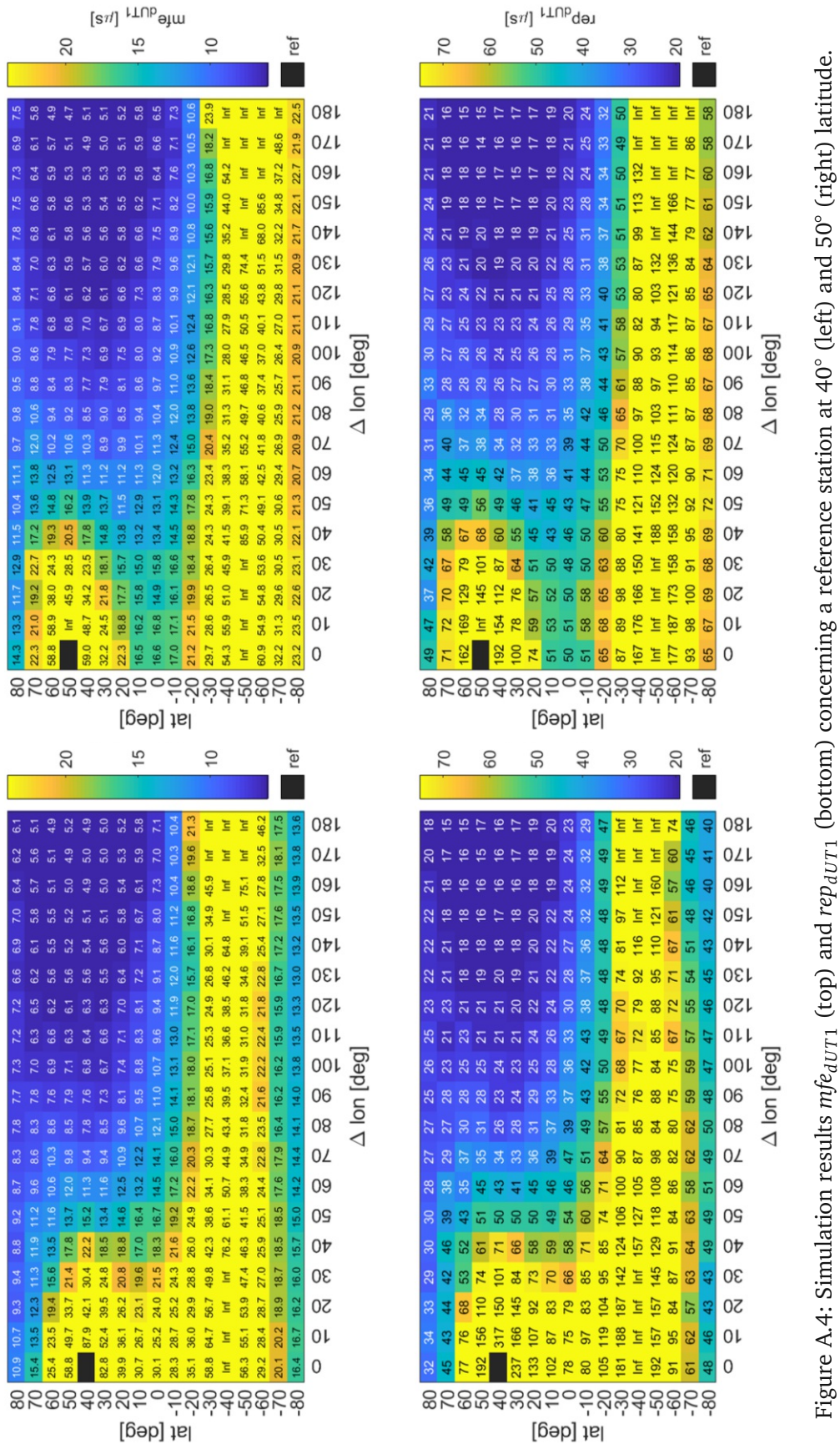

Figure A.4: Simulation results mfe_{dUT1} (top) and rep_{dUT1} (bottom) concerning a reference station at 40° (left) and 50° (right) latitude.

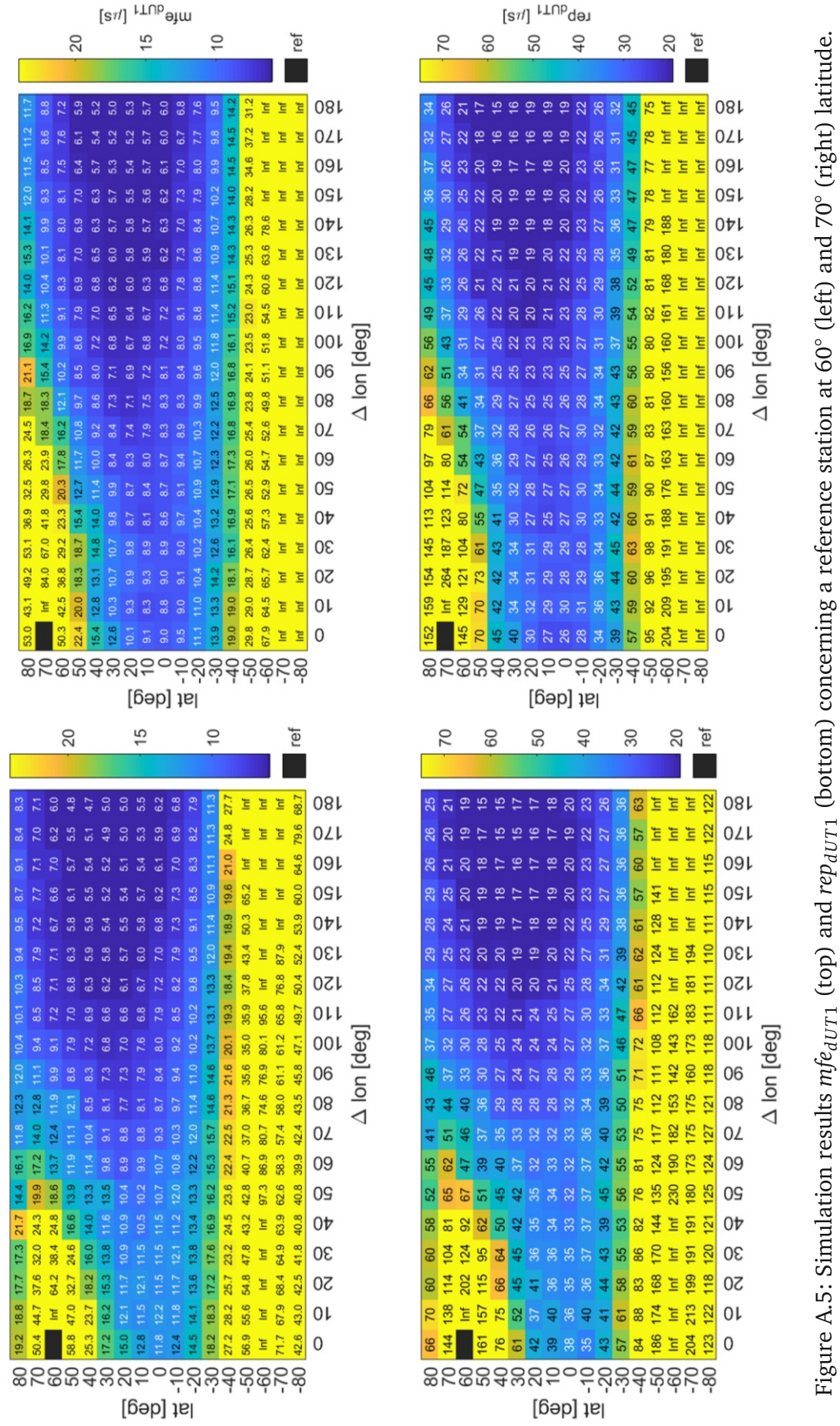

Figure A.5: Simulation results mfe_{dUT1} (top) and rep_{dUT1} (bottom) concerning a reference station at 60° (left) and 70° (right) latitude.

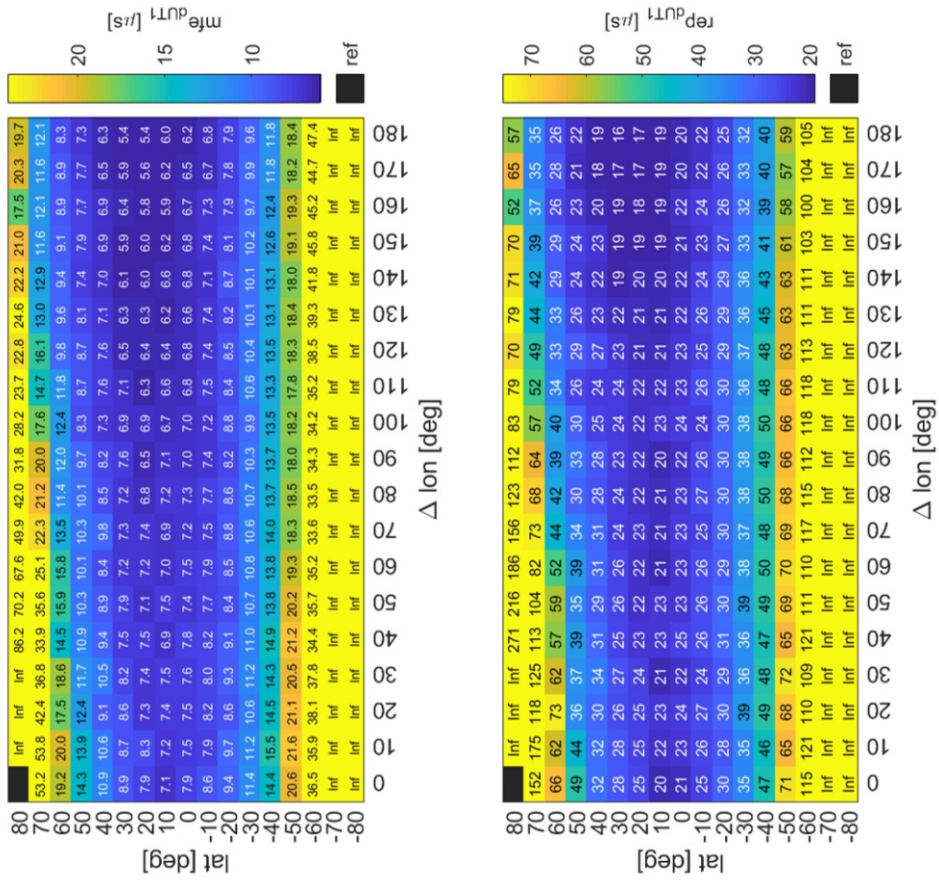

Figure A.6: Simulation results mfe_{dUT1} (top) and rep_{dUT1} (bottom) concerning a reference station at 80° latitude.

References

Artz, T., Leek, J., Nothnagel, A., & Schumacher, M. (2012). VLBI Intensive Sessions Revisited. *Seventh General Meeting (GM2012) of the international VLBI Service for Geodesy and Astrometry (IVS)*, 276–280.

Baver, K., & Gipson, J. (2014). Balancing Sky Coverage and Source Strength in the Improvement of the IVS-INT01 Sessions. In D. Behrend, K. Baver, & K. Armstrong (Eds.), *International VLBI Service for Geodesy and Astrometry 2014 General Meeting Proceedings* (pp. 267–271).

Baver, K., & Gipson, J. (2015). Minimization of the UT1 Formal Error Through a Minimization Algorithm. *Proceedings of the 22nd European VLBI Group for Geodesy and Astrometry Working Meeting*. http://www.oan.es/raege/evga2015/EVGA2015%5C_proceedings.pdf

Baver, K., & Gipson, J. (2018). UT1 Formal Errors from the BA 50 Balanced Scheduling Strategy INT01 R&Ds. *IVS 2018 General Meeting Proceedings*, 209–213.

Baver, K., & Gipson, J. (2020). Balancing source strength and sky coverage in IVS-INT01 scheduling. *Journal of Geodesy*, *94*(2), 18. https://doi.org/10.1007/s00190-020-01343-1

BKG. (2021). Radiointerferometrie (VLBI). Retrieved May 21, 2021, from https://www.bkg.bund.de/DE/Observatorium-Wettzell/Messverfahren/Radiointerferometrie/radiointerferometrie_cont.html

Böhm, J., Böhm, S., Boisits, J., Girdiuk, A., Gruber, J., Hellerschmied, A., Krásná, H., Landskron, D., Madzak, M., Mayer, D., McCallum, J., McCallum, L., Schartner, M., & Teke, K. (2018a). Vienna VLBI and Satellite Software (VieVS) for Geodesy and Astrometry. *Publications of the Astronomical Society of the Pacific*, *130*(986), 044503. https://doi.org/10.1088/1538-3873/aaa22b

Böhm, J., Bolaño, R., Garcia-Espada, S., González, J., Gruber, J., Kronschnabl, G., Neidhardt, A., Phogat, A., Plötz, C., Schartner, M., Schönemann, E., Schüler, T., & de Vicente, P. (2018b). European Intensive Sessions for the Estimation of UT1. *IVS 2018 General Meeting Proceedings*, 214–218.

Böhm, J., Nilsson, T., & Schuh, H. (2010). Prospects for UT1 Measurements from VLBI Intensive Sessions. *IVS 2010 General Meeting Proceedings*, 251–255.

Böhm, S., Gruber, J., Kern, L., McCallum, J., McCallum, L., Quick, J., & Schartner, M. (2021). Probing a southern hemisphere VLBI intensive baseline configuration fur dUT1 determination. *Scientific Assembly of the International Association of Geodesy Abstract Book*.

Campbell, J. (2000). From Quasars To Benchmarks: VLBI Ties Heaven and Earth. *IVS 2000 General Meeting Proceedings*, 19–34.

Charlot, P., Jacobs, C. S., Gordon, D., Lambert, A., S. and. de Witt, Böhm, J., Fey, A. L., Heinkelmann, R., Skurikhina, E., Titov, O., Arias, E., Bolotin, S., Bourda, G., Ma,

C., Malkin, Z., Nothnagel, A., Mayer, D., MacMillan, D. S., Nilsson, T., & Gaume, R. (2020). The third realization of the International Celestial Reference Frame by very long baseline interferometry. *Astronomy & Astrophysics*. https://doi.org/10.1051/0004-6361/202038368

Corbin, A., Niedermann, B., Nothnagel, A., Haas, R., & Haunert, J. (2020). Combinatorial optimization applied to VLBI scheduling. *Journal of Geodesy*, *94*(2), 19. https://doi.org/10.1007/s00190-020-01348-w

Geiger, N. P., Fey, A., Dieck, C., & Johnson, M. (2018). Intensifying the Intensives with the VLBA. *IVS 2018 General Meeting Proceedings*, 219–222.

Gipson, J. (2010). An Introduction to Sked. In R. Navarro, S. Rogstad, C. E. Goodhart, E. Sigman, M. Soriano, D. Wang, L. A. White, & C. S. Jacobs (Eds.), *International VLBI Service for Geodesy and Astrometry 2010 General Meeting Proceedings* (pp. 77–84). https://ivscc.gsfc.nasa.gov/publications/gm2010/IVS-2010-General-Meeting-Proceedings.pdf

Haas, R., Varenius, E., Matsumoto, S., & Schartner, M. (2021). Observing UT1-UTC with VGOS. *Earth, Planets and Space*, *73*(78). https://doi.org/10.1186/s40623-021-01396-2

Herring, T., Davis, J., & Shapiro, I. (1990). Geodesy by radio interferometry: The application of Kalman Filtering to the analysis of very long baseline interferometry data. *Journal of Geophysical Research: Solid Earth*, *95(B8)*, 12561–12581. https://doi.org/10.1029/JB095iB08p12561

Hobiger, T., Kondo, T., & Schuh, H. (2006). Very long baseline interferometry as a tool to probe the ionosphere. *Radio Science*, *41*(1). https://doi.org/10.1029/2005RS003297

IVS. (2021a). Intensive Master Schedule 2021. Retrieved May 25, 2021, from https://ivscc.gsfc.nasa.gov/sessions/

IVS. (2021b). Network Stations - Map of Stations. Retrieved May 25, 2021, from https://ivscc.gsfc.nasa.gov/stations/ns-map.html

Kahmen, H. (2006). *Angewandte Geodäsie Vermessungskunde* (20th ed.). Walter de Gruyter GmbH & Co. KG, Berlin.

Kareinen, N., Klopotek, G., Hobiger, T., & Haas, R. (2017). Identifying optimal tag-along station locations for improving VLBI Intensive sessions. *Earth, Planets and Space*, *69*(1). https://doi.org/10.1186/s40623-017-0601-y

Klopotek, G., Hobiger, T., Haas, R., & Otsubo, T. (2020). Geodetic VLBI for precise orbit determination of Earth satellites: a simulation study. *Journal of Geodesy*, *94*(56). https://doi.org/10.1007/s00190-020-01381-9

Landskron, D., & Böhm, J. (2019). Improving dUT1 from VLBI intensive sessions with GRAD gradients and ray-traced delays. *Advances in Space Research*, *63*, 3419–3435. https://doi.org/10.1016/j.asr.2019.03.041

Leek, J., Artz, T., & Nothnagel, A. (2015). Optimized scheduling of VLBI UT1 intensive sessions for twin telescopes employing impact factor analysis. *Journal of Geodesy*, *89*(9), 911–924. https://doi.org/10.1007/s00190-015-0823-3

Merkowitz, S., & Gipson, J. (2021). IVS Contribution to ITRF2020. Retrieved May 26, 2021, from https://ivscc.gsfc.nasa.gov/IVS_AC/IVS-AC_ITRF2020.htm

Napier, P., Bagri, D., Clark, B., Rogers, A., Romney, J., Thompson, A., & Walker, R. (1994). The Very Long Baseline Array. *Proceedings of the IEEE*, *82*(5), 658–672. https://doi.org/10.1109/5.284733

Nilsson, T., Haas, R., & Elgered, G. (2007). Simulations of atmospheric path delays using turbulence models. In J. Böhm, A. Pany, & H. Schuh (Eds.), *Proceedings of the 18th European VLBI for Geodesy and Astrometry Work Meeting* (pp. 175–180).

Nothnagel, A. (2019a). The correlation process in Very Long Baseline Interferometry. *GEM - International Journal on Geomathematics*, *10*(18). https://doi.org/10.1007/s13137-019-0130-x

Nothnagel, A. (2019b). Very Long Baseline Interferometry. *Handbuch der Geodäsie* (pp. 1–58). Springer Spektrum Berlin Heidelberg. https://doi.org/10.1007/978-3-662-46900-2110-1

NVI. (2021). sked catalogs. Retrieved June 1, 2021, from https://github.com/nvi-inc/sked_catalogs

Pany, A., Böhm, J., MacMillan, D., Schuh, H., Nilsson, T., & Wresnik, J. (2010). Monte Carlo simulations of the impact of troposphere, clock and measurement errors on the repeatability of VLBI positions. *Journal of Geodesy*, *85*, 39–50. https://doi.org/10.1007/s00190-010-0415-1

Petit, G., & Luzum, B. (2010). IERS Conventions (2010). *IERS Technical Note*, *36*.

Petrachenko, B., Niell, A., Behrend, D., Corey, B., Boehm, J., Charlot, P., Collioud, A., Gipson, J., Haas, R., Hobiger, T., Koyama, Y., MacMillan, D., Malkin, Z., Nilsson, T., Pany, A., Tuccari, G., Whitney, A., & Wresnik, J. (2009). Design Aspects of the VLBI2010 System. Progress Report of the IVS VLBI2010 Committee - Progress Report of the IVS VLBI2010 Comittee, NASA/TM-2009-214180.

Petrachenko, W. T., Niell, A. E., Corey, B. E., Behrend, D., Schuh, H., & Wresnik, J. (2012). VLBI2010: Next Generation VLBI System for Geodesy and Astrometry. In S. Kenyon, M. Pacino, & U. Marti (Eds.), *Geodesy for Planet Earth* (pp. 999–1005). Springer Berlin Heidelberg.

Plank, L., Lovell, J., McCallum, J., Mayer, D., Reynolds, C., Quick, J., Weston, S., Titov, O., Shabala, S., Böhm, J., Natusch, T., Nickola, M., & Gulyaev, S. (2017). The AUSTRAL VLBI observing program. *Journal of Geodesy*, *91*, 803–817. https://doi.org/10.1007/s00190-016-0949-y

Plank, L., Lovell, J., Shabala, S., Böhm, J., & Titov, O. (2015). Challenges for geodetic VLBI in the southern hemisphere. *Advances in Space Research*, *56*(2), 304–313. https://doi.org/10.1016/j.asr.2015.04.022

Plötz, C., Schüler, T., Hase, H., La Porta, L., Schartner, M., Böhm, J., Bernhart, S., Brunini, C., Salguero, F., Vera, J., Müskens, A., Kronschnabl, G., Schwarz, W., Phogat, A., Neidhardt, A., & Brandl, M. (2019). INT9 - Δ UT1 Determination Between the Geodetic Observatories AGGO and Wettzell. *Proceedings of the 24th European VLBI Group for Geodesy and Astrometry Working Meeting*, 124–128.

Raut, S., Heinkelmann, R., Modiri, S., & Schuh, H. (2020). Effect of VLBI intensive sessions on daily and sub-daily ERP determined from CONT17 IVS data. *Proceedings of the Journees 2019 "Astrometry, Earth Rotation, and Reference Systems in the GAIA era*, 141–145.

Robertson, D. (1991). Geophysical applications of very-long-baseline interferometry. *Reviews of Modern Physics*, *63*(4).

Schartner, M. (2021). Templates. Retrieved May 31, 2021, from https://github.com/TUW-VieVS/VieSchedpp_AUTO/tree/master/Templates

Schartner, M., & Böhm, J. (2019a). Optimizing schedules for the VLBI global observing system. *Journal of Geodesy*, *94*(12). https://doi.org/10.1007/s00190-019-01340-z

Schartner, M., & Böhm, J. (2019b). VieSched++: A New VLBI Scheduling Software for Geodesy and Astrometry. *Publications of the Astronomical Society of the Pacific*, *131*(1002). https://doi.org/10.1088/1538-3873/ab1820

Schartner, M., Böhm, J., Mayer, D., McCallum, L., & Hellerschmied, A. (2017). Recent Developments in Scheduling With VieVS. *23th Meeting of the European VLBI Group for Geodesy and Astrometry*, 113–116.

Schartner, M., Böhm, J., & Nothnagel, A. (2020). Optimal antenna locations of the VLBI Global Observing System for the estimation of Earth orientation parameters. *Earth, Planets and Space*, *72*(1), 87. https://doi.org/10.1186/s40623-020-01214-1

Schartner, M., Kern, L., Nothnagel, A., Böhm, J., & Soja, B. (2021). Optimal VLBI baseline geometry for UT1-UTC Intensive observations. *Journal of Geodesy*, *95*(75). https://doi.org/10.1007/s00190-021-01530-8

Schnell, D. (2006). *Quality aspects of short duration VLBI observations for UT1 determinations* (Doctoral dissertation). Hohe Landwirtschaftliche Fakultät der Rheinischen Friedrich-Willhelms-Universität zu Bonn.

Schuh, H., & Behrend, D. (2012). VLBI: A fascinating technique for geodesy and astrometry. *Journal of Geodynamics*, *61*, 68–80. https://doi.org/https://doi.org/10.1016/j.jog.2012.07.007

Seeber, G. (2003). *Satellite Geodesy, 2nd completely revised and extended edition*. Walter de Gruyter GmbH & Co. KG, Berlin.

Sekido, M., Takefuji, K., Ujihara, H., Kondo, T., Tsutsumi, M., Kawai, E., Hachisu, H., Nemitz, N., Pizzocaro, M., Clivati, C., Perini, F., Negusini, M., Maccaferri, G., Ricci, R., Roma, M., Bortolotti, C., Namba, K., Komuro, J., Ichikawa, R., ... Ido, T. (2021). A broadband VLBI system using transportable stations for geodesy and metrology: an alternative approach to the VGOS concept. *Journal of Geodesy*, *95*(41). https://doi.org/10.1007/s00190-021-01479-8

Shuygina, N., Ivanov, D., Ipatov, A., Gayazov, I., Marshalov, D., Melnikov, A., Kurdubov, S., Vaselyev, M., Ilin, G., Skurikhina, E., Surkis, I., Mardyshkin, V., Mikhailov, A., Salnikov, A., Vytnov, A., Rakhimov, I., Dyakov, A., & Olifirov, V. (2019). Russian VLBI network "Quasar": Current status and outlook. *Geodesy and Geodynamics*, *10*(2), 150–156. https://doi.org/https://doi.org/10.1016/j.geog.2018.09.008

Spicakova, H. (1991). A Consensus model for relativistic effects in geodetic VLBI. *Proceedings of the USNO workshop on relativistic models for use in space geodesy*, 60–82.

Spicakova, H., Böhm, J., Böhm, S., Nilsson, T., Pany, A., Plank, L., Teke, K., & Schuh, H. (2010). Estimation of Geodetic and Geodynamical Parameters with VieVS. *2010 General Meeting Proceedings, Hobart, Tasmania, Australia*, 202–206.

Sun, J. (2013). VLBI scheduling strategies with respect to VLBI2010. *Geowissenschaftliche Mitteilungen*, (92). http://www.aoc.nrao.edu/software/sched/index.html

Uunila, M., Nothnagel, A., & Leek, J. (2012). Influence of Source Constellations on UT1 Derived from IVS INT1 Sessions. In D. Behrend & K. Baver (Eds.), *International VLBI Service for Geodesy and Astrometry 2012 General Meeting Proceedings* (pp. 395–399).

Vandenberg, N. (1997). *sked's Catalogs - Program Reference Manual*. NVI Inc. NASA/Goddard Space Flight Center, Space Geodesy Program.

Vandenberg, N. (1999). sked: Interactive/Automatic Scheduling Program.

Walker, R. (2018). *The SCHED User Manual, version 11.4*. http://www.aoc.nrao.edu/software/sched/index.html

Whitney, A. (2000). How Do VLBI Correlators Work? *IVS 2000 General Meeting Proceedings*, 187–205.